TU Delft

EVALUATING THE RESILIENCE OF URBAN DRAINAGE SYSTEMS IN ROTTERDAM UNDER EXTREME PRECIPITATION

HOW HYDRODYNAMIC MODELS CAN GUIDE CLIMATE ADAPTATION STRATEGIES?

CARLO SOBRAL DE VITO

SUPERVISORS:
PROF. ZORAN KAPELAN
DR. BORIS VAN BREUKELEN
IR. ALBERT KEMELING
DR. IR. NIKOLA STANIĆ

Gemeente Rotterdam

This page is intentionally left blank

Evaluating the Resilience of Urban Drainage Systems in Rotterdam Under Extreme Precipitation

How hydrodynamic models can guide climate adaptation strategies?

by

Carlo Sobral de Vito

in partial fulfilment of the requirements for the degree of

Master of Science
in Environmental Engineering

at Delft University of Technology,
to be defended publicly on Friday, November 15, 2024 at 10:45 AM.

Student Number: 5833337

Project Duration: February 2, 2024 – November 15, 2024

Thesis Committee: Prof. Zoran Kapelan (TU Delft)
Dr. Boris van Breukelen (TU Delft)
Ir. Albert Kemeling (IBR Gemeente Rotterdam)
Dr. Ir. Nikola Stanić (IBR Gemeente Rotterdam)

Cover Design: João Paulo Sant'Anna

Photos from MediaTV.nl (upper-left) and AD.nl (bottom-left)

This page is intentionally left blank

Acknowledgments

My passion for urban drainage began during my bachelor's studies, guided by Prof. Sergio Koide at the University of Brasília, and continuously supported by daily insights from my father, Marco de Vito, a dedicated water resources engineer. Motivated by the famous saying 'God created the earth, but the Dutch created the Netherlands', I dreamed of advancing my studies in this country. Here, I have been privileged to learn from remarkable mentors. Prof. Zoran Kapelan, my main supervisor, has profoundly inspired me with his clear and structured method of teaching and his vast expertise in hydrodynamic modelling and risk assessments. Dr. Jeroen Langeveld has greatly enhanced my learning experience by demonstrating both successful and less successful water management practices in the Netherlands, encouraging innovative thinking. Dr. Job van der Werf has been important in deepening my enthusiasm for the field, providing well-designed modelling assignments during the course and generously sharing his extensive coding knowledge. I am also grateful to Dr. Boris van Breukelen for his guidance as my second supervisor, offering insightful contributions during the final stages of this thesis.

Beyond my activities at the university, I also had the opportunity to grow under the guidance of distinguished professionals during internships. At Deltares, Dr. Antonio Moreno provided me the opportunity to work on an international project presented at ICUD, which greatly enhanced my GIS and writing skills. Later, at Gemeente Rotterdam, where I conducted this research, I was fortunate to be guided by Dr. Nikola Stanic, who insightfully identified my strengths and weaknesses, consistently challenging me not only to explore innovative modelling methods but also to effectively communicate the results of this thesis. Additionally, Ir. Albert Kemeling made a significant contribution to this research, always eager to share his extensive knowledge of Rotterdam's drainage systems and helping me navigate the complexities of the city's looped networks. I would also like to extend my gratitude to Koen Tromp, Farhan Meke, and Tije Bakker for their expert guidance with InfoWorks ICM; to Nadia Mobron, Emma Oosterveld, and Márcio Bittar Bigonha for their valuable insights in modeling SuDS; and to Tobias Mulder for his assistance in processing rainfall data.

Lastly, this acknowledgments would be incomplete without a special mention of beloved family, whose support has enabled me to experience and enjoy every moment of my life here in Europe. Thank you for making this dream come true!

Abstract

In response to the growing risks of pluvial flooding due to climate change, this thesis presents a framework to assess the resilience of urban drainage systems and guide adaptation strategies using coupled 1D-2D modelling and economic flood risk assessments. The research begins by exploring methods in InfoWorks ICM to simulate interactions between surface and subsurface flows in urban environments, focusing on a simplified approach to model gully flow that reduces data requirements and computational load. Building on this, flood hazards from the simplified model are used to identify buildings at risk of internal flooding, estimate potential financial losses, and calculate expected annual damages under current and future climate conditions, accounting for climate change impacts. Subsequently, this research evaluates blue, green, and grey infrastructure measures, through cost-benefit analysis where benefits are quantified as reductions in expected damages.

A detailed case study from Spangen, a densely populated residential area in Rotterdam, applies the proposed framework, demonstrating that a simplified 1D-2D modelling approach without individual gully data can realistically estimate pluvial flood hazards and support economic flood risk assessments. The findings of the risk assessment suggest that existing infrastructure investments in the neighborhood have effectively reduced current pluvial flood risks. Looking ahead, for future climate conditions, a combination of green, blue, and grey infrastructure proves to be the most effective adaptation strategy as these measures synergistically enhance the resilience. Despite this, the cost-benefit analysis revealed a negative net present value when considering only flood damage reduction due to low flood risks under current climate conditions. Nonetheless, comprehensive decision-making should account for the additional benefits of green infrastructure, such as urban cooling and associated energy savings, improved air quality, and enhanced biodiversity.

This page is intentionally left blank

Content

List of Figures

List of Tables

1 Introduction

1.1 Background

Scientists agree that human activity is one of the primary drivers of climate change, thus leading to global warming. These changes result in more frequent and intense extreme weather events globally (IPCC, 2021), increasing the likelihood of pluvial flooding. In order to protect both public and private urban infrastructure, it is necessary to adapt urban water systems to these changes and enhance their resilience (Willems & Olsson, 2012). In the Netherlands, where about 25% of the land is below sea level and up to 60% is at significant flood risk during extreme weather conditions, the threat from climate change is particularly severe (Kabat *et al.*, 2005). In response, Dutch authorities are integrating climate-proofing and water-resilient strategies into their policies and actions to safeguard the country against future climate conditions (Delta Programme, 2020).

Urban drainage systems are crucial for managing runoff during storms and mitigating flood risks. However, their effectiveness is limited by design capacities that may not accommodate heavy rainfall events. In Rotterdam, the sewer system is well-designed and established, and consequently its performance is well-understood. Nevertheless, The Municipality of Rotterdam is responsible for managing stormwater runoff in public spaces and is focused on preparing the city for extreme weather conditions. To this end, Rotterdam is engaged in developing adaptation strategies to mitigate increased flood risk driven by climate change; thereby preventing excessive damage and hazardous conditions in urban environments.

Economic feasibility is one of the main factors when establishing climate adaptation strategies. For this purpose, different infrastructure investment options are evaluated. A common method to estimate the efficiency of risk-reduction measures is cost-benefit analysis. For flood management, the comparison is typically between the investment plus maintenance costs of measures and the expected damages (Alves *et al.*, 2019). In assessing pluvial flooding risks, damages are often estimated from maximum water depths during specific flood events, using mathematical models that simulate hydrologic and hydraulic processes within urban drainage systems to predict flood hazards (Nicklin *et al.*, 2019).

Conventional urban drainage modelling involves two main steps: (i) hydrological model that converts rainfall into runoff, taking into account various losses as rainwater reaches the catchment surface, and (ii) this runoff is transported through a sewer network conceptualized as nodes (manholes) and links (sewers or open channels) in one-dimensional (1D) representation (Barreiro *et al.*, 2023). Over the years, The Municipality of Rotterdam has efficiently used this conventional modelling approach to ensure the systems meet design standards and to identify flood-prone areas. However, relying solely on 1D sewer flow models limits the analysis to predicting surcharge volumes at the surface and fails to simulate the flood propagation over the ground level (Chang *et al.*, 2015). To provide a comprehensive assessment of urban flood risks, a more realistic representation of complex surface flows is essential (Bulti *et al.*, 2020).

To address the limitation, Djordjević *et al.* (1999) proposed to couple these minor system's 1D models with the major system, employing the dual drainage concept. Advancements in urban flood modelling have resulted in commercial software coupling two-dimensional (2D) surface models with 1D sewer models. This integration is typically achieved by generating a unstructured

mesh to represent the urban topology, using a high-resolution elevation model for 2D numerical modelling of surface flow (Yang *et al.*, 2020).

Despite these advancements, transitioning to a 1D-2D urban flood modeling approach presents challenges. Although detailed topographic data is available at national level in the Netherlands, these models require methodologies that carefully account for the interactions between the major and minor drainage layers (Russo *et al.*, 2015). The literature, including studies by Chang *et al.* (2018) and Jang *et al.* (2019), recommends incorporating gully inlets to more realistically model the water exchange between surface and the underground network. Yet, accurately locating these inlets is time-consuming and impractical on a city-wide scale. Incorporation of every gully and its connecting pipe to the main sewer system makes the urban drainage model excessively complex to build, use and maintain. Moreover, 1D-2D simulations that incorporate detailed gully data in Rotterdam have long simulation time, complicating the evaluation of large system performance across different scenarios and hydraulic loads.

1.2 Problem Statement

Due to limited financial resources, Rotterdam's decision-makers are in need of tools to select cost-effective measures to mitigate pluvial flood risks. The municipality is transitioning to a 1D-2D urban flood modeling approach to simulate flood hazards, but determining the best method to represent surface-network flow interactions remains challenging. Furthermore, to determine flood risks, economic tools are favored to quantify in monetary terms, enabling comparison of investment options through cost-benefit analysis. Additionally, the long technical lifetimes of urban drainage systems necessitate the inclusion of climate predictions in these economic flood risk assessments.

This thesis presents an integrated approach to evaluate adaptation options, incorporating climate change impacts, 1D-2D pluvial flood modeling, GIS analysis, economic risk assessment, and cost-benefit analysis. Specifically, for 1D-2D modeling, various methodologies to account for interactions between surface and underground networks were assessed, seeking an efficient and reliable method that simulates gully flow without directly including their data. To author's knowledge, based on the literature review, no attempt has been made until now to represent gullies in a simplified manner within the urban drainage system model.

1.3 Thesis Objectives and Research Questions

This research has two main objectives: (i) identify best approach to simulate pluvial flood hazards in an urban environment in a realistic, reliable and efficient manner, i.e. by using a simplified 1D-2D model without gully data; and (ii) develop an integrated flood risk assessment framework to guide the selection of cost-effective adaptation measures. These objectives can be framed through the following main and sub-questions:

Main Question:

How can the cost-effectiveness of climate adaptation measures be evaluated using flood hazard estimates derived from an efficient and reliable 1D-2D modeling approach without gully data?

Sub-Questions:

1) How can gully flow be modelled in a simplified manner (resulting in reduced data requirements and computational time) without significantly compromising the quality of obtained results?
2) How best to incorporate climate change impacts into the evaluation of pluvial flood risks in the urban environment?
3) How can estimates of pluvial flood risks be generated from simulated flood hazards using the simplified model?
4) How can the effectiveness of climate adaptation measures be assessed using pluvial flood risk estimates?

2 Theoretical Background

2.1 Pluvial Flooding

2.1.1 Causes and Impacts

In today's cities the response to intense rainfall is primarily determined by its stormwater management practices. Over the years, the conventional approach to stormwater runoff management aimed to quickly collect and convey runoff, maximizing available land for urban development needs. This initially appeared to be effective for flood mitigation, however this method overlooked the risks posed by extreme rainfall. Stormwater systems are engineered to handle runoff from a "design storm" i.e. rainfall event with specific return period. Nevertheless, more extreme rainfall events may occur thus exceeding system's drainage capacity, leading to pluvial flooding (Rosenzweig *et al.*, 2018).

In the Netherlands, growing concerns about increased pluvial flooding arise from four main drivers (Rehder, 2024). Firstly, climate change has led to more frequent heavy rains in Europe due to a warming atmosphere that holds more moisture (IPCC, 2021). Secondly, urbanization has replaced permeable surfaces with impermeable materials like concrete and asphalt, decreasing water absorption and modifying flow paths (Costa *et al.*, 2021). Thirdly, aging of the infrastructure and differential land settlement rates caused by soil subsidence lead to system failures and diminished in-sewer storage capacity (Dirksen *et al.*, 2013). Lastly, the low soil bearing capacity in many Dutch cities, along with soil subsidence, causes surface depressions in stressed areas, raising the risk of localized flooding (Jansen *et al.*, 2023).

The impacts of pluvial flooding are wide-ranging and manifest across economic, environmental, and social dimensions. They can be categorized into direct and indirect, as well as tangible and intangible. Direct damages result from immediate contact with floodwaters, such as physical damage to vehicles, buildings, and their contents, or harm to people and ecosystem losses. Indirect damages, such as business and infrastructure disruptions, can emerge later or beyond the flooded area. Tangible damages, such as building and infrastructure losses, are easily quantifiable in monetary terms, while intangible ones, like mortality and psychological trauma, lack clear market values (Nicklin *et al.*, 2019).

The financial implications of pluvial flooding in the Netherlands has been proven to be significant, with a total damage of €674 million between 1986 and 2009 (Spekkers *et al.* 2012). With increasing flood risks due to climate change, these economic losses are likely to be even greater. Therefore, there is an urgent need to review design practices and incorporate adaptation measures. However, quantifying the benefits of these measures for effective planning is often a challenge (Zhou *et al.*, 2012).

2.1.2 Economic Flood Risk Assessment

According to the European Commission (2021), economic risk assessment that incorporates climate change impacts is the most comprehensive method for assessing the effectiveness adaptation investments or policy decisions. Although there is no universally accepted definition of risk, it is most commonly defined as the product of the likelihood of an event and its impact (Kaplan and Garrick, 1981). In the context of pluvial flooding, the likelihood is calculated as the inverse of the return period of rainfall events, while the impact is represented by the associated financial loss due to flood damage. When financial loss estimates are weighted by the rainfall

return period and averaged over all flood events, the end result is an estimate of the expected annual damage (EAD), which can be used as a risk indicator to reflect adverse effects in terms of cost (Sušnik *et al.*, 2015; Zhou *et al.*, 2012).

Estimating financial loss for a given flood event typically involves three steps (Nicklin *et al.*, 2019): hazard analysis (simulating the flood hazard), exposure analysis (identifying assets exposed to flooding), and vulnerability analysis (translating characteristics of exposed objects into monetary costs). In hazard analysis, impact parameters like flood depth, duration, and flow velocity are estimated often using a simulation model. Next, exposure analysis identifies objects affected by a flood event. This is typically done by intersecting land use with inundation data using a geographic information system (GIS). For example, Bertsch *et al.* (2022) intersected water depth information with building geometry data to estimate flood exposure through buffer analysis, classifying the likelihood of internal flooding. In vulnerability analysis, flood damages to these exposed objects are computed based on its asset value (i.e., maximum potential damage) and the hazard parameters.

Given that object-level assessment is often impractical, assets are often aggregated by land use classification (Merz *et al.*, 2010). Estimates of asset values are then made for categories (e.g., houses, industries, commercial companies, primary roads, and secondary roads); though uncertainties is significant due to different susceptibilities of the exposed objects (Wagenaar *et al.*, 2016). Once asset values are defined, flood damage is typically estimated using depth-damage curve, which correlates surface water levels to monetary loss for the specific category (Smith, 1994). This loss is often expressed as a fraction of the asset values (FLOODsite, 2009).

Besides flood depth, additional hazard parameters, such as duration and flow velocity also affect structural integrity of assets (Marvi *et al.*, 2020). Some loss models for fluvial flooding include these parameters and also resistance factors like building material, age, and size (Penning-Rowsell *et al.*, 2013, Kreibich *et al.*, 2010). However, pluvial flooding requires different considerations due to its unique flow properties, making direct use of fluvial damage functions inappropriate (Kellens *et al.*, 2013). Efforts to incorporate additional hazards into pluvial flood damage assessments using insurance data or victim surveys have been made (Spekkers *et al.*, 2012; Zhou *et al.*, 2013); however, developing a reliable regional depth-damage curve remains challenging (Zhou *et al.*, 2012). Thus, correlation between damage and pluvial flooding characteristics has been mainly limited to simplified regression laws considering flood depth only (Freni *et al.*, 2010).

2.1.3 Flood Risk Management

Flood risk management aims to reduce (or maintain) future flood consequences, recognizing that risks can only be mitigated, not eliminated, often at the cost of other societal goals (FLOODsite, 2009). A key element is to develop long-term, cost-effective intervention strategies to reduce potential damages (Woodward *et al.*, 2011). Traditional urban resilience strategies relied on robust but inflexible and costly grey infrastructure like sewer pipes and canals (Depietri and McPhearson, 2017). However, recognizing their limitations in adapting to future climate conditions, recent decades have seen a shift toward nature-based solutions that enhance infiltration and water retention, aiming to maintain the urban hydrological cycle closer to its pre-development state (Ferreira *et al.*, 2021).

Even before climate change became a dominant concern in urban water management, the Netherlands began adopting nature-based solutions to address the following challenges of their traditional systems: (i) sewage systems were often overwhelmed by heavy rainfall, leading to rapid water processing and flooding in low-lying areas; (ii) frequent CSOs led to contamination of surface water systems; and (iii) fluctuating groundwater levels (GWLs) e.g.too low GWLs during summer droughts can cause compromise structural integrity of the buildings, and too high GWLs often during winter period can lead to groundwater floods. By 1998, the Dutch Ministry of Infrastructure and Water Management (*Ministerie van Infrastructuur en Waterstaat*) initiated a transition/shift from conventional sub-surface water runoff conveyance via sewere systems to more surface-level runoff solutions. This became national policy, mandating that new neighborhoods disconnect stormwater runoff from sewer systems, with various strategies encouraging the adoption of nature-based solutions (Koning and Boogaard, 2023).

During this transition, the Netherlands introduced its first swales, which are green ditches designed to facilitate drainage, infiltration, and rainwater storage. Recognizing the growing impacts of climate change, these became a cornerstone in the country's strategy to achieve climate resilience by 2050 (Boogaard, 2019). However, in densely populated urban areas, available green space for installing this infrastructure is limited. As an alternative, permeable pavements have been widely adopted by many municipalities to reduce peak flows and stormwater discharge into sewers (de Graaf-van Dinther *et al.*, 2021; Veldkamp *et al.*, 2020). Another common measure involves disconnection by installing stormwater piping networks that direct water to underground infiltration crates. These crates gradually release water into the groundwater and generally provide more storage capacity than above-ground infrastructures, though implementation is constrained by available underground space (Gehrels *et al.*, 2018).

Besides public spaces, nature-based solutions have been increasingly adopted in private properties, particularly in social housing areas in the Netherlands to also promote environmental justice. For instance, housing corporations are integrating green roofs in new developments or during renewals, often supported by stormwater subsidies from municipalities (Snep *et al.*, 2023). However, while green roofs offer multifunctional urban benefits, their storage capacity during extreme rainfall events is relatively low (Zhang *et al.*, 2021). To enhance their effectiveness, recent innovations include the integration of blue water retention layers, which can add up to 70 mm of storage (Pelorosso *et al.*, 2021; Busker *et al.*, 2021). Additionally, smart flow controls are being developed to enable remote management water levels ahead of heavy rainfall and to supply irrigation during dry spells. This innovative concept was applied in Amsterdam through the RESILIO project, where approximately 7,500 m² of roofs from three housing corporations were retrofitted (Langewen *et al.*, 2022).

As numerous investment options exist to mitigate flood risks, it is essential to evaluate their effectiveness for informed climate adaptation planning within a specific urban setting. This typically involves a cost-benefit analysis to assess the economic impacts of implementing risk-reduction measures. In the context of pluvial flooding, benefits are categorized as primary and secondary. Primary benefits consist of avoided damages, calculated as the net present value of the difference in EAD with and without the investment (de Bruin *et al.*, 2014). Secondary benefits extend beyond flood management, encompassing water and energy savings, air quality improvements, and carbon sequestration. Though challenging to quantify and often neglected in decision-making, these benefits can enhance the viability of adaptation strategies. For example,

Alves *et al.* (2019) found that nature-based solutions only become cost-effective for the urban catchment under investigation when secondary benefits are included, and a combined blue-green-grey solution maximizes net benefits.

2.2 Modelling of Urban Drainage Systems

Simulation models of urban drainage systems offer a mathematical approximation of hydrological and hydraulic processes in a specific geographic and geometric contexts. A well-defined model can simulate a change in the system and provide a realistic projections of potential consequences (Pedersen *et al.*, 2021). Thus, their usage as planning tool has increased considerably over the last decades, facilitating tasks such as prioritizing areas for rehabilitation (Suryanto, 2021), assessing economic impacts of urbanization and climate change (Ortiz *et al.*, 2021), evaluating upgrade scenarios to comply with water quality regulations (Benedetti *et al.*, 2013), making comparative assessments of adaptation measures to reduce overflow emissions (Montoya-Coronado *et al.*, 2024) and to mitigate pluvial flood risks (Cheng *et al.*, 2024).

2.2.1 Different Modelling Approaches

Simulation models of urban drainage systems must be tailored to specific needs, as there is no 'one-size-fits-all' approach. Models that are overly simplistic may not yield accurate enough results, while highly detailed models can be prohibitively costly in terms of data requirements and computational efforts. An effective model finds a balance between simplicity and the level of detail necessary to accurately describe the processes under investigation. Essential components to be represented in the model include rainfall-runoff processes, urban water infrastructure, surface water systems, and ground-level flow, which can be depicted in zero, one, two, or three dimensions – 0D, 1D, 2D, 3D (RIONED, 2019).

One popular modelling approach is the traditional 1D sewer model conceptualization, which is employed by the open-source software Storm Water Management Model – SWMM (Rossman *et al*., 2016). This approach uses a lumped (0D) rainfall-runoff process, where land use percentages are assigned to sub-catchments delineated by drainage areas that lead to specific outlets. Each sub-catchment is modeled as a uniformly shaped area with consistent morphological and hydrological characteristics, such as mean slope, imperviousness, and infiltration properties. Rainfall is applied uniformly across each sub-catchment, and runoff volumes are calculated and routed to the outlets using either conceptual or physically-based methods (Pina *et al*., 2016).

In this approach, sub-catchment outlets are modeled as nodes within an underground pipe network, where water flow is governed by 1D equations. Each pipe, acting as a link, possesses uniform hydraulic properties like shape and hydraulic roughness. Links may also be used to model flow regulators such as weirs and pumps. Nodes are typically associated with physical structures like manholes, but they can also represent storage units or act as outfalls (Rossman *et al*., 2016). When hydraulic loads exceed system capacities, node overflow is treated as a system loss or stored in virtual volumes. Therefore, traditional 1D sewer models alone fail to provide detailed surface flow and depth calculations, crucial for identifying nuisance locations and evaluating their severity (Barreiro *et al*., 2023; RIONED, 2019). The dual drainage concept addresses this by integrating above and below ground systems, using either 1D or 2D approach to model surface flows (Djordjević *et al*., 1999).

In 1D-1D dual drainage models, water that overflows from the sewer system onto the streets is modeled as flowing in a 1D network at ground level. Although this approach can give insights on the water nuisance locations, 1D surface flow models are only effective for urban flood risk assessments when water is confined within the street profiles (Mark *et al.*, 2004), and when the urban topography is relatively uniform, often implying a unidirectional flow (Barreiro *et al.*, 2023). When flood water overflows the street curbs and potentially changes direction, 2D surface flow modelling provides a more accurate representation of flood propagation (Leandro *et al.*, 2009).

Conversely, in 1D-2D dual drainage models, water from the 1D sewer network that spills onto the surface is modeled as flowing over a 2D mesh generated using topographical data. In this approach, rainfall can either be converted into runoff hydrographs at the sub-catchments' outlets, a method known as Semi-Distributed (SD); or directly applied to each 2D element of mesh to generate grid-point runoff, a method referred to as Fully-Distributed (FD). The differences in how SD and FD models link rainfall to overland and sewer flows are illustrated in Figure 1.

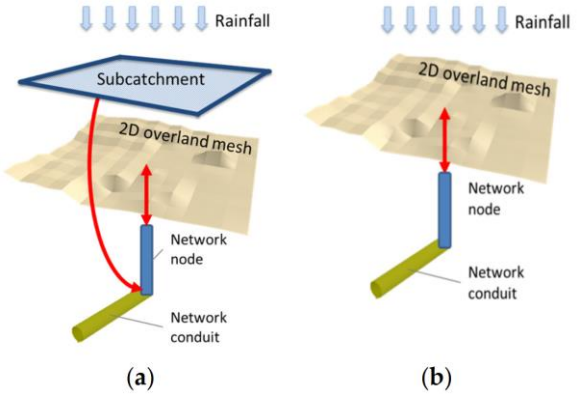

Figure 1 – Connections of rainfall-runoff with overland and sewer flow models: (a) traditional connections for SD models; (b) traditional connections for FD models (Pina *et al.*, 2016).

FD models simulate runoff flow across a 2D mesh before it enters the sewer system through inlets with limited hydraulic capacity. This allows FD models to realistically account for flooding conditions where runoff bypasses inlets or exceeds these capacities. However, the accuracy of these models hinges on detailed urban topography and comprehensive data on drainage connections, which is often incomplete or imprecise. This can lead to errors such as water erroneously pooling in non-existent depressions or missing inlet data. Research by Pina et al. (2016) indicates that FD models can overestimate surface runoff volumes, leading to underestimations of the sewer network's hydraulic conditions compared to actual measurements.

Furthermore, directly applying rainfall to the 2D surface significantly increases simulation times, as more mesh elements are involved in the numerical calculations. Given this drawbacks, Dutch sewerage guidelines recommend this approach only when necessary for accuracy, such as in areas with significant unpaved runoff or when (direct) runoff overflows street curbs. In flat, urban areas with dense inlet networks, coupled 1D-2D models with the SD approach are generally adequate for assessing flood risks during extreme weather (RIONED, 2019). Nevertheless, even within an SD framework, incorporating information about gully inlet influence the flow dynamics between the major and minor drainage layers. For instance, Chen *et al.* (2007) noted that if the inlets were taken into account in their SD model, flood water in local depressions next to buildings could be drained and returned to the sewer system.

2.2.2 General Modelling Aspects

2.2.2.1 Rainfall-Runoff simulation

The rainfall-runoff processes can be modeled in two ways: directly applying rainfall on the 2D surface elements (FD models), or indirectly via sub-catchments (SD models). As discussed in the previous section, SD models are typically preferred for their efficiency. In these models, sub-catchments are often conceptualized as non-linear reservoirs to estimate stormwater inflows. As illustrated in Figure 2, this reservoir collects the precipitation and from here the rainwater infiltrates and evaporates. Runoff occurs when the water level, denoted by depth d, surpasses a predefined threshold. This threshold, indicated by the depth d_s, represents initial losses such as surface ponding, surface wetting, and interception (Rossman *et al.*, 2016).

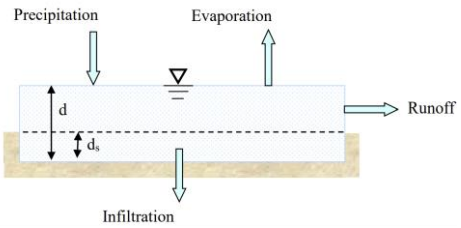

Figure 2 – Non-linear reservoir model of a sub-catchment (Rossman *et al.*, 2016).

In this schematization, the dynamics of this reservoir can be calculated using a simple mass balance equation that accounts for the change in depth per unit of time. This rate of change is expressed as the difference between inflow and outflow rates over the sub-catchment (Rossman *et al.*, 2016):

$$\frac{\partial d}{\partial t} = i - e - f - q \tag{1}$$

where i is the inflow flux represented by the rate of rainfall and snowmelt (mm/hr), e is the surface evaporation rate (mm/hr), f is the infiltration rate (mm/hr), and q is the runoff rate (mm/hr). Note: these fluxes are expressed as flow rates per unit area.

When modeling extreme precipitation events characterized by short, intense periods, evaporation is usually minimal and often omitted from simulations. For infiltration losses, Dutch sewerage guidelines (RIONED, 2019) suggest using either a fixed runoff coefficient or Horton's infiltration method. The fixed runoff coefficient applies a constant percentage of rainfall directly to runoff, ideal for impervious surfaces. In contrast, Horton's method, based on empirical data, indicates that infiltration rates decrease exponentially during rainfall events (Figure 3).

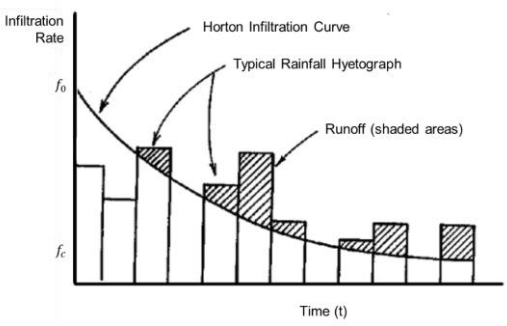

Figure 3 – The Horton infiltration curve (adapted from Rossman *et al.*, 2016).

Once the rainfall losses are computed, the SWMM5 Runoff Method is commonly used to simulate inflow hydrographs. This method simplifies the sub-catchments as uniform rectangular areas characterized by a uniform slope (S) and width (W) that drains to a single outlet channel, as shown in Figure 4.

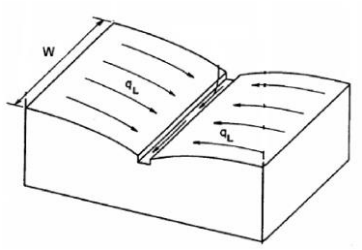

Figure 4 – Idealized representation of a sub-catchment (Rossman *et al.*, 2016).

Another simplification made by this method is the assumption that the drainage system reacts immediately to runoff, and therefore the travel time from the channel to the outlet is neglected. Under this assumption, with open channel flow across the sub-catchment at an effective depth of $d - d_s$, the Manning Equation can be applied to determine the volumetric runoff flow rate (Q) delivered to the underground drainage network (Rossman *et al.*, 2016):

$$Q = \frac{1.49}{n} W S^{1/2} (d - d_s)^{5/3} \quad (2)$$

Here, n represents the Manning's roughness coefficient, which indicates the hydraulic resistance encountered by runoff flow. The values of n for overland flow are less well-established than those for pipe flow due to the considerable variability in landscape features, the transitions between laminar and turbulent flow, and the minimal flow depths involved (Rossman *et al.*, 2016). Empirical estimates made by Engman (1986) of roughness values for overland flow shows roughness values between 0.01 and 0.013 for concrete and asphalt and 0.1 to 0.48 for grass.

The parameter W represents the width perpendicular to overland flow in an idealized rectangular sub-catchment. However, actual sub-catchments often lack of rectangular shape, symmetry, and uniformity, necessitating adjustments to estimate W for general cases. This estimation is crucial as width variations affect the hydrograph shape: a narrower width increases the time to equilibrium outflow, causing the sub-catchment to retain more water and release it more slowly. A practical method to estimate W is by calculating the average maximum length of overland flow and dividing the sub-catchment's area by this length (Rossman *et al*., 2016). Lastly, the sub-catchment slope (S) should reflect the average slope along the pathway of overland flow to inlet locations. A recommended approach for determining S involves delineating several overland flow paths, computing the slope of each, and calculating a weighted average (DiGiano *et al.*, 1977).

2.2.2.2 1D sewer flow simulation

Sewer flow modeling involves complex, non-uniform, and unsteady flow conditions driven by daily variations in wastewater discharge and changes in stormwater inflows following rainfall events. Thus, once water enters the drainage network, hydrodynamic models typically solves the complete form of the 1D Saint-Venant equations to simulate various possible flow regimes, such as backwater effects and pressurized flows. These equations employs the principles of continuity and momentum conservation through a set of partial differential equations (Yen, 1973):

$$\frac{\partial A}{\partial t} + \frac{\partial Q}{\partial x} = 0 \tag{3}$$

$$\frac{\partial Q}{\partial t} + \frac{\partial}{\partial x}\left(\frac{Q^2}{A}\right) + gA\left(\cos\theta \frac{\partial h}{\partial x} - S_0 + \frac{Q|Q|}{K^2}\right) = 0 \tag{4}$$

where Q is the discharge (m^3/s); A is the cross-sectional area (m^2); g is the accelerations due to gravity (m/s^2); θ is the angle of bed to horizontal (degrees); h is the depth (m); S_0 is the bed slope and K is the conveyance (m^3/s).

The conveyance function in sewers is typically modeled using either the Manning or Colebrook-White formulas. In the Netherlands, where sewers frequently operate under pressurized conditions, the Colebrook-White formula is favored for estimating friction losses, using Nikuradse's roughness values (Nikuradse, 1933). Initially, new concrete sewer pipes have roughness values ranging from 0.06 to 1.5 mm, and PVC pipes from 0.03 to 0.06 mm. Due to factors like corrosion and biological growth, these values can increase significantly over time, with recommended roughness values up to 6.0 mm for concrete and 1.5 mm for PVC (Butler and Davies, 2018). Further, research by Stanić *et al*. (2017) using laser scanning reveals that roughness in deteriorated Dutch sewers can escalate up to 12 mm.

2.2.2.3 2D overland flow simulation

The shallow water equations (SWE), which provide a depth-averaged version of the Navier-Stokes equations, are often used for the mathematical representation of 2D surface flow. These equations are based on the on the assumption that the flow is primarily horizontal, allowing the vertical velocity variations to be neglected. To solve the SWE, numerical methods like the finite volume are utilized, which rely on discretizing the equations into a conservative form to preserve mass and momentum across the computational domain. The conservative formulation of the SWE can be described as (Wei *et al.*, 2022):

$$\frac{\partial h}{\partial t} + \frac{\partial (hu)}{\partial x} + \frac{\partial (hv)}{\partial y} = q_{1D} \tag{5}$$

$$\frac{\partial (hu)}{\partial t} + \frac{\partial}{\partial x}\left(hu^2 + \frac{gh^2}{2}\right) + \frac{\partial (huv)}{\partial y} = S_{0,x} - S_{f,x} + q_{1D}u_{1D} \tag{6}$$

$$\frac{\partial (hv)}{\partial t} + \frac{\partial}{\partial x}\left(hv^2 + \frac{gh^2}{2}\right) + \frac{\partial (huv)}{\partial y} = S_{0,y} - S_{f,y} + q_{1D}v_{1D} \tag{7}$$

where h is the water depth; u is the velocity component in the x-direction; v is the velocity component in the y-direction; $S_{0,x}$ is the bottom slope component in the x-direction; $S_{0,y}$ is the bottom slope component in the y-direction; $S_{f,x}$ is the friction component in the x-direction; $S_{f,y}$ is the friction component in the y-direction; q_{1D} is the outflow rate per unit area; u_{1D} is the velocity component of q_{1D} in the x-direction; v_{1D} is the velocity component of q_{1D} in the y-direction.

2.2.3 Composite Design Storms

Hydraulic simulations for urban drainage in the Netherlands have historically used pre-defined storms (Bui01 to Bui10) from sewerage guidelines, based on De Bilt data (1955-1979). However, these standardized events do not accurately represent current rainfall patterns or the actual return periods for every rainfall duration. Additionally, not all sewer systems reach full capacity at the peak intensity, as the response to precipitation can vary significantly. Consequently, estimating the return period of water on the streets using these storms can be inaccurate, as the recurrence period of the rainfall may not align with the system's actual response (RIONED, 2019).

To address these challenges, many recent municipal sewerage plans across the Netherlands now refer to most recent developed composite storms to assess hydraulic functioning. These storms, based on the Chicago method developed by Keifer and Chu (1957) and the Flemish composite storms detailed by Vaes and Berlamont (1996), feature a symmetrical structure with rainfall intensities increasing towards a central peak. This peak corresponds to the intensity specified by the intensity-duration-frequency (IDF) curve for the chosen return period and duration of 10 minutes. One key advantage is that all the durations for a specific return period are incorporated in a single storm. Therefore, composite storms provide indicative precipitation load for both short and long rainfall durations (RIONED, 2019).

Precipitation data collected until 2014, as reported by STOWA (Beersma *et al.*, 2019), led to the creation of 13 composite storms covering return periods from 0.5 to 1000 years. New storms for 2030, 2050, and 2085 account for projected increases in rainfall due to climate change, based on KNMI's four climate scenarios (Klein *et al.*, 2014). Under the most severe projection (referred to as WH), maximum hourly rainfall could rise by 25% by 2050, halving return periods (e.g., a 73 mm/hour peak, currently a 2-year event, may occur annually by 2050). Figure 5 shows composite storms for 2014 and future years considering the most severe climate projection.

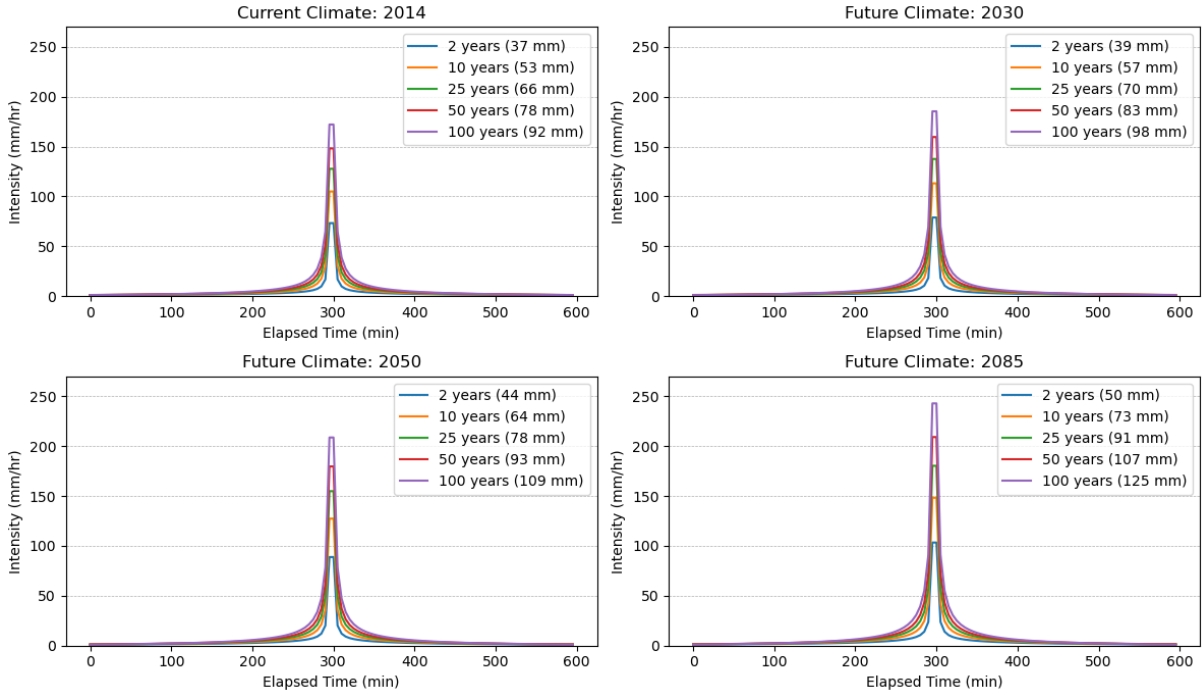

Figure 5 – Composite storms for various return periods under current and future climate conditions. Data source: RIONED (2019).

2.2.4 Uncertainties in Urban Drainage Modelling

Uncertainties are intrinsic to any modelling activity. Modelling itself involves creating a representation based on assumptions about how a system functions or behaves. Given system observations, the mathematical model can be adjusted so it achieves a quantifiable degree of representativity. Then, this mathematical representation can be used to infer further knowledge, predict future system state or test the effect of hypothetical scenarios (Moreno Rodenas, 2019).

Recent research has increasingly focused on model calibration, i.e., reducing the uncertainty contribution related to model parameters based on mostly relatively few measurements. However, uncertainties in urban drainage models stem from multiple sources, not just parameters. Although developing error models and calibrating parameters might enhance model performance in the short term and for specific applications, this approach can obscure the true underlying source of errors that affect the model's accuracy (Pedersen *et al.*, 2022a).

Pedersen *et al.* (2022b) combined the content of Walker *et al.* (2003) and Gupta *et al.* (2012) into a unified framework explaining the locations of uncertainties present in the semi-distributed integrated urban drainage models, illustrated in Figure 6.

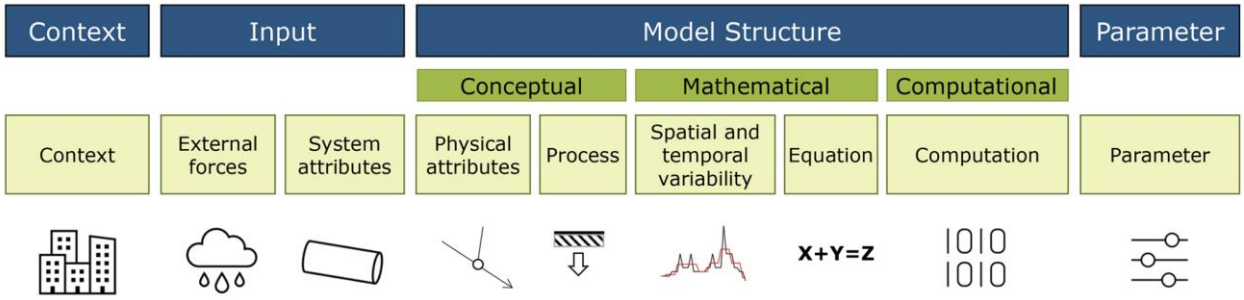

Figure 6 – Classification of the location of uncertainties in models, based on Walker *et al.* (2003) and Gupta *et al.* (2012). Graphically adapted by Pedersen *et al.* (2022b).

Related to input uncertainties, Korving and Clemens (2005) explored how database errors in system attributes, like incorrect invert levels, storage and pumping capacities, and weir heights, affect sewer emission modelling. Rainfall input is also a major source of error, thus the choice of precipitation dataset plays a crucial role in model calibration (Tscheikner-Gratl *et al.*, 2017). Model structure uncertainties arise from oversimplifications of physical processes, omission of key attributes, or inadequate representation of spatial and temporal dynamics. Errors can also result from human mistakes in model development (e.g., equation derivation or coding), poorly defined numerical methods, and boundary conditions, which may cause numerical dispersion or instabilities (Deletic *et al.*, 2012).

Given the challenges in identifying uncertainties in urban drainage models, Pedersen *et al.* (2022a, 2022b) recommend a structured error diagnostics framework over relying heavily on calibration with limited data. When routinely comparing model results with sewer measurements from an increasing number of locations, uncertainties previously not realized become visible. Employing hydrological signatures (e.g., peak levels, durations, and areas under the curve) during these diagnostics helps to reveal the true underlying errors and provides deeper insights into the processes driving the observed phenomena.

2.2.5 InfoWorks ICM Modelling Software

InfoWorks ICM, developed by Innovyze, is an advanced software designed for fully integrated catchment modeling. The term "integrated" refers to the creation of a 1D-2D coupled model, where 1D modeling can simulate flows within pipes and channels, and 2D captures the spread of water on surface landscapes. Therefore, the software provides the ability to model the natural and engineered above and below ground drainage system within a single simulation engine (Innovyze, 2023a).

In 1D hydraulic modeling, InfoWorks ICM employs the Preissmann 4-point scheme to approximate the full Saint-Venant equation and incorporates a narrow slot above the pipe to maintain a conceptual free surface during pressurized flows (Innovyze, 2022b). For surface flow, the 2D engine employs a finite volume semi-implicit scheme to solve the SWE, requiring iterative stability adjustments each simulation period. Stability is maintained by calculating the minimum timestep for each 2D mesh element using the Courant-Friedrichs-Lewy (CFL) condition (Innovyze, 2023c). The 2D mesh, generated using Shewchuk Triangle functionality, interpolates elevation data to accurately depict urban topography (Innovyze, 2023d).

The interaction between the 1D network and 2D surface layers in InfoWorks ICM typically takes place at designated 2D nodes. Water transfer between these nodes and the adjacent mesh element is governed by the node's flood type designation. For nodes labeled as '2D', water transfer is calculated using weir equations, assuming the crest is at ground level and the length is equivalent to the node's perimeter, with a discharge coefficient specified by the user (Innovyze, 2023e). For 'Gully 2D' nodes, the exchange is modeled through head-discharge tables that handle two main scenarios: limit inflow, where water moves from the 2D surface to the node, and limit outflow, where water exits the node to flood the surface (see Figure 7).

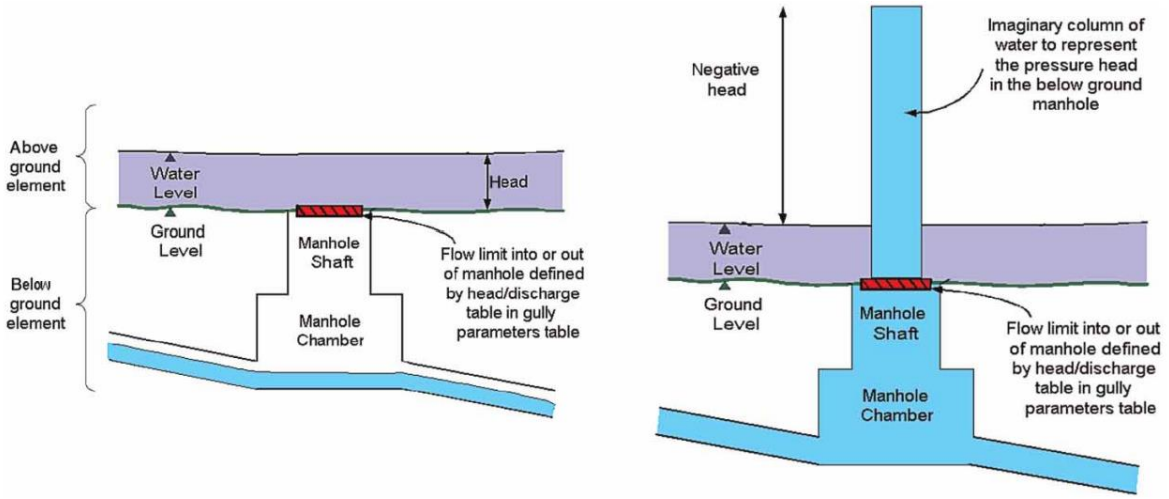

Figure 7 – Modelling of flow interchanges between the surface and 2D nodes: limit inflow, on the left, and limit outflow, on the right (Innovyze, 2012).

InfoWorks ICM also supports these interactions with other modelling objects beyond 2D nodes. For instance, users can define infiltration zones to represent physical areas within the 2D mesh where infiltration characteristics, defined through infiltration surfaces, are applied (Innovyze, 2023f). Permeable zones intersecting one or more infiltration zones can be then defined to link the infiltrated volume from the 2D surface to a specific object (e.g., node and conduits) of the 1D network (Innovyze, 2023g).

3 Methodology

3.1 Overview

The methodology of this thesis begins with selecting a representative case study area in Rotterdam. After describing the urban catchment and drainage network, three models were tested to identify the most efficient and reliable. These models were calibrated, validated, and compared against each other in terms of data requirements, level of detail of flood predictions, and runtimes. Using results from the best-performing model, an economic flood risk assessment was conducted considering the existing infrastructure and climate change impacts. Subsequently, structural solutions aimed at reducing flood risks under current and future climate conditions were proposed, and their economic feasibility was evaluated through cost-benefit analysis. This workflow is presented in Figure 8.

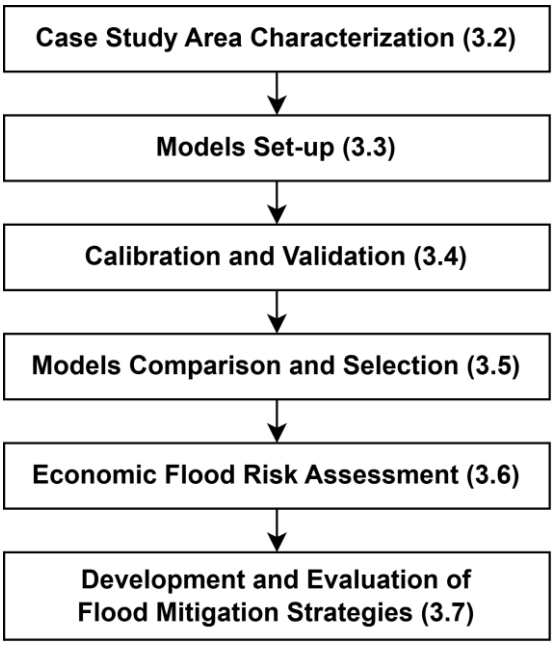

Figure 8 – The schematic diagram of the methodology used in this thesis

3.2 Case Study Area Characterization

3.2.1 Description

Spangen is a densely urbanized 50-hectare neighbourhood in Rotterdam's Delfland hydraulic area (Figure 2), home to over 10,000 residents. Characterized by minimal open water and a high proportion of paved surfaces, Spangen faces drainage challenges. These are further exacerbated by uneven settlement from soil subsidence that reduces in-sewer pipe storage and forms surface depressions. Moreover, growing incidence of intense rainfall linked to climate change increases the risk of flooding. Despite investments to make the area climate-proof, it remains uncertain whether these adaptations have sufficiently enhanced the drainage system's capacity to handle extreme weather events to acceptable levels. Therefore, Spangen was selected as a representative case study to assess the current system's performance and explore additional flood mitigation strategies.

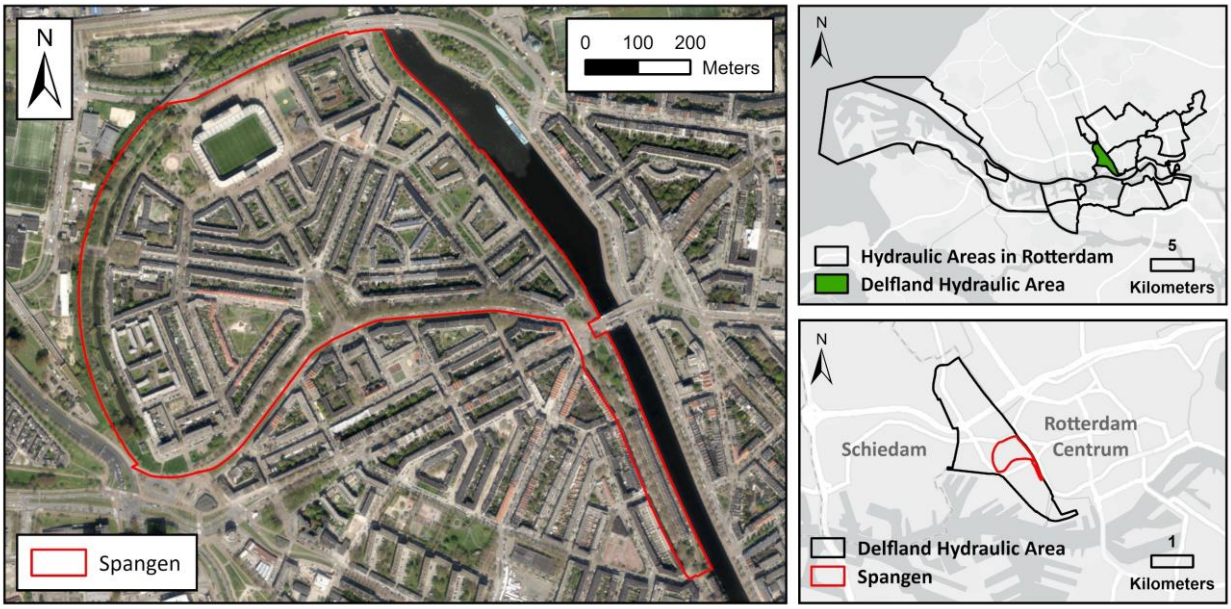

Figure 9 – Location of the case study area.

3.2.2 Land Use Cover and Runoff Surfaces

The land use cover of the study area was identified using the *Basisregistratie Grootschalige Topografie* – BGT (Kadaster, 2022), an open-source digital map of the Netherlands that records the locations of physical objects such as buildings, roads, water bodies, and railway lines. For hydrological modeling purposes, we consolidated the 44 land use categories found in the BGT dataset into 8 runoff surface types, as shown in Table 1, with their spatial distribution in Figure 10. Courtyards were excluded from these categories because they are often disconnected from the municipal sewer system, and they are situated at lower elevations due to soil subsidence (see Annex B), preventing runoff from entering public systems. Moreover, due to the lack of reliable data on private drainage connections all courtyards are considered as non-sewered areas. This practice is often adopted by the municipality of Rotterdam when simulating the performance of their urban water systems.

Table 1 – Classification and extent of surface types in Spangen's Sewer System.

Surface Type	Description	Total Area (ha)	Percentage
Paved Area (Open)	Open paving consisting of clinkers or tiles with sand joints.	17.82	43.6%
Paved Area (Close)	Closed paving consisting of asphalt.	1.27	3.1%
Flat Roof Connected	Flat roofs (<4% slope) connected to combined sewer pipes.	7.67	18.8%
Sloped Roof Connected	Flat roofs (< 4% slope) disconnected; runoff is discharged into surrounding areas.	2.59	6.3%
Flat Roof Disconnected	Sloped roofs (> 4% slope) connected to combined sewer pipes.	0.05	0.1%
Sloped Roof Disconnected	Sloped roofs (> 4% slope) disconnected; runoff is discharged into surrounding areas.	0.44	1.1%
Unpaved Areas	Natural surfaces with high infiltration rates.	10.31	25.2%
Open Water	Areas covered by water bodies.	0.69	1.7%
Total Sewered Area	Sum of all areas contributing to the municipal drainage system.	40.84	100.0%

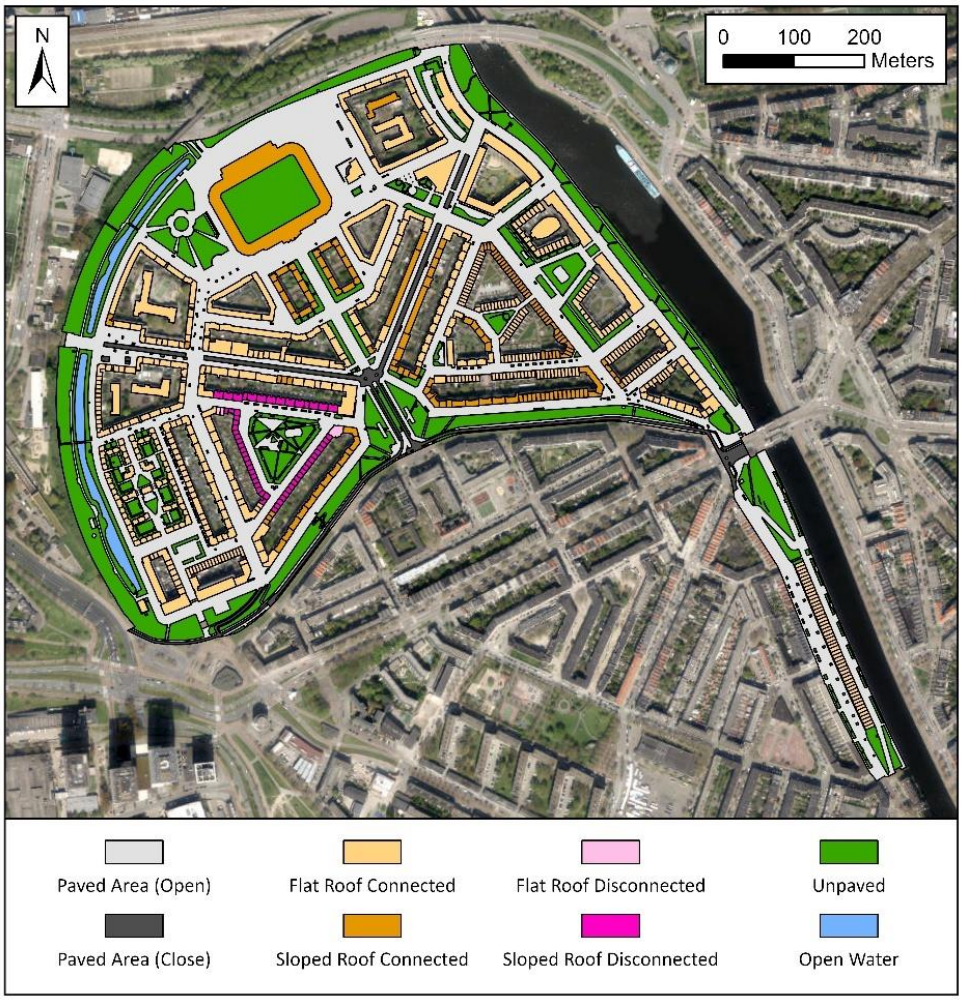

Figure 10 – Land use map of Spangen.

3.2.3 Topographical Characteristics

To ensure accurate flood modeling it is crucial to use a detailed representation of urban topography. In this research, a high-resolution DTM sourced from the 2023 *Actueel Hoogtebestand Nederland* (AHN) was used. This terrain model, produced using advanced airborne laser altimetry, has a resolution of 50 cm. This fine level of detail is essential for accurately characterizing the predominantly flat terrain and capturing subtle elevation changes (see, Figure 11). The elevation map derived from this data is presented in Figure 12, highlighting the topographical variations within the study area, especially the sloped areas in the south and east, which are surrounded by a dike.

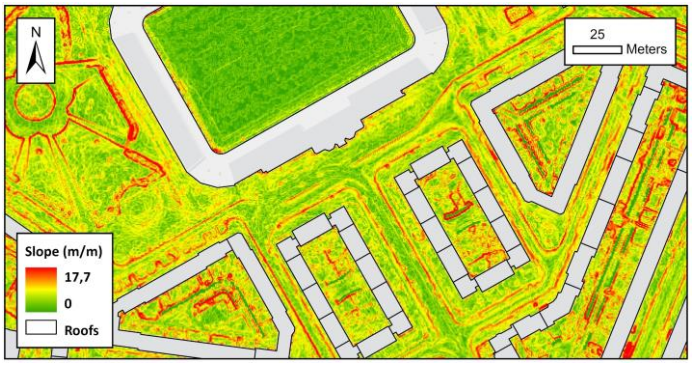

Figure 11 – Slope map highlighting elevated areas around street curbs.

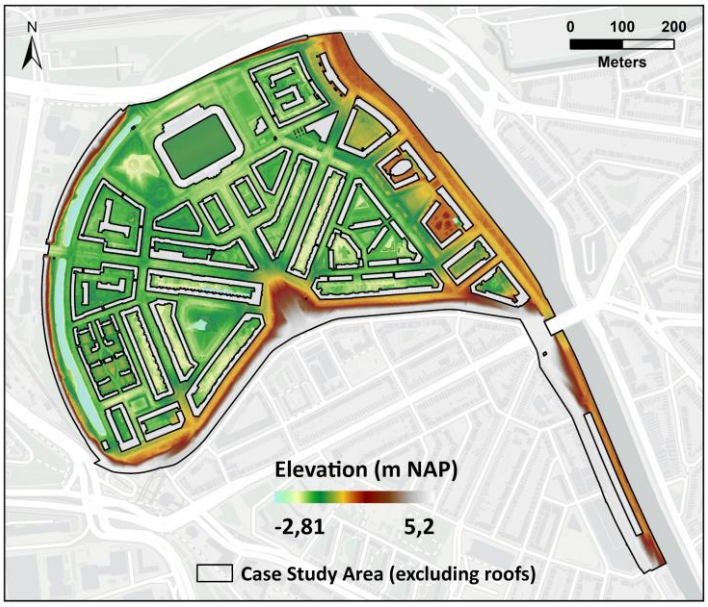

Figure 12 – Elevation map derived from high-resolution DTM.

3.2.4 Drainage Network Layout

The drainage system in Spangen is mostly combined with some areas disconnected to enhance its resilience. This was done by implementing three stormwater systems that increased the storage capacity by around 67%. First, Bellamyplein water square, constructed in 2012 in a low-lying western region, consists of a 91 m³ above-ground concrete tank, and 628 m³ of below-ground infiltration crates. The Urban Water Buffer (UWB), established in 2018, collects and stores runoff from Sparta Rotterdam's stadium and nearby paved areas, later pumping it into an aquifer for non-potable reuse. More recently, the Municipality of Rotterdam and Woonstad housing

corporation redeveloped Staringplein, incorporating a green square with a 105 m³ underground infiltration crate system and an additional 20 m³ crate near Multatulistraat.

During heavy rainfall, when drainage capacities are exceeded, discharges from the combined system and UWB enter the Spaansebocht canal. Besides degrading water quality, these spills raise the canal levels, which increases upstream flooding risk as overflow weirs submerge. To manage this, a primary pumping station with a capacity of 500 m³/hr controls water levels by directing excess flow to *Merwedehaven*. Additionally, a smaller 120 m³/hr station can also support the main pump during extreme weather conditions.

Figure 13 shows the current network layout of the study area and Table 2 provides essential information about the various systems in the area. More information about these systems can be found in Annex A.

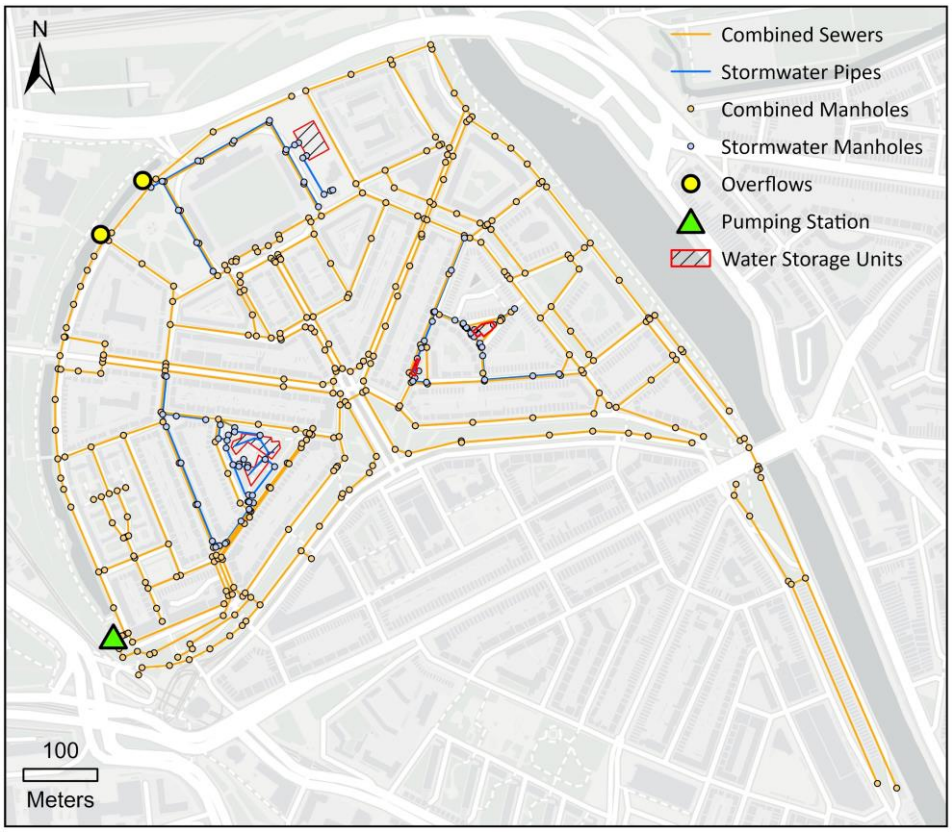

Figure 13 – Drainage network layout.

Table 2 – Total conduit length and storage volumes for combined and stormwater systems.

System	Conduits Length (km)	Conduit Storage (m³)	Manhole Storage (m³)	Storage Units Volume (m³)	Total Storage Volume (m³)
Combined	14.1	3445	715	0	4174
Bellamyplein	0.8	60	41	819	920
Urban Water Buffer	0.6	51	22	1400	1473
Staringplein	0.5	35	20	135	190
Total	**16.0**	**3591**	**798**	**2354**	**6757**

3.3 Models Set-Up

Conventional 1D sewer models struggle to accurately simulate surface flows during extreme precipitation, failing to identify potential nuisance locations or assess the severity of these nuisances (RIONED, 2019). To address this, the Spangen 1D sewer model was enhanced by integrating it with a 2D surface model derived from the district's DTM. Considering the extensive paved surfaces and numerous gully inlets in Spangen, pluvial flooding predominantly results from the overloading of the underground network rather than direct surface runoff. Thus, a simpler 0D conceptualization was adopted to model runoff processes, which discretizes the study area into sub-catchments and routes runoff directly to the 1D network. Additionally, the Spaansebocht canal is modeled using a 0D approach with storage units to simulate water level dynamics, suitable due to the minimal bed slope and uniform water levels along the canal. The model schematization adopted is presented in Figure 14.

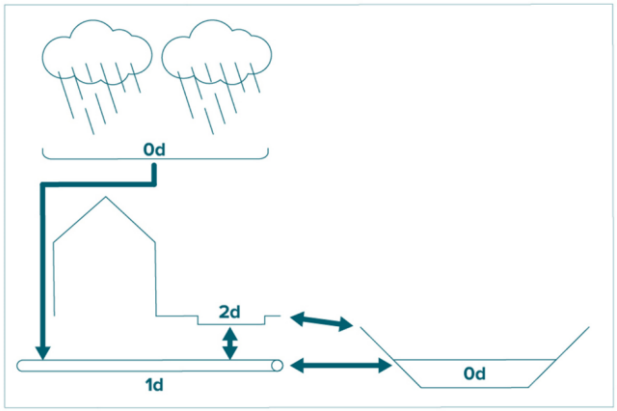

Figure 14 – Graphical representation of the conceptualization adopted. Source: RIONED (2019).

This model concept was implemented using InfoWorks ICM version 2024.5.1, which allows for different methods to represent the interaction between the 1D sewer network and the 2D surface model. To compare different methodologies, we developed three distinct modelling approaches:

- Model without Gullies: only manholes are represented as 2D nodes;
- Model with Gullies: gully inlets are modelled as 2D nodes and water exchange between the two drainage layers can occur from both manholes and gullies;
- Model with Permeable Zones: similar to the model without gullies; however it include a constant infiltration rate at the surface, and infiltrated volumes are re-directed to specific manholes via permeable zone to simulate gully flow in a simplified manner.

The upcoming sections will first outline the general aspects common to all three modelling approaches. Subsequently, it is provided details of the unique features specific to each approach.

3.3.1 General Aspects

3.3.1.1 Initial and Boundary Conditions

For numerical stability purposes, we assume as initial condition that nodes and conduits have a base flow depth equal to 5% of the conduit's height, which is also a default setting in the InfoWorks ICM. Storage units are initially considered empty, except for those representing the canal, where water levels are set to match observed conditions during periods without rain, as determined from monitoring data. Water pumped from the canal out of the study area is

considered lost, thus the node downstream of the surface pumping system is modelled as an outfall.

The external inflow received by the nodes and conduits comprises dry weather flow and stormwater inflows. Groundwater infiltration has been excluded from this analysis due to the complexities in estimating its signal response, which can vary from days to months (Wright *et al.*, 2001). Dry weather flow (DWF) is calculated based on a daily wastewater discharge of 120 liters per capita. The number of inhabitants is estimated based on available data from Evides, water supply company in Rotterdam area. The daily variation of the wastewater discharge (Figure 15) adheres to usage patterns suggested by Dutch sewerage guidelines (RIONED, 2019).

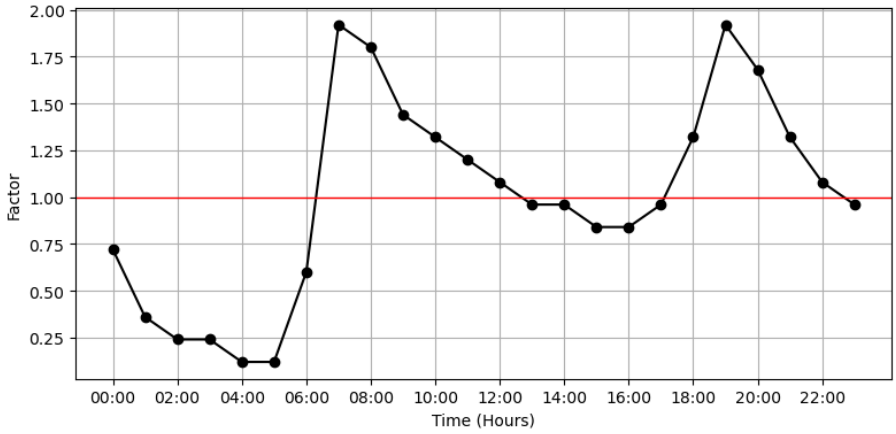

Figure 15 – Daily pattern of the dry weather flow for the study area. Data source: RIONED (2019).

In order to estimate the stormwater inflows, this research uses the SWMM runoff block within InfoWorks ICM (Innovyze, 2023h), adopting a lumped approach with the non-linear reservoir method for rainfall-runoff modeling (Rossman *et al*., 2016). The study area was divided into sub-catchments, each characterized by unique runoff surfaces percentages, as identified on the land use map. Delineation of these sub-catchments at ground level vary with the modeling approach and will be further elaborated in subsequent sections. Nevertheless, for sub-catchments that model runoff from roofs, all approaches use the original delineation provided in the dataset from the BGT data (Kadaster, 2022). Hydrological parameters for the runoff surfaces were determined using Dutch sewerage guidelines (RIONED, 2019) and are summarized in Table 3.

Table 3 – Hydrological parameter values estimated for the runoff surfaces based on Dutch sewerage guidelines (RIONED, 2019).

Runoff Surface Type	Runoff Volume Model	Fixed Runoff Coefficient	Initial Infiltration (mm/hr)	Limiting Infiltration (mm/hr)	Decay Factor (h^{-1})	Initial Loss (mm)
Flat Roofs	Fixed	1	-	-	-	2
Sloped Roofs	Fixed	1	-	-	-	0
Paved (Close)	Fixed	1	-	-	-	0.5
Paved (Open)	Horton	-	2	0.5	3	0.5
Unpaved	Horton	-	60	10	7	10

After calculating runoff volumes, inflow hydrographs are estimated using the SWMM5 Runoff Method, which routes flows directly to specific nodes, conduits, or adjacent sub-catchments. Thus, flooding is modeled to occur only when the system's capacity is exceeded, rather than from limited hydraulic capacity of inlets or direct runoff accumulating on the surface. The width and slope of sub-catchments at ground level vary by modeling approach. For sub-catchments that model roof runoff, width is calculated as the square root of the roof area and slopes are set at 2% for flat roofs and 45% for sloped roofs. Manning's roughness coefficients, based on Dutch sewerage guidelines (RIONED, 2019) and Engman (1986), are 0.011 for closed paved areas and roofs, 0.013 for open paved areas, and 0.2 for unpaved areas.

3.3.1.2 1D sewer flow modelling

The 1D sewer flow was modeled using the full Saint-Venant equations and the Preissmann 4-point scheme in InfoWorks ICM, with conveyance calculated via the Colebrook-White expression. Although this method requires a smaller timestep, it was selected for its ability to simulate various flow regimes and pressurized flow conditions. Furthermore, the looped configuration of the network requires the simultaneous modelling of water levels at nodes and flows in conduits, a task facilitated by these methods. Additionally, to address the absence of equations that adequately represent the transition from free surface to pressurized flow, pipes include a Preissmann slot, ensuring a conceptual free surface remains during surcharge conditions (Innovyze, 2022b).

The network in Spangen was modeled using design invert levels, despite the non-uniform settling caused by the low bearing capacity of the soil in Rotterdam. This decision was made because the information on current sewer invert levels is limited and of questionable quality. Sewer pipes are modeled as links, with their lengths and dimensions based on as-built drawings and GIS data. Initial roughness values were set at 3 mm for combined sewer pipes (concrete or steel), following van Bijnen *et al.* (2012) and Dutch guidelines (RIONED, 2004). For stormwater pipes, a roughness of 0.1 mm was used, which is the minimum value recommended by InfoWorks ICM and the lower bound value suggested for older PVC pipes by Butler and Davies (2018).

Nodes in the model correspond to physical structures like manholes and storage units. Manholes have a chamber and shaft area of 0.5 m², in line with Rotterdam's modeling practices, and the chamber floor level set at the lowest pipe invert. Ground and flood levels are based on the DTM. Water buffer structures, such as infiltration crates, are modeled as storage units with fixed plan areas from GIS data and depth-area curves from as-built drawings. A dummy slot is used to reduce inflow when capacity is exceeded, approach suggested by Meng (2022). The Bellamyplein retention tank is modeled differently, with stormwater pipes connected to a 2D outfall discharging onto the 2D surface, using DTM elevation data to represent the tank's storage.

The weirs in the system vary in type and shape, but for modeling purposes, based on expert judgment from the municipality, all are assumed to be rectangular sharp-crested. Crest levels and widths are derived from as-built drawings, with a discharge coefficient of 0.4, the lower recommended value from Bagheri *et al.* (2014). Discharge through these weirs is modeled using the Kindsvater and Carter formula (1957) within InfoWorks ICM. Pumps are modeled as links, with operations controlled by switch-on and switch-off levels based on upstream water levels and defined according to current operational time series.

3.3.1.3 2D surface flow modelling

Overland flow on 2D surfaces is modeled using the InfoWorks ICM, i.e. using the Shallow Water Equations (SWE) within a finite volume semi-implicit scheme (Godunov, 1959) and the Riemann solver (Alcrudo & Mulet-Martí, 2015). The 2D surface is represented by an unstructured triangular grid created using Shewchuk's Triangle meshing algorithm (Shewchuk, 1996). To prevent inaccurate water flow simulation, buildings and enclosed courtyards are treated as voids due to the absence of data on potential water ingress points like doors and windows.

The mesh resolution is selected to balance detail level and computational efficiency. The minimum element area is set at 0.5 m², and the maximum triangle area at 2 m². Surface roughness is varied based on land use, with Manning's coefficients set at 0.011 for closed paved areas and roofs, 0.013 for open paved areas, and 0.2 for unpaved areas. Figure 16 shows a detailed view of the 2D grid overlaid on the land use map.

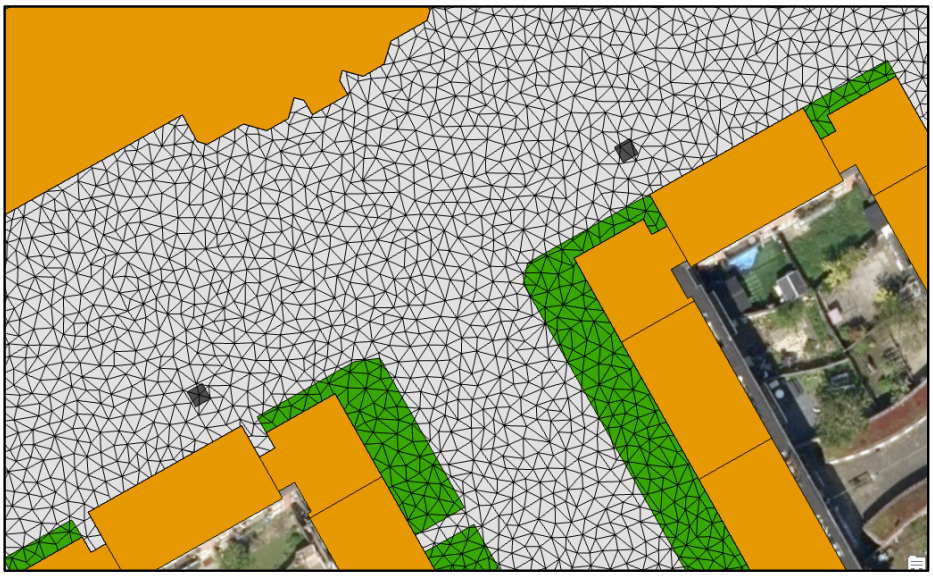

Figure 16 – Example of the 2D grid overlayed the land use map.

3.3.1.4 Interaction between 1D network and 2D surface

As mentioned before, the main distinction among the methodologies evaluated in this thesis lies in their approach to model the interaction between the 1D network and the 2D surface. However, all approaches share a common feature: manholes are represented as 2D nodes, allowing water to exit from these nodes to the surface when the system is surcharged and re-enter the network when capacity becomes available. Water exchange between the 2D manholes and the surface is estimated using the weir equation, with the crest level at ground level and the weir width equal to the manhole circumference. A discharge coefficient of 0.5 is used, based on previous studies investigating surface-sewer flow interaction (Russo *et al.*, 2015; Djordjević *et al.*, 2013).

3.3.2 Model without Gullies

In the model without gullies, 293 manholes were selected as outlets for sub-catchment delineation. Since manholes do not represent actual surface flow endpoints, a distance-based method, not reliant on the DTM, was used for sub-catchment delineation. Sub-catchments were delineated using least-cost allocation tools in ArcGIS Pro 3.3.0, based on a cost-surface raster. On this raster, high values were assigned to cells representing flow obstructions, like buildings,

while open areas had a cost of one unit. The least-cost path for runoff to reach the nearest manhole was then calculated (see Figure 17), following similar procedure used by Jain *et al.* (2016). Since actual flow paths weren't generated, sub-catchment width was estimated as the square root of the area, and slope was set at 2.5% per RIONED (2022) street slope guidelines.

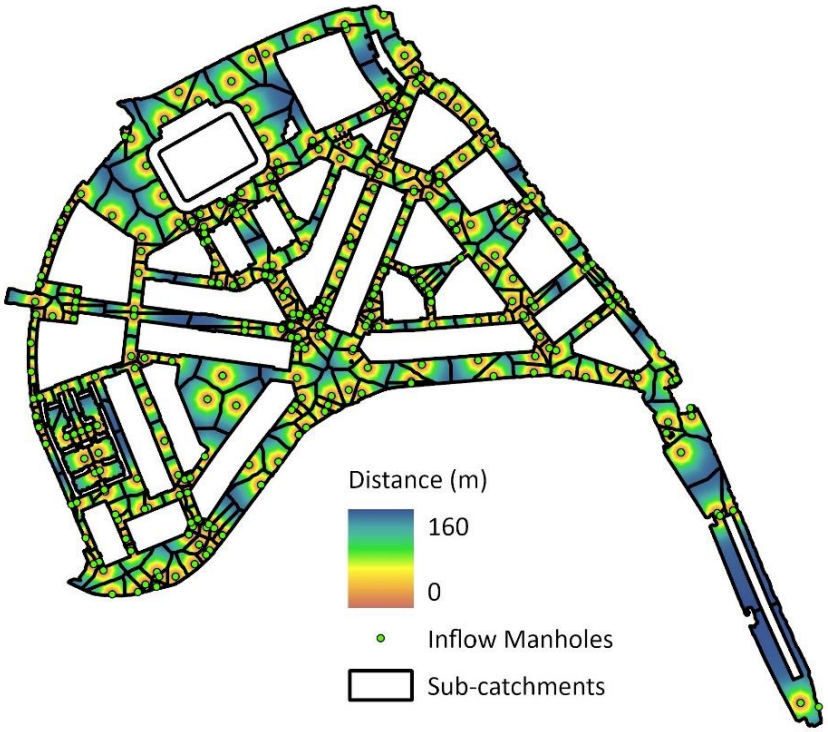

Figure 17 – Sub-catchment delineation using distance-based method in the model without gullies.

3.3.3 Model with Gullies

In the model with gullies, a total of 1,447 inlet locations were identified during on-site field visits. These locations were then adjusted to the center of the lowest elevation cell on the DTM within a 2-meter buffer. This adjustment ensures that the inlets are optimally placed at the lowest points of depressions where water accumulation is greatest within their respective area of influence, as illustrated in Figure 29.

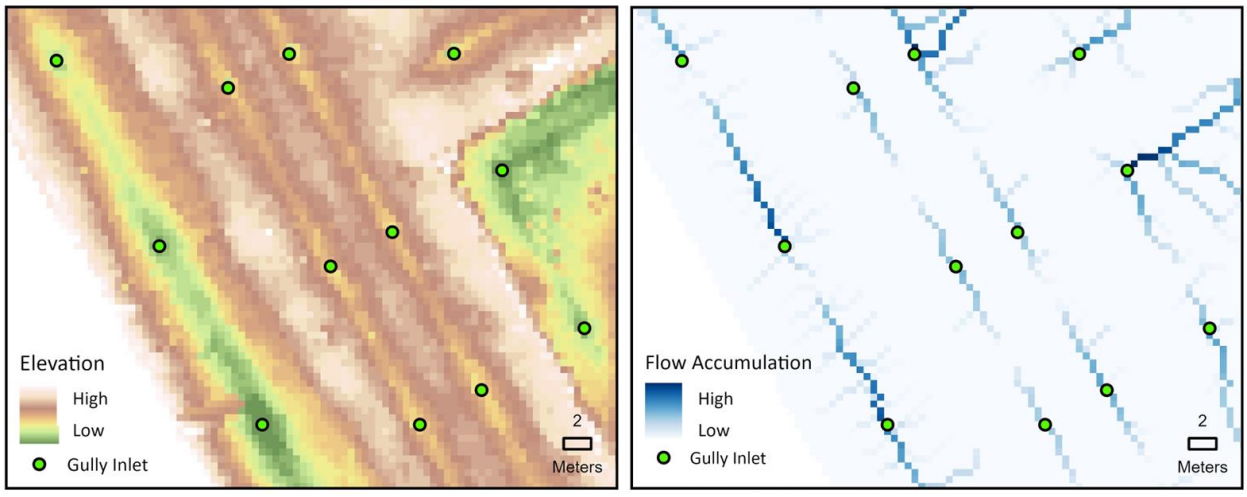

Figure 18 – Placement of gully inlets at depressions where flow accumulation is highest.

The optimal placement of gully inlets facilitated the delineation of sub-catchments across the terrain using GIS tools through the following steps:

- Pre-processing the DTM: buildings are removed, and elevation values at building boundaries are raised to better represent actual surface flow conditions.
- Generating flow direction raster: using the Derive Continuous Flow tool (ESRI, 2024a) in ArcGIS Pro 3.3.0, a flow direction raster is created, with gully inlets designated as known depressions to guide continuous flow paths toward them.
- Sub-catchment delineation: With gully inlets as outlets, the flow direction raster is input into the Watershed tool (ESRI, 2024b) in ArcGIS Pro 3.3.0 to delineate sub-catchments.

A total of 1,447 sub-catchments were delineated across the terrain. Figure 19 provides a detailed view, focusing on the southern part of the study area characterized by high slopes due to a dike.

Figure 19 – Detail of the flow paths and sub-catchments delineated in the model with gullies.

After mapping the primary flow paths, the width of each sub-catchment is estimated by calculating the average length of these paths and then dividing the total area of the sub-catchment by this average length, following the method outlined by Rossman *et al.* (2016). To determine the slope of each flow path, the elevation difference between the farthest drainage point and the nearest gully inlet is divided by the length of the path. The overall slope of the sub-catchment is then calculated as the average of these individual slopes, according to the approach described by DiGiano *et al.* (1977). Figure 20 shows the calculated widths and slopes for the sub-catchments.

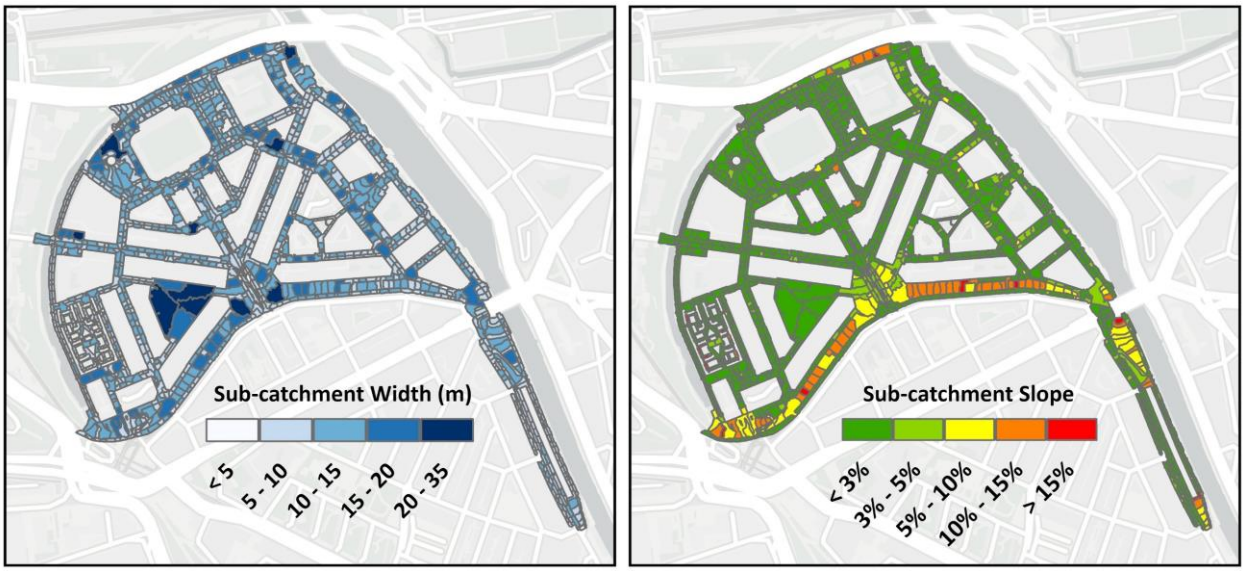

Figure 20 – Sub-catchment width and slope in the model with gullies.

In InfoWorks ICM, gully inlets are classified as 'Gully 2D', allowing surface flow to be intercepted based on head-discharge tables. Despite potential variations in gully geometry or clogging, the head-discharge curve from Figure 24 recommended by Ally (2011) and applied by Hoogmoet (2019) in Dutch drainage studies.

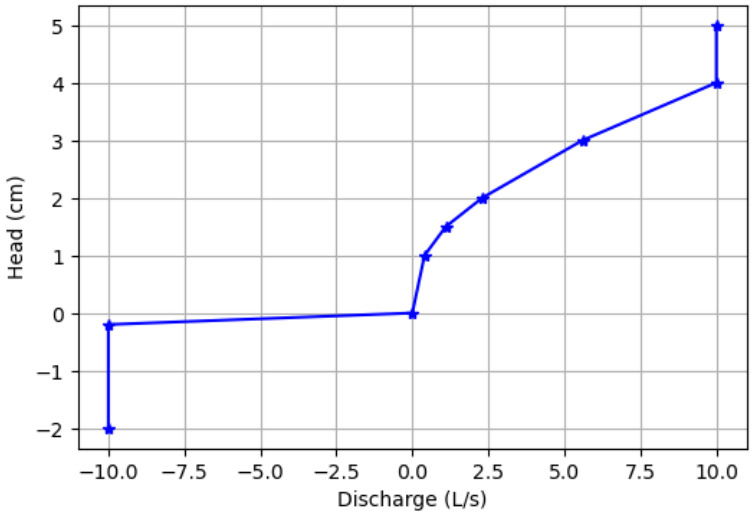

Figure 21 – Head-discharge curve adopted for gully inlets.

Gully inlets were connected nearest manhole using synthetic pipes following the inlet-manhole approach by Jang *et al.* (2018). These synthetic pipes were specified with a 150 mm diameter, a minimum slope of 1%, and installed at least 70 cm below the connected manhole, adhering to Dutch sewerage guidelines (RIONED, 2022). Assuming PVC pipes, the initial roughness value for synthetic pipes was set at 0.1 mm.

3.3.4 Model with Permeable Zones

This model simulates gully flow by enhancing the model without gullies with two additional elements on the 2D mesh: infiltration and permeable zones. It includes a single infiltration zone that spans the entire mesh, maintaining a constant infiltration rate that is calibrated based on the simulation outcomes from the model with gullies (detailed in section 3.4.5). Infiltrated water is calculated at each timestep and routed to the 1D network via 293 permeable zones that correspond to the sub-catchments of the previous model. Each zone directs the flow to the corresponding sub-catchment outlet. Figure 22 illustrates the schematic representation of this approach.

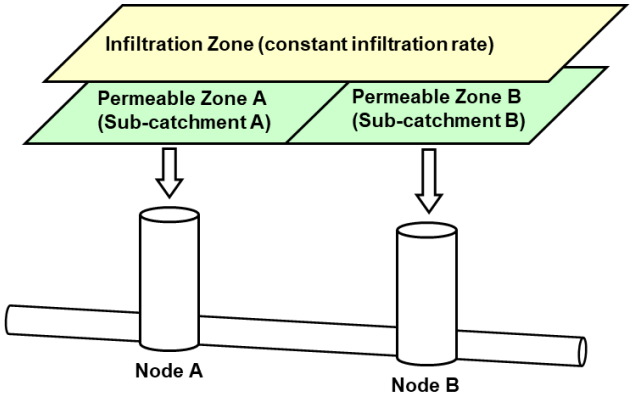

Figure 22 – Schematic representation of infiltration and permeable zones to simulate gully flow.

3.4 Model Calibration and Validation

3.4.1 Observed Data

The Municipality of Rotterdam provided data for six distinct rainfall events during which water levels were continuously monitored (every minute) at upstream manholes of two key locations, CSO weir and pumping station. Four of these events were selected for calibration, while the remaining two were used for validation. Due to the significant spatial variability of rainfall in the Netherlands (van Leth *et al.*, 2021), local rain gauge data would have been ideal for simulating these events. However, complete rainfall records were only available from KNMI meteorological station 344, located at Rotterdam Airport, approximately 4.8 km from Spangen.

As Spangen is a small urban catchment, the hourly rainfall data provided by KNMI was insufficient to capture the fast response of the drainage system, a challenge frequently encountered in urban drainage modeling (Aronica *et al.*, 2005). To address this, the data was interpolated to a minute-level resolution. Table 4 presents the main characteristics of the rescaled rainfall events used for calibration and validation. These events are representative of typical conditions in the area. Ideally, urban flood models should be calibrated using both sewer system data and flood records from heavy rainfall events; however, this study faced limitations due to the absence of extreme weather data for Spangen.

Annex C contains hyetographs and the associated water level measurements at the CSO weir and pumping station, along with the 1,000-minute initialization period adopted in the simulations to depict the system's state prior to rainfall peaks.

Table 4 – Characteristics of rainfall events selected for calibration and validation of the models.

Event	Start Date	Cumulative Rainfall (mm)	Max Intensity (mm/hr)	Total Duration (h)	Event Used For
1	02/11/2023	39.5	8.7	42	Calibration
2	16/06/2020	43.1	16	27	Calibration
3	31/07/2021	22.3	14.8	10	Calibration
4	25/11/2021	25.6	5	37.5	Calibration
5	19/06/2021	34.4	14.9	11.5	Validation
6	27/07/2020	31.7	12.7	21.3	Validation

3.4.2 Assessment Criteria

The quality of the model's predictions against observed data was assessed using the Nash-Sutcliffe Efficiency (NSE), widely recognized as a key index for measuring simulation accuracy in hydrological models (Pushpalatha *et al.*, 2012). Mathematically, it is defined as:

$$NSE = 1 - \frac{\sum_{i=1}^{n}\left(Q_{obs,i} - Q_{sim,i}\right)^2}{\sum_{i=1}^{n}\left(Q_{obs,i} - \overline{Q}_{obs}\right)^2} \quad (8)$$

where n is the total number of time-steps; $Q_{sim,i}$ represents the simulated variable at timestep i; $Q_{obs,i}$ represents the observed variable at timestep i; and $\overline{Q}_{obs}$ is the average value of the observed variable. When the NSE equals 1, it indicates a perfect match between the observed and simulated flows. An NSE value between 0 and 1 suggests that the simulated flow is generally acceptable. If the NSE is greater than 0.5, the model's simulation results are considered satisfactory (Moriasi *et al.*, 2007).

3.4.3 Parameter Selection

The rainfall events used for calibration and validation corresponded to typical rainfall patterns where flooding is unlikely. Thus, it was not possible to calibrate the parameters of the 2D surface model. Instead, the focus was on adjusting seven parameters of the 1D sewer flow and rainfall-runoff models. The initial values and calibration ranges are summarized in Table 5. Hydrological parameters related to unpaved areas were excluded from calibration, assuming these areas absorbed all rainwater during the monitored events.

Table 5 – Initial values and calibration interval for the parameters selected to be calibrated

Parameter	Initial Value	Calibration Interval	References
Roughness of Combined Pipes (mm)	3.0	1.5 – 9.0	Stanić *et al.* (2017)
Roughness of PVC Pipes (mm)	0.1	0.1 - 0.6	Butler and Davies (2018)
Discharge Coefficient of the Weirs	0.4	0.3 - 0.6	Bagheri *et al.* (2014)
Sub-catchment Width and Slope	-	± 50%	Temprano *et al.* (2007)
Initial Loss of Paved Areas (mm)	0.5	0.25 - 1.25	RIONED (2019); Rossman (2010)
Initial Loss of Flat Roofs (mm)	2.0	1.0 – 5.0	RIONED (2019); Rossman (2010)

3.4.4 Optimization Procedure

After selecting parameters and setting their calibration intervals, the next step was determining the optimal set of parameter values that best match the observed data. For this purpose, we used Monte Carlo sampling to generate 1,000 random parameter sets. Each set was then used to simulate the four observed rainfall events, with results reported only after the initialization period. The optimal parameter set was the one that produced the maximum average NSE across water level data from the CSO weir and pumping station during the four calibration events:

$$\frac{1}{8}\sum_{i=1}^{4} NSE_{CSO,i} + NSE_{PS,i} \rightarrow max \tag{9}$$

where $NSE_{CSO,i}$ is the NSE value for the CSO water level at event i and $NSE_{PS,i}$ for the pumping station water level for event i.

3.4.5 Optimal Infiltration Rate for the Model with Permeable Zones

The same calibrated parameters values defined for the model without gullies were used for the model with permeable zones. However, an additional parameter, the constant infiltration rate across the 2D surface, required calibration. To determine the optimal rate, it was necessary to use hydraulic loads that would result in water on the streets. In the absence of such flood records, composite storms developed based on 'current' climate conditions (see section 2.2.3) were adopted. During calibration, storms with return periods of 2, 10, and 25 years were selected, while validation used a 100-years event, in line with the return periods outlined in Rotterdam's Municipal Sewerage Plan (Municipality of Rotterdam, 2021) for assessment of urban water system performance.

The calibration interval for the rainfall rate ranged from 25 to 200 mm/h. Calibration and validation compared the flooded area time series between models with permeable zones and gullies, using the NSE to measure performance. Flooded area time series were chosen because they can illustrate gully effects on flood extent and duration. The model with gullies served as a reference because it can more accurately represents the bi-directional interaction between the 2D surface and 1D drainage network (Chang *et al.*, 2018). The optimal infiltration rate was determined by maximizing the average NSE across the three calibration storms.

3.5 Models Comparison and Selection

The three methodologies were compared based on data requirements, flood hazard predictions and simulation times. The comparison began with an analysis of flood extent predictions, where time series of flooded areas from the three models were plotted for return periods of 2, 10, 25, and 100 years. Following this, maximum flood depths for the 100-year return period, which exhibited the largest flooded extent among the analyzed events, were visually depicted through inundation maps for all the approaches. Flood duration predictions for this same event were also analyzed, with the spatial distribution presented on maps and the value distribution illustrated through Violin plots. Execution times for simulations of various storm events were then carefully evaluated, ensuring that runtimes were comparable by maintaining a consistent minimum 2D timestep for each simulation, ranging from 0.08 to 0.15 seconds, as calculated by InfoWorks ICM under the Courant-Friedrichs-Lewy condition. The model that combined realistic flood hazard estimates, manageable data requirements, and efficient runtimes was ultimately chosen for the subsequent economic flood risk assessment.

3.6 Economic Flood Risk Assessment

In this phase of the research, an economic flood risk assessment was conducted under the assumption that no new investments would be made beyond maintaining existing infrastructure. The methodology involved several key steps: simulating flood hazards (3.6.1), identifying exposed assets (3.6.2), converting these exposures into monetary terms based on asset vulnerability (3.6.3), and developing a risk model for present and future climate (3.6.4).

3.6.1 Hazard Analysis

The hazard analysis characterizes floods by examining the probability distribution of their magnitudes, mapping overland flow paths, and identifying key hazard indicators like flood extent, depth, and duration (Zhou *et al.*, 2012). In this research, the best-performing 1D-2D model was used to simulate flood hazards using composite storms with return periods of 2, 10, 25, 50, and 100 years. Considering the expected increase in the frequency of extreme events (and thus flood hazards) due to climate change, these return periods were modeled under both current conditions (2014) and future extreme projections for 2030, 2050, and 2085 (refer to 2.2.3). The storms, designed to fill the system to its full capacity before the peak, effectively represent both the short and long durations associated with each return period (RIONED, 2019). Therefore, it is assumed that these return periods correspond to the recurrence intervals of the flood events under specific climatic conditions.

3.6.2 Exposure Analysis

In this research, the assets affected during a flood event were evaluated with GIS tools by intersecting land use with inundation data from the simulations. Assessing the streets exposed to flooding was straightforward as the model predicts maximum water depths at ground level. However, evaluating the exposure of the buildings was more complex due to the lack of data on potential water entry points such as doors, windows, or air bricks, leading to buildings being represented as voids in the 2D mesh. To address this limitation of the model, we applied a generic exposure analysis method proposed by Bertsch *et al.* (2022), which involved spatially intersecting the surface water depth grid with building geometry (see Figure 23).

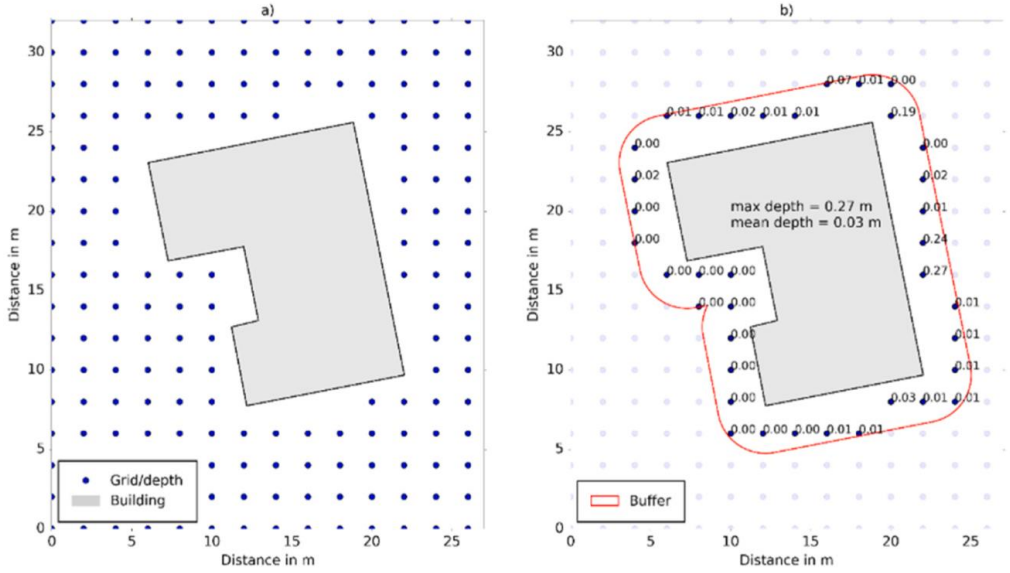

Figure 23 – Building level flood exposure analysis: (a) surface water depth grid and building geometry; and (b) buffered zone and depth statistics. Source: Bertsch *et al.* (2022).

Initially, a buffer is created around the buildings to extract maximum and mean depths from surrounding areas. These depths are then used to assess the risk of internal flooding, based on criteria presented in Table 6. The maximum water depth threshold was set at 15 cm, given that about 65% of Rotterdam doorsteps are at this height (see Annex D). A mean threshold of 5 cm is used to mitigate the impact of outliers in the DTM caused by measurements inaccuracies or abrupt elevation changes near structures (Meng *et al.*, 2010).

Table 6 – Classification scheme to assess likelihood of internal flooding of buildings based on mean and maximum water depth values obtained from spatial intersection.

Exposure Class	Mean (cm)	Maximum (cm)	Internally Flooded
Low	0 < 5	≤ 15	No
Medium	0 < 5	≥ 15	No
	5 < 15	≤ 15	
High	≥ 5	≥ 15	Yes

3.6.3 Vulnerability Analysis

Vulnerabilities describe the potential adverse effects caused by exposure of susceptible areas to flooding (Zhou *et al.*, 2012). In this study, these effects were quantified in monetary terms using the 'WaterSchadeSchatter' (WSS, 2017), a web-based tool developed by STOWA for estimating pluvial flood damage costs in the Netherlands. The WSS tool only requires three main inputs: maximum water level, DTM, and a land use map. Figure 24 shows a schematic flowchart detailing the key inputs and outputs used to estimate final damage costs.

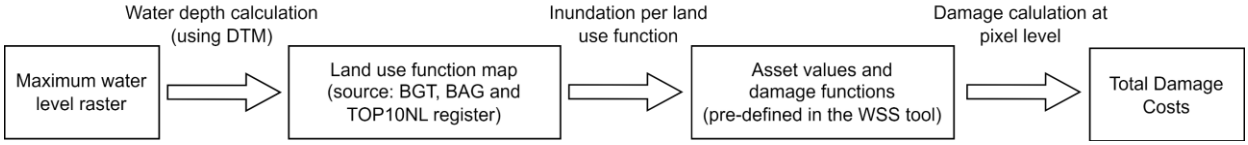

Figure 24 – Workflow of the WSS tool for estimating flood damage.

The maximum water level map was generated based on simulated flood hazards from the best-performing model. Because the WSS tool calculates damages at the pixel level, water levels must be defined inside each building exposed to flooding. For this purpose, if a building is classified as internally flooded during the exposure analysis, it is assumed to have a uniform flood depth across its entire surface area. This flood depth is calculated as the maximum depth, identified in the buffer analysis, minus the previously assumed doorstep height of 15 cm.

The land use map presented earlier in section 3.2.2, used to define runoff surface percentages of sub-catchments in the simulation model, does not provide sufficient detail for damage assessment since asset values depends on their function (e.g., a school typically incurs higher indirect damages than a residential house). To address this, information of building function from the BAG register (*Basisregistratie Adressen en Gebouwen*) was combined with the BGT data. Furthermore, street categories must also be defined, as the potential for indirect damages due to disruption varies depending on factors like traffic volume and connectivity of the road. Given that Spangen is a residential area with primarily minor streets with low traffic, indirect damages were considered negligible. Hence, streets were classified as 'local roads' and sidewalks as 'other road sections' based on the TOP10NL data. The functional land use map used in this analysis is presented in Annex E.

After uploading these three main input data to the WSS website, other additional parameters were specified: flood duration, recovery time for buildings, and whether to use minimum, average, or maximum damage costs. The flood duration was set to the average of durations predicted across all 2D elements for the specific event. While the WSS tool assumes that direct damage to buildings is not dependent on flood duration, direct damage to roads does increase with longer flooding due to reduced pavement bearing capacity and increased traffic-induced stress. Regarding indirect damage to buildings, recovery time was established at one day to consider financial losses due to factors like temporary accommodations for displaced families or lost business revenue for commercial properties. For both direct and indirect damages, average costs were used for calculations.

The direct and indirect damage costs, predefined by the WSS tool at 2015 price levels, are outlined in Table 7. These costs represent the maximum potential losses. Figure 25 illustrates the damage functions used by the WSS tool to translate flood depth and duration into a percentage of these costs, using damage factors that ranges from 0 to 1.

Table 7 – Average damage costs for each land use function (from WSS 2017).

Land Use Function	Direct Damage (€/m²)	Indirect Damage (€/m²/day)
Residential Building	271	11
Assembly Building	271	11
Industrial Building	271	87
Office Building	271	87
Commercial Building	271	87
Educational Building	271	87
Healthcare Building	271	87
Courtyards	0.076	0
Unpaved Areas	0	0
Local Roads	0.076	0
Other Road Sections	0.076	0

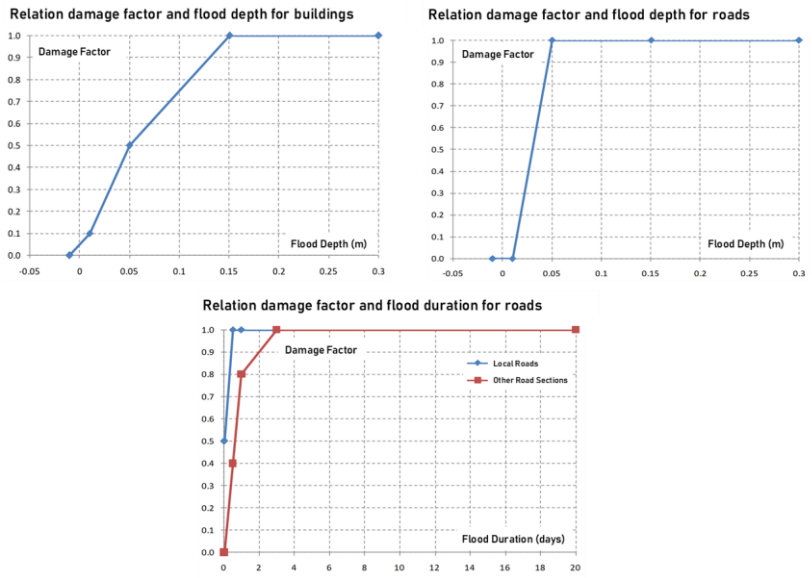

Figure 25 – Damage functions for buildings and for roads. Adapted from WSS (2017).

3.6.4 Flood Risk Model for Present and Future Climates

The flood risk model combines calculated hazards and vulnerabilities to provide a 'snapshot' in time of these factors at a specific urban layout and under given climatic conditions. This involves calculating the annual flood risk density curve by multiplying the estimated damage costs of flood events by their annual occurrence probabilities (i.e., the inverse of the return periods) (Zhou *et al.*, 2012). This curve helps identify the contributions of different return periods to the expected annual damage (EAD), guiding adaptation measures that address events with the highest annual risk (Merz *et al.*, 2009). The EAD, representing the area under the flood risk density curve, can be computed by summing the flood risk across several return periods (Alves *et al.*, 2019):

$$EAD = \sum_{i=1}^{n} \left(\frac{D_i + D_{i+1}}{2}\right)\left(\frac{1}{RP_i} - \frac{1}{RP_{i+1}}\right) \quad (10)$$

where D_i is the damage corresponding to the event of return period RP_i, and n is the number of return periods considered.

This study limits the EAD calculation to return periods of 2, 5, 10, 25, 50, and 100 years, excluding events beyond the 100-year event, which may lead to an underestimation of the EAD. Furthermore, with climate change likely increasing the frequency of severe rainfall events, the flood risk density curves and EAD are expected to shift significantly over time (Zhou et al., 2012). Accordingly, density curves and EAD were estimated for current climatic conditions (2014) and projected future conditions for 2030, 2050, and 2085, under the most extreme climate projections by the KNMI, referred to as 'WH' climate scenario (Klein et al., 2014).

3.7 Development and Evaluation of Flood Mitigation Strategies

3.7.1 Risk-Reduction Scenarios

Different forms and levels of responsibility were taken into consideration (e.g., with publicly and privately owned space) when proposing risk-reduction measures, integrating both gray and green infrastructure. For gray solutions, a capacity analysis identified pipes needing enlargement to handle high flows. Pipes requiring upgrades were those experiencing hydraulic gradients during a 100-year return period storm that exceeded 1.5 times their bed slope, indicating significant hydraulic losses. Additionally, the segments selected for replacement were set at a minimum total length of 20 meters to avoid fragmented interventions that may not enhance the system's overall resilience.

For green solutions, it was proposed to install permeable pavements in low-traffic streets close to the main hydraulic bottlenecks identified in the flood hazard analysis. This strategy targets the sub-catchments adjacent to nodes where high overflow incidents occur, achieving a larger flooding control effect with a smaller investment (Cheng *et al.*, 2024). Additionally, the installation of blue-green roofs was proposed for buildings with flat roofs constructed after 1950 and owned by the housing corporation Woonstad, which has already collaborated with the municipality on retrofitting projects to mitigate climate change impacts. These roofs, combining vegetation and a water retention layer that provides up to 70 mm of additional storage capacity, have been successfully implemented in Amsterdam (Busker *et al.*, 2021; Langewen *et al.*, 2022). Other green solutions, such as vegetated swales, were not considered due to the limited availability of green spaces for implementing this infrastructure.

A total of five risk-reduction scenarios with these solutions implemented individually or in combination were selected to be evaluated (see Table 8).

Table 8 – Summary of the flood risk-reduction scenarios.

Scenario	Description	Abbreviation
1	Enlargement of under-performing pipes to the next commercially available size.	Pi
2	Installation of permeable pavements in selected streets close to bottlenecks.	PP
3	Installation of blue-green roofs on suitable buildings.	BGR
4	Combination of permeable pavements and blue-green roofs.	PP + BGR
5	Combination of pipe enlargement, permeable pavements, and blue-green roofs.	Pi + PP + BGR

3.7.2 Simulation of the Scenarios

For sake of simplicity, it is assumed that all adaptation measures will be implemented immediately. To simulate the impact of risk reduction measures in InfoWorks ICM, the best-performing model was adjusted for each scenario in order to represent its measures. To simulate the gray solution, the diameters of selected under-performing pipes were increased to the next commercially available size. This modification did not consider changes to hydraulic roughness that might occur with the installation of new pipes, given the challenges in predicting changes in roughness over time.

For green solutions, the study did not focus on the detailed performance of specific infrastructures or their exact modeling in InfoWorks ICM. Instead, the focus was on their collective impact on the system's overall performance. Therefore, green solutions were simplistically modelled by modifying the initial losses of sub-catchment to mimic storage and infiltration structures, approach also selected by other studies (Stovin *et al.*, 2013, Moore *et al.*, 2012). Following RIONED (2019), an initial loss of 25 mm was designated for streets with permeable pavements. Similarly, an initial loss of 70 mm was assigned to blue-green roofs to reflect the typical storage capacity of the water retention layer (Busker *et al.*, 2021). Simulations were conducted using composite storms representing both ‘current’ (2014) and projected future climates (2030, 2050, 2085) across return periods of 2, 10, 25, 50, and 100 years.

3.7.3 Cost-Benefit Analysis

To evaluate the effectiveness of the proposed risk-reduction measures for Spangen, a cost-benefit analysis (CBA) was conducted. The cost-benefit estimations span a 60-year period from 2025 (now) to 2085 (future). This horizon is considered appropriated without the need of replacement of the proposed infrastructures. For example, van de Riel *et al.* (2014) suggest that Dutch sewer systems may last up to 90 years, but conditions in Rotterdam like poor soil and uneven settling might limit their effective lifespan to 60 years. Similarly, certain permeable pavements are advertised to last up to 60 years (TRUEGRID, 2024), and blue-green roofs are expected to have a lifespan of 60 years (Langewen *et al.*, 2022).

Climate change impacts were considered in this analysis, as the risk-reduction scenarios were analyzed under both current and future climate conditions up to 2085. For each scenario, it was estimated damage costs related to return periods of 2, 10, 25, 50, and 100 years, annual flood risk density curves, and the EAD for 2014, 2030, 2050, and 2085 using the economic framework presented in the previous chapter. These EAD estimates are linearly interpolated over the years, chosen for its simplicity when there is no strong justification for another method (Smith *et al.*,

2001). The analysis then compared the avoided flood damages across the horizon (benefits) with the present value of costs associated with implementing and maintaining the measures. While a comprehensive CBA would also include co-benefits like heat stress reduction and air quality improvement (Alves *et al.*, 2019), this study focuses only on primary benefits related to damage reduction due to challenges in quantifying co-benefits and time constraints.

To calculate present values, both benefits and costs are discounted. The rationale is that the further in time costs and benefits occur, the lower the weight assigned to it (Sušnik *et al.*, 2015). This weighting is achieved by applying a discounting rate. In this study, a discounting rate of 2.5% is adopted, as recommended by the Ministry of Infrastructure and Water Management. Although this rate was set in 2021, it remains the prevailing standard in the Netherlands unless an updated guidance is issued (Rijkswaterstaat, 2021).

3.7.3.1 Present Value of Benefits

Benefits are the reduction in EAD due to risk-reduction measures, estimated for each period over the horizon. The sum of all discounted benefits across the analysis period represent the present value of benefits for a specific risk-reduction scenario:

$$PV\ (B)_k = \sum_{t=0}^{60} \frac{B_t}{(1+r)^t} \tag{11}$$

where $PV\ (B)_k$ is the present value of benefits for risk-reduction scenario k; B_t is the benefit in year t (with t=0 representing the year 2025 and t=60 the year 2085); and r denotes the discounting rate.

3.7.3.2 Present Value of Costs

Data on investment and maintenance costs for pipe enlargement and permeable pavements were sourced from Dutch sewerage guidelines (RIONED, 2022), while costs for blue-green roofs were estimated from Amsterdam's RESILIO project (Langewen *et al.*, 2022). Given that these costs were based on 2021 price levels, and damage estimates from the WSS tool were calculated at 2015 price levels, all cost estimates were adjusted to 2015 price levels using the Consumer Price Index (CPI). This adjustment ensures that the CBA is performed using *real* values from which the overall effect of a general price inflation has been removed (Prokofieva *et al.*, 2011). The sum of all discounted costs provides the present value of costs for a risk-reduction scenario:

$$PV\ (C)_k = \sum_{t=0}^{60} \frac{C_t}{(1+r)^t} \tag{12}$$

where $PV\ (C)_k$ is the present value of costs for risk-reduction scenario k; C_t is the investment and/or maintenance costs in year t (with t=0 representing the year 2025 and t=60 the year 2085); and r denotes the discounting rate.

4 Results and Discussion

4.1 Model Calibration and Validation

The calibration results show that all the 1,000 sets of model parameter value combinations generated for both the model with and without gullies consistently produce accurate predictions when compared to observed water level measurements. This consistency indicates that initial parameter values and assumptions are sufficiently adequate for predicting the behavior of the sewer system under normal rainfall conditions.

As it can be seen in Figure 26, the distribution of average NSE values for both models ranges narrowly from 0.76 to 0.78. Although the model without gullies exhibits a slightly better performance according to the selected assessment criteria, this difference is minimal and negligible. This finding implies that a more detailed hydrological characterization of the sub-catchments in the model with gullies does not enhance accuracy for this specific urban catchment. Therefore, the simpler, distance-based method adopted in the model without gullies is sufficient. This indicates that accurately predicting flow dynamics hinges more on having robust estimates of runoff volumes rather than on the detailed routing of these volumes to specific network components.

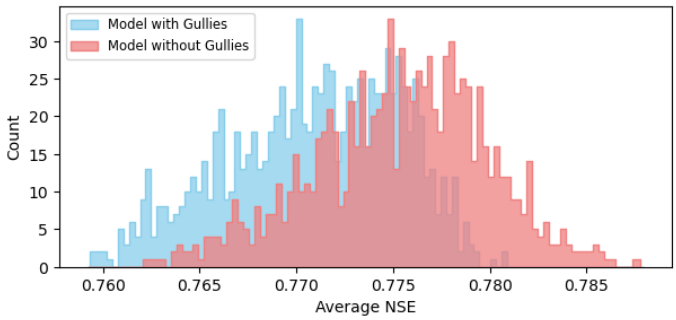

Figure 26 – Average NSE distribution for models with and without gullies during calibration.

Further, the results show that the selected calibration parameters exhibited low sensitivity during typical rainfall events with mild peaks and runoff volumes. However, relying solely on such events may be insufficient as it does not test the model to the limit. Small inaccuracies in a model calibrated under these conditions can lead to significant errors when predicting outcomes for rainfall events with higher return periods. Consequently, the impact of these parameters under extreme precipitation conditions should not be underestimated.

Despite these concerns, the limited access to sewer data and the absence of flooding records constrained our calibration process to these typical rainfall events. Recognizing that these parameter adjustments might only address short-term deviations rather than the underlying sources of error, it is recommend that the municipality engage in ongoing monitoring of the network. The collected data should be used to regularly assess the predictions of the model by implementing a structured error diagnostic framework, as proposed by Pedersen *et al.* (2022a).

The calibrated parameter values for the models with and without gullies are detailed in Table 9. The high roughness coefficients for pipes in both models may balance local hydraulic losses in sewer flow, which were explicitly omitted in our models. Additionally, higher initial loss values for impervious surfaces in the model without gullies likely compensate for its lower in-sewer storage, as representing gullies through nodes and conduits increases storage by about 10%.

Table 9 – Calibrated parameter values for models with and without gullies.

Parameter	Calibrated Values (with Gullies / without Gullies)
Roughness of Concrete/Steel Pipes (mm)	9 / 9
Roughness of PVC Pipes (mm)	0.6 / 0.6
Discharge Coefficient of the Weirs	0.5 / 0.6
Sub-catchment Width and Slope	-50% / -50%
Initial Loss of Paved Areas (mm)	0.25 / 0.75
Initial Loss of Flat Roofs (mm)	1 / 3

Despite slight differences in calibrated parameter values, both models predict nearly identical water level time series at the CSO weir and upstream of the pumping station across all calibration events (Figure 27). The similarity extends to the NSE values, with both models achieving an aggregated NSE of about 0.78 for the CSO. For the pumping station, the aggregated NSE values are also closely matched, at 0.83 and 0.82 for the models without and with gullies, respectively.

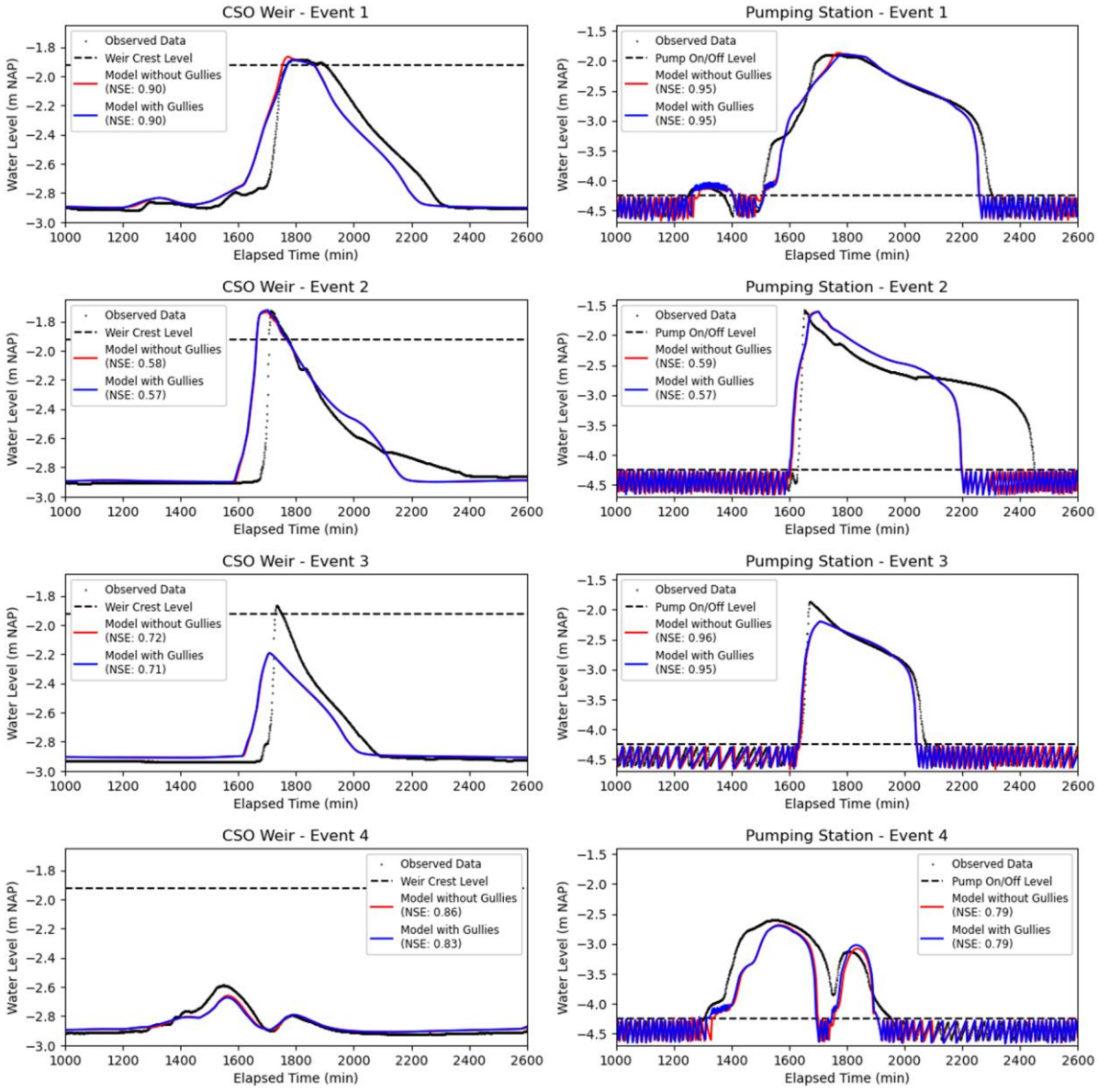

Figure 27 – Water level predictions at CSO and pumping station during calibration.

Following calibration, the models were validated against two additional rainfall events. The validation results show that water level predictions from both models closely matched observed data, reflected in satisfactory NSE values (Figure 28). The aggregated NSE for the CSO time series was 0.69 without gullies and 0.68 with gullies. For the pumping station, both models achieved an aggregated NSE of about 0.83.

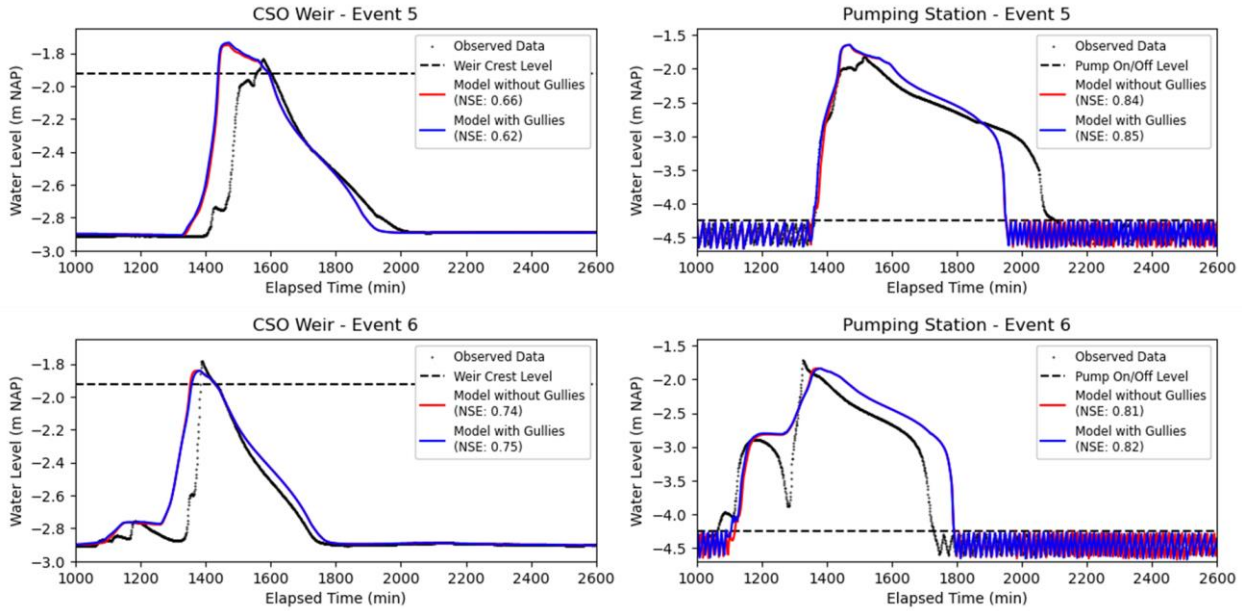

Figure 28 – Water level predictions at CSO and pumping station during validation.

Although both models yielded satisfactory NSE values, they inaccurately predict the peak water levels at the CSO weir for Events 3 and 5, failing to estimate discharges for the former and overestimating for the latter. The specific causes of these inaccuracies are not fully known, but one likely explanation is the use of rainfall data from a gauge nearly 5 km away, which may not capture the localized intensities typical of summer rainfall events. Moreover, timing discrepancies in the rising limbs of most CSO time series suggest that interpolating hourly rainfall data to minute intervals may distort the actual timing of rainfall within the catchment. Other factors, such as reduced system storage due to sediment buildup or differential subsidence rates, may also contribute to these inaccuracies. Regarding the pumping station time series, the mismatches in the recession limbs for Events 2, 5, and 6 are likely due to variations in pump operation during those events, as the model applied current rules based on the latest municipal data. This is not observed in Event 1, which is the most recent event under investigation.

After calibrating a model without gullies, the same parameters were applied to a model with permeable zones. Yet, determining a constant infiltration rate across the 2D surface to represent gully flow was necessary. Calibration against simulation results from the gully model, based on composite storms with return periods of 2, 10, and 25 years, set an optimal rate of 50 mm/hr. This rate aligned relatively well with the flooded area time series (see Figure 29) from the model with gullies, achieving an average NSE of 0.6 across these three events. For validation, this rate was tested against a 100-year storm, yielding a NSE of 0.57. Lower performance for storms with return periods of 25 and 100 years was noted, likely due to substantial amount of water exiting through gully inlets at locations without manholes, leading to unaccounted flooded areas in the models with permeable zones and also without gullies.

Finally, it is crucial to acknowledge that the optimal infiltration rate identified for this specific sewer district may not directly translate to other drainage systems within the city of Rotterdam. Further research is necessary to refine and generalize this modelling methodology. Preliminary analyses in a smaller district indicate significantly higher optimal constat infiltration rate, likely due to a faster system response to stormwater inflows and the CSO weir not submerging during extreme events, allowing quicker availability of underground network post-peak.

4.2 Models Comparison and Selection

Figure 29 presents the time series of flood extent predictions from the three modeling approaches. The presence of an inflection point at the start of flooding in all models indicates varying response times of the stormwater and combined sewer systems in Spangen. For instance, the Bellamyplein water square begins to flood earlier than other systems, a pattern that diminishes with more severe storms. Post-peak, models without gully data stabilize at higher flood extents due to minimal 2D surface and 1D network interaction, whereas models with gullies is able to redirect more surface flow back into the sewers. Nonetheless, localized ponding remains in depressed areas lacking inlets. On the other hand, the model with permeable zones shows complete drainage from the streets post-simulation.

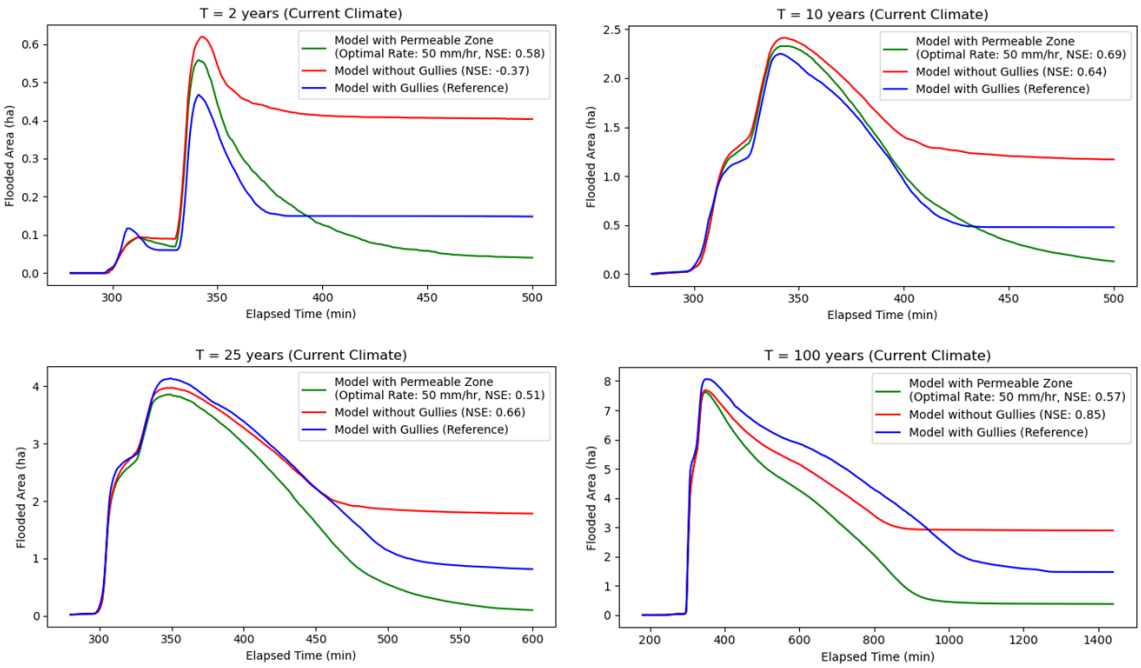

Figure 29 – Time series of flooded area predictions across the different modelling approaches.

For return periods of 2 and 10 years, the model with gully data show reduced maximum flood areas compared to those without, due to synthetic pipes that connect inlets to manholes, enhancing storage by about 10% and lessening flood peaks for milder rainfall events. For 25- and 100-year return periods, however, this additional storage is insufficient and the model with gullies predicts larger flood areas at peak of rainfall. This increase is attributed to more 2D nodes allowing water to spread extensively on the surface. Figure 30 illustrates this effect, showing significant flooding in the park west of the stadium during the 100-year storm, whereas the models without gully data report no flooding due to the absence of manholes and the presence of only inlets in that area. Despite these variations, maximum flood depths in vulnerable areas like residential streets remain similar across all models.

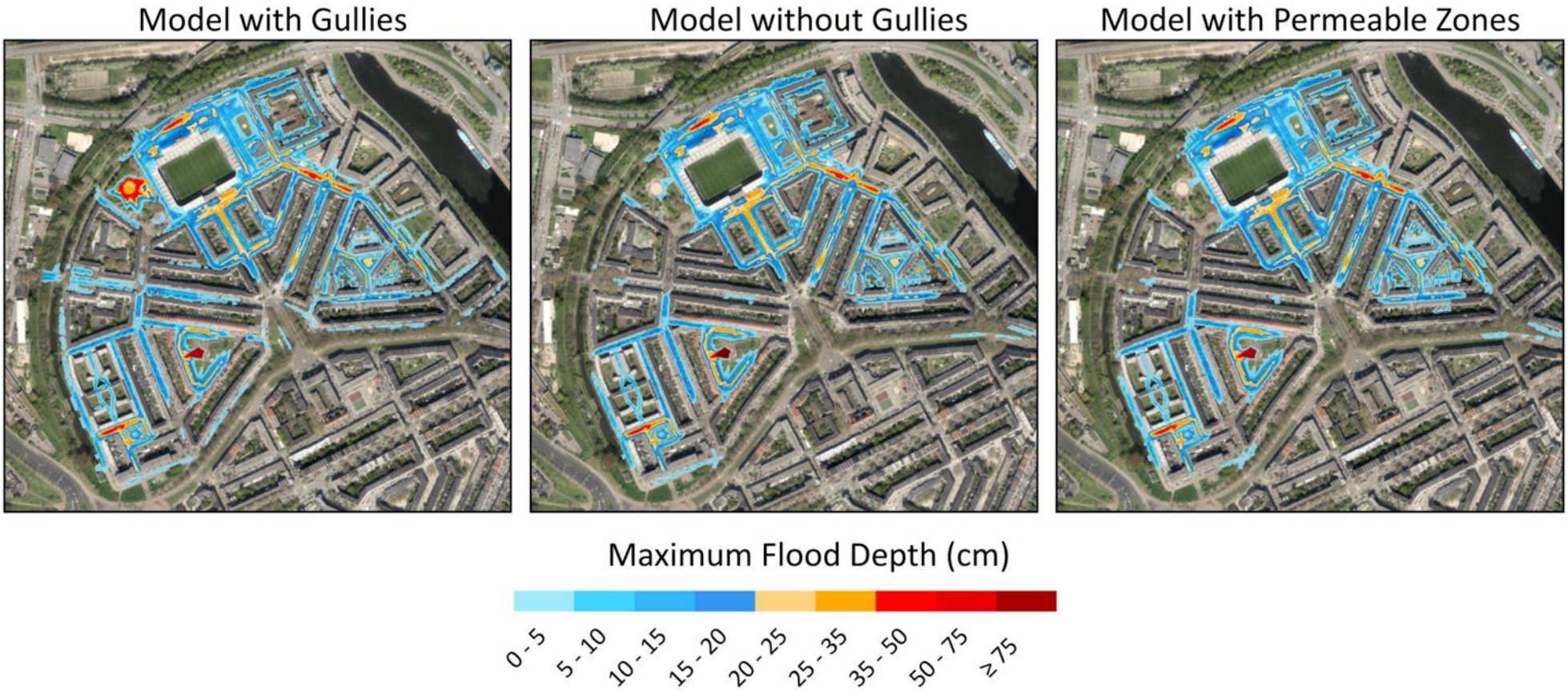

Figure 30 – Comparison of maximum flood depth across the models for a 100-year composite storm based on current climate conditions.

Despite minor differences in flood depth and extent predictions, the critical distinction between these methodologies is the duration of flooding on the 2D surface. For example, consider the simulation results from a 100-year storm (see Figure 32), where a significant amount of water accumulates on the street. In the model with gullies, almost all the street is drained post-simulation, although some water fails to reach the 2D nodes (i.e., gully inlets and manholes) and accumulates in depressions, never flowing back to the 1D network. In the model without gullies, more water stays on the 2D surface through the whole simulation, since it accumulates in depressions where inlets are actually located but not represented in this approach. In contrast, the model with permeable zones allows all the water on the 2D surface to flow back to the network within about 10 hours after the peak. These findings are illustrated in the “violin” plots presented in Figure 31 and the flood duration maps in Figure 33.

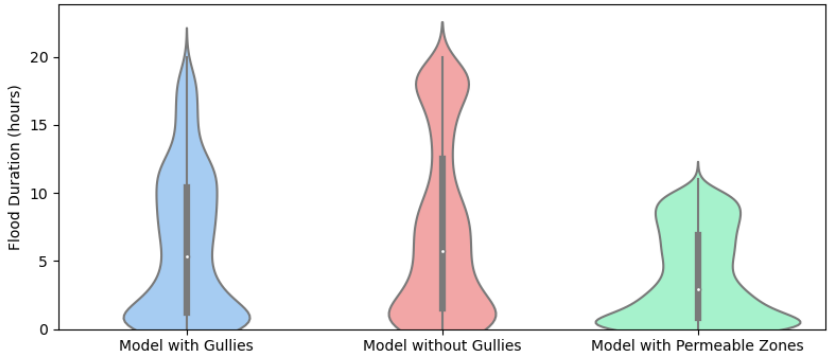

Figure 31 – Violin plots of flood duration across the models for a 100-year composite storm.

While the model with gullies may offer a more realistic depiction of surface flow behavior, acknowledging that in practice not all floodwaters are captured by gullies, this approach comes with significant drawbacks. Firstly, it requires extensive data collection on precise inlet locations, a process that is extremely time-consuming. Additionally, the complexity of the model increases significantly as it also must account for connections between inlets and manholes. Most critically, the model impacts computational efficiency. In InfoWorks ICM, 2D calculations are performed only on wet elements, so the model with permeable zones, which dries faster, markedly reduces simulation runtime compared to other methods. Although the model with gullies dries elements quicker than the model without gullies, its runtime is longer, especially for extreme events, due to complex interactions of the 2D surface with the 1D network through head-discharge tables. Execution times for the analyzed storm eventes across the models are presented in Figure 32.

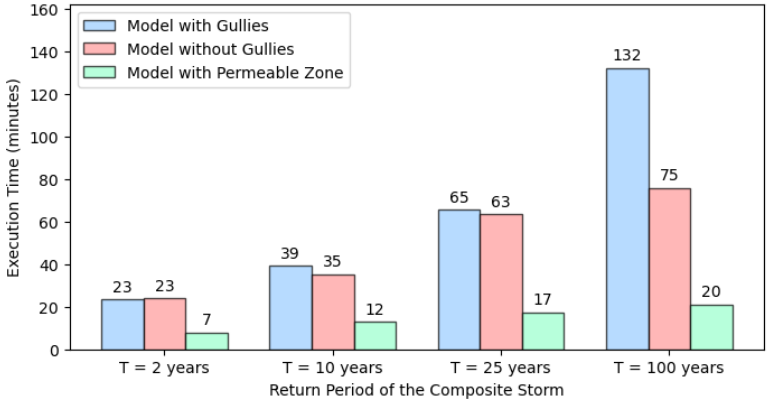

Figure 32 – Comparison of computational times for different models.

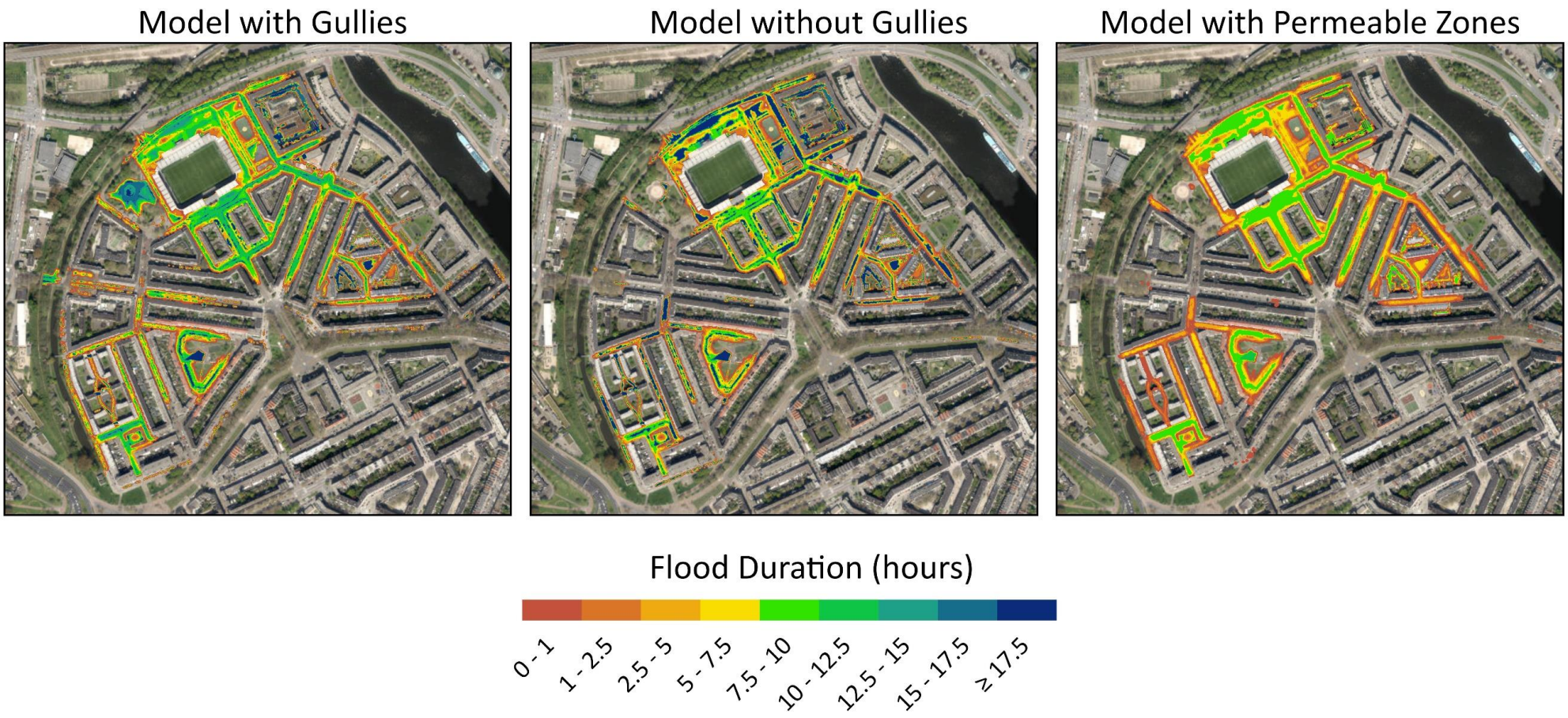

Figure 33 – Comparison of flood duration across the models for a 100-year composite storm.

Based on the above comparison analysis, the model with permeable zones was selected for further analysis due to its significantly shorter simulation times while maintaining similar maximum flood depth and duration predictions to the most detailed (hence likely most accurate) model with gullies. The reduced simulation times make this model particularly advantageous for economic flood risk assessments and the evaluation of mitigation strategies, both of which require multiple simulations to be conducted efficiently.

4.3 Economic Flood Risk Assessment of the Current System

4.3.1 Hazard and Exposure Analysis

The primary hazards in assessing pluvial flood impacts in Spangen are flood extent and depths, given the area's flat terrain which results in low surface flow velocities. For instance, in a simulated 100-year event projected for 2085 under severe climate conditions, the maximum flow velocity reaches only 1.3 m/s, well below the 2 m/s threshold identified by van Ginkel *et al.* (2021) where severe structural damage and high repair costs are expected.

Figure 48 illustrates the simulated maximum water depths during various rainfall return periods under current climate conditions, indicating areas susceptible to flooding. With longer return periods, flooding becomes more extensive and severe, especially in regions with local depressions where hydraulic heads in the network are likely to exceed ground levels and surface flows accumulate. Notably, areas like Nicolaas Beetsstraat in the northeast and Jan Luykenstraat in the southwest, which have high soil subsidence rates (see Annex B), experience flooding during all the analyzed events. Conversely, northwest areas with minimal uneven ground settlement are rarely affected by flooding across any return period.

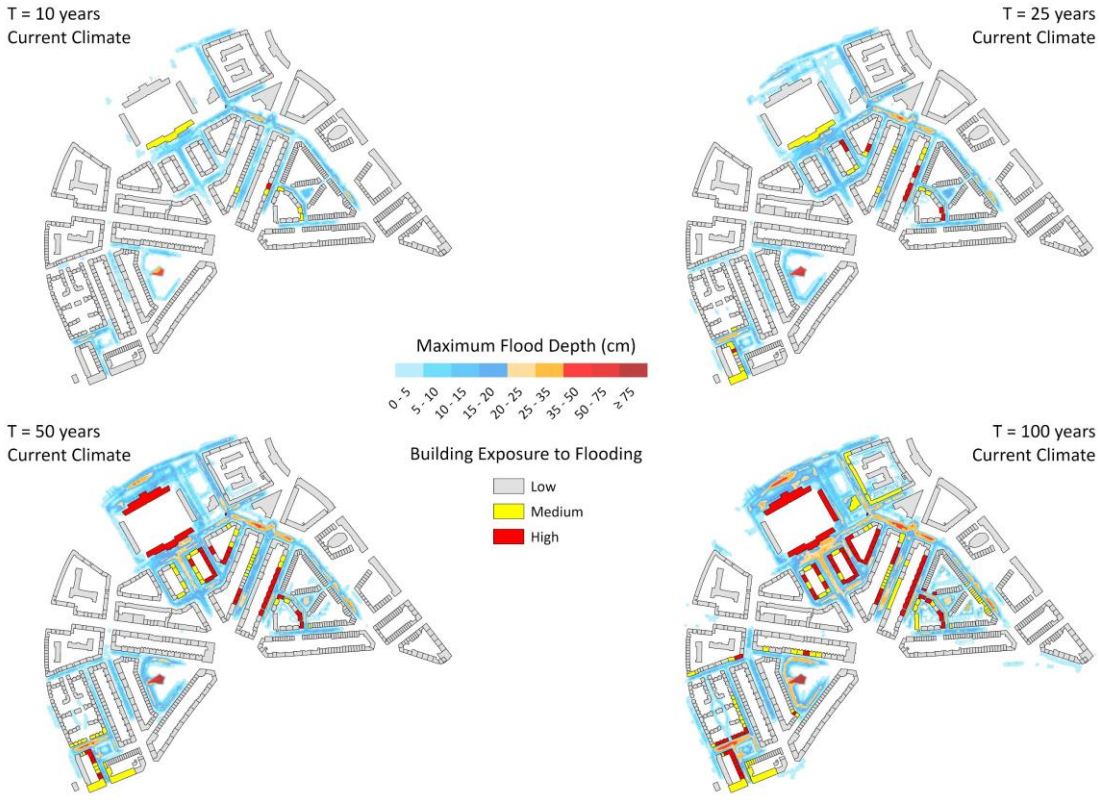

Figure 34 – Inundation maps showing building exposure to flooding for 2, 10, 25, and 100-year return periods under current climate conditions.

The inundation maps reveal that stormwater systems in the area differ in their ability to manage rainfalls with the same magnitude. The Urban Water Buffer (UWB) effectively manages runoff from the stadium and nearby areas up to a 10-year return period. However, once its storage capacity is exceeded, substantial flooding impacts nearby areas. This situation is worsened by an overflow weir that is nearly at the same level as the canal, making it prone to become submerged. Meanwhile, the Bellamyplein water square effectively handles surface water for up to a 50-year event, with its above-ground retention tank holding more than 75 cm of water depth, effectively keeping sidewalks and buildings dry. Conversely, the Staringplein stormwater system encounters challenges managing runoff from even a 10-year rainfall event, resulting in flooding of both streets and buildings due to the limited storage capacity of its infiltration crates.

Despite the Staringplein system's underperformance compared to others, the overall system performance remains satisfactory, likely meeting the qualitative standards defined in the latest municipal sewerage plan for Rotterdam (GRP, 2021). However, simulation results based on future climate projections indicate escalating flood hazards, suggesting the system may struggle with moderate events by 2085. Simulations show that a 10-year rainfall event could lead to flooding of sidewalks and buildings by that year, as shown in Figure 35. This trend is consistent across most return periods, illustrated in Figure 36, with the exception of the 2-year event, which shows no anticipated internal flooding for all future climates. Inundation maps including building exposure classification for all flood events analyzed under present and future climate conditions are available in Annex G.

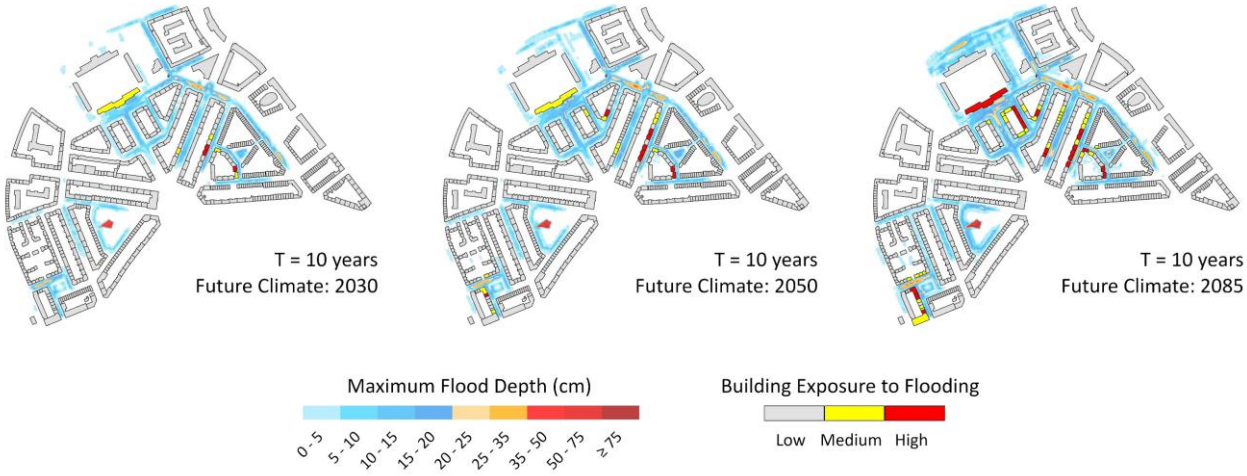

Figure 35 – Projected impact of a 10-year return period on maximum flood depth and building exposure by 2030, 2050, and 2085.

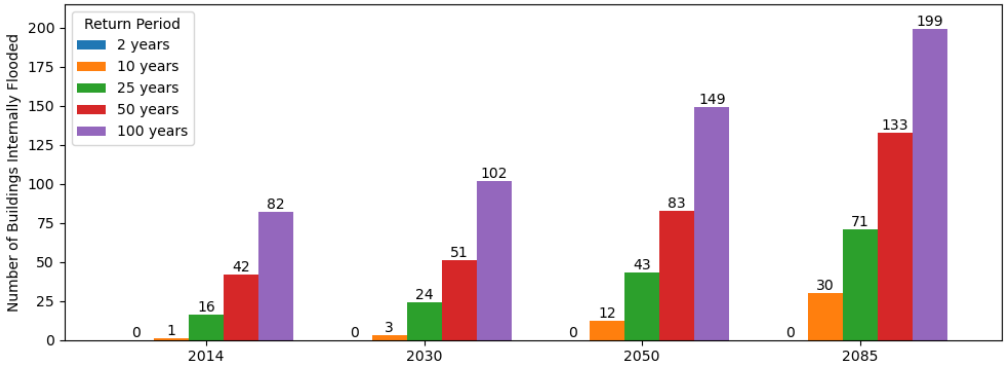

Figure 36 – Projected impact of climate change on building flooding incidence by return period.

In this analysis, distinguishing whether uncertainties stem from the hydrodynamic model or the exposure assessment is challenging. The latter takes into account water depth estimates and building geometries in order to estimate flood exposure based on a simple buffer analysis, not directly modelling flow exchanges of the building with the surrounding streets. While this method can still yield high accuracy in classifying exposed buildings, the water depth thresholds and buffer distances should be validated using data such as resident surveys from areas known or suspected to have experienced flooding during observed events (Bersch *et al.*, 2022). More advanced methods exist like using LiDAR data to map building openings and integrating these detections with flood simulation results to predict flow intrusion (Feng *et al.*, 2022).

Despite potential enhancements through validated thresholds and advanced mapping techniques, the simulation model will continue to face uncertainties from various sources. For instance, pipe invert levels, based on as-built drawings, may no longer be accurate due to differential settlement in sewers causing reduced in-sewer storage (Dirksen *et al.*, 2013). Moreover, the model omitted factors like groundwater infiltration and inflow, which can increase hydraulic loading and more frequently overwhelm the system (Dirckx *et al.*, 2019). It also overlooks issues such as limited gully inlet capacity and potential blockages, which can largely affect flooding occurrence and extent (Leitão *et al.*, 2017). Moreover, sediment accumulation in sewers was neglected, although can affect flow more significantly than high hydraulic roughness due to pipe aging (van Bijnen *et al.*, 2012).

Uncertainties also arise from the conceptual framework of the model, which employs a semi-distributed approach to simulate rainfall-runoff processes across sub-catchments. Because this method does not apply direct rainfall on the 2D surface, it neglects flooding that occurs when runoff does not reach inlets, thus accumulating in surface depressions. Additionally, courtyards, often disconnected from the municipal network, are also not modeled to receive direct rainfall. Consequently, despite the susceptibility for low-lying inner courtyards in Rotterdam to flood during heavy rainfall events (Dai *et al.*, 2018), the simulation predicts negligible water accumulation as the model only accounts for surface flow that reaches these areas through node overflows from adjacent public spaces. Moreover, this approach neglects potential gully connections that could direct runoff from these areas into the municipal sewer network, thus underestimating the contribution of courtyards to stormwater inflow.

4.3.2 Vulnerability Analysis

Figure 37 displays the distribution of flood damage in Spangen for different return periods under present climate conditions. Economic losses are significant only during the 50- and 100-year events when buildings experience internal flooding, with the majority of damage occurring in the eastern part of the study area. Interestingly, buildings incurring the most damage are not always on the streets with the deepest floodwaters. For example, buildings along Brederodestraat and Spiegelstraat, south of the stadium, are highly exposed to floodwater that accumulates on sidewalks, even though the water depths on the streets are not as high as in Nicolaas Beetsstraat, where water remains confined to the street curbs, thus sparing buildings from internal flooding. This suggests that the additional storage capacity provided by some streets might be enough to prevent building damage in a 100-year event.

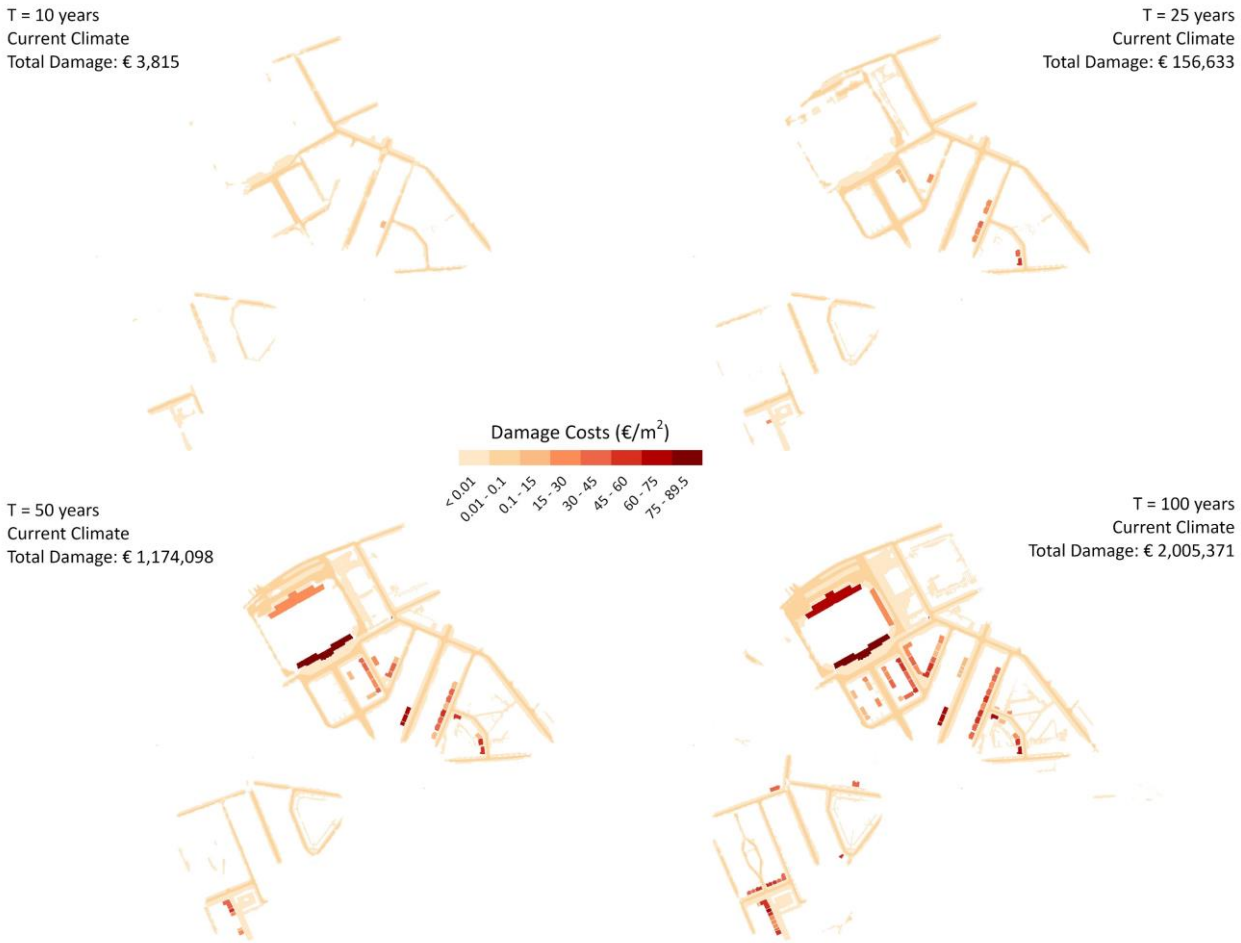

Figure 37 – Flood damage maps for 2, 10, 25, and 100-year return periods under current climate conditions.

Table 10 breaks down flood damage under current climate conditions by land use function for various return periods. Notably, the commercial buildings are the most affected by flood events with high return periods. This apparent vulnerability largely stems from the methodology that assigns a uniform flood depth to the entire surface area of exposed buildings, likely overestimating the extent of internal flooding. Specifically, the damage estimates for commercial buildings in the 50- and 100-year flood events might be inflated because the model simulates extensive flooding across the entire stadium facade. Moreover, the WSS tool applies a constant maximum average asset value for all buildings within the same category, failing to account for potentially lower actual values of stadium facilities, which are used less frequently and therefore probably experience less indirect damages. The model further assumes a uniform one-day recovery period for all buildings, an oversimplification given that recovery times can significantly vary based on flood depth and duration, likely resulting in underestimated indirect damages for some buildings. Additionally, the WSS tool does not consider the duration of flooding when estimating direct damages, potentially resulting in underestimated structural damage, especially in older buildings that are more prone to such impacts.

Table 10 – Estimated flood damage by land use function for various return periods under current climate conditions.

Land Use Function	Damage (€ thousands)				
	T = 2 years	T = 10 years	T = 25 years	T = 50 years	T = 100 years
Residential	0	3.1	109	410	912
Industrial	0	0	46	61	66
Retail	0	0	0	701	1,024
Courtyards	0	0	0	0	0.1
Local Roads	0.2	0.7	1	2	3
Other Road Sections	0	0	0	0.2	0.5
Total	0.2	3.8	156	1,174	2,005

The data presented in Table 10 indicates that building damage constitutes 82% of total damage for 10-year floods, rising to over 99% for 25-year floods or longer, significantly higher than other studies suggest (Fenn *et al.*, 2016; Schröter *et al.*, 2014). This difference partly results from not including indirect road damages in the analysis, assuming that streets in Spangen mainly access few houses. Furthermore, the analysis only considered direct road damages for minimal repair and sludge removal costs, based on estimates from the WSS tool. While these assumptions may hold due to Spangen's residential setting and low surface flows, significant water accumulation on streets can cause additional nuisances. For instance, direct damage to vehicle is possible in flood-prone parking areas, especially where uneven ground settlement like in Nicolaas Beetsstraat leads to localized deep water accumulation over 30 cm, far above the 14 cm estimated threshold for standard sedan car damage (Abdulla *et al.*, 2020). Moreover, floodwaters resulting from combined sewer flooding incidents are likely to be contaminated and may pose potential health risks to citizens exposed to pathogens (Ten Veldhuis *et al.*, 2010).

Other intangible damages not considered in this assessment include environmental impacts of the release of pollutants, psychological trauma due to ongoing disruptions, and causalities from hazards like electrocution due to submerged electrical outlets during basement flooding. Although pluvial floods typically cause less intangible damage than coastal floods, a comprehensive flood risk assessment should consider all damage types. Overemphasizing building damage estimates could lead to prioritizing only economically valuable areas over those most in need, potentially exacerbating social inequalities. Even though the WSS applies uniform average damage values across all buildings regardless of building quality, this approach might favor risk mitigation strategies for larger buildings which aren't always the most vulnerable. Moreover, less affluent and socially vulnerable communities often suffer more from flood impacts due to limited information and resources, a significant concern that remains unaddressed in assessments focused solely on asset damage (Nicklin *et al.*, 2019).

Despite uncertainties and limitations in capturing the full spectrum of damages, the estimates from this research remain valuable for assessing future flood impacts. As climate change is expected to increase the frequency and intensity of pluvial flood hazards, damages will also rise. While current infrastructure can manage up to a 25-year return period with minimal economic losses, extreme climate projections for 2030, 2050, and 2085 indicate that more frequent extreme events will cause significantly higher losses. For instance, Figure 38 shows that damages from a 10-year flood event will rise substantially over time. By 2085, such an event could incur

damages close to €800 thousands, greatly surpassing the estimate of approximately €155 thousands for a 25-year return period event in present climate.

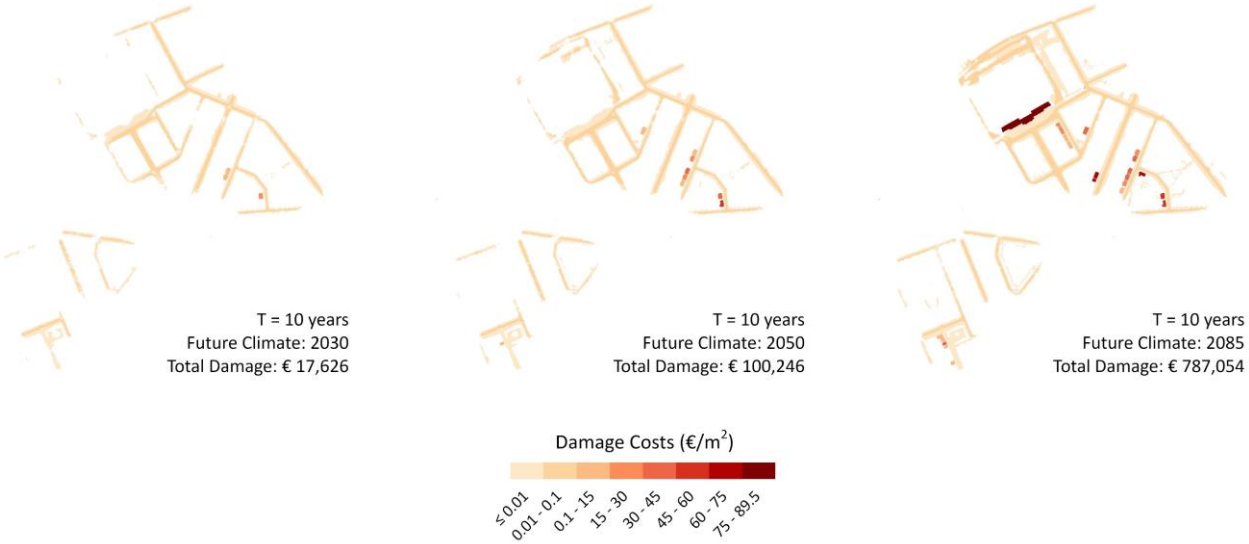

Figure 38 – Projected impact of a 10-year return period on flood damage by 2030, 2050, and 2085.

4.3.3 Flood Risk Model for Present and Future Climates

The damage costs and annual risk density curves for both present and future climates are shown Figure 39. Currently, flood risk in Spangen is primarily influenced by high-return period events (50, 100 years). Future climate projections, however, suggest a trend towards more frequent events dominating the overall risk as climate change intensifies flood hazards. While damage costs from events up to a 25-year return period in future climates are relatively low compared to more severe events (see Figure 39, left panel), their contribution is quite significant (see Figure 39, right panel), especially by the year 2085 where flood risk will be dominated by a 10-year rainfall event.

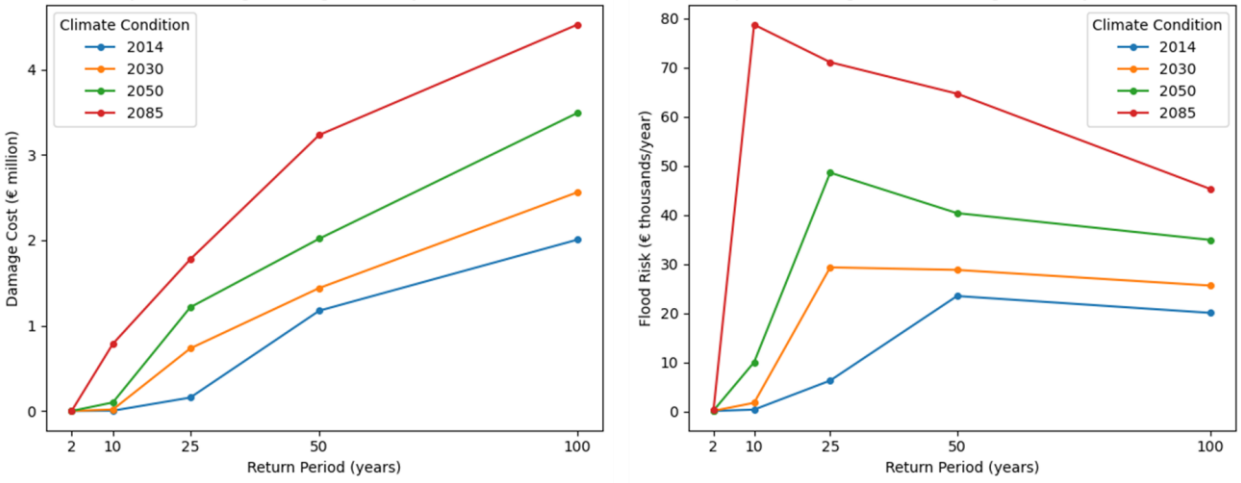

Figure 39 – Damage cost (left) and annual flood risk density curves (right) as function of the return period for current and future climate conditions.

The evolution of expected annual damage (EAD) over time, excluding inflation and considering climate change impacts, is presented in Figure 40. While current climate conditions result in low EAD, by 2085 it is projected to exceed €300 thousands. Cumulative damages from 2025 to 2085 are estimated at €10.12 million when accounting for climate change, compared to €2.12 million without these impacts. Therefore, disregarding the discount rate and focusing solely on benefits from avoided flood damage, the maximum economically justifiable investment in adaptation would be approximately €8 million, assuming it could reduce future flood risks to current climate condition levels.

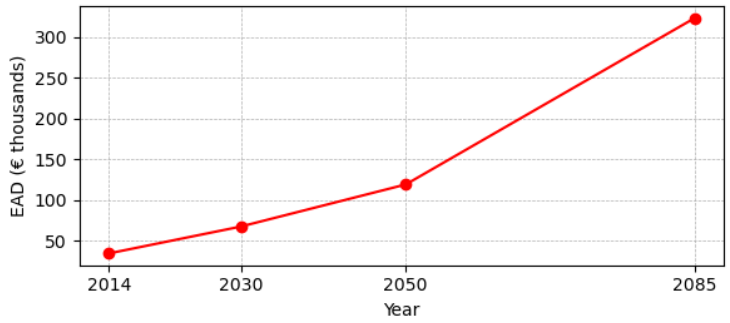

Figure 40 – Projected expected annual damage over time considering climate change impacts.

Lastly, it is important to mention that these EAD estimates were based only on return periods of 2, 10, 25, 50, and 100 years, likely underestimating risks, as events beyond the 100-year return period still pose significant annual risks, as suggested by the density curves presented before (see Figure 39, right panel). Nonetheless, this simplification is sufficient for comparing the costs and benefits of adaptation strategies, as indicated by the literature (e.g., Sušnik *et al.*, 2015).

4.4 Flood Mitigation Interventions

This research proposes three different interventions to mitigate flood risks in Spangen: enlarging pipes, installing permeable pavements, and implementing blue-green roofs. A total of 2.2 km of underperforming pipes were selected for enlargement based on capacity analysis, and approximately 1 hectare of permeable pavements was designated for installation on low-traffic streets near bottlenecks. For blue-green roofs, a total area of 1.7 hectare was selected to be implemented on suitable buildings. Notably, these buildings were situated near the identified bottlenecks, predominantly in the eastern part of the study area, as shown in Figure 41.

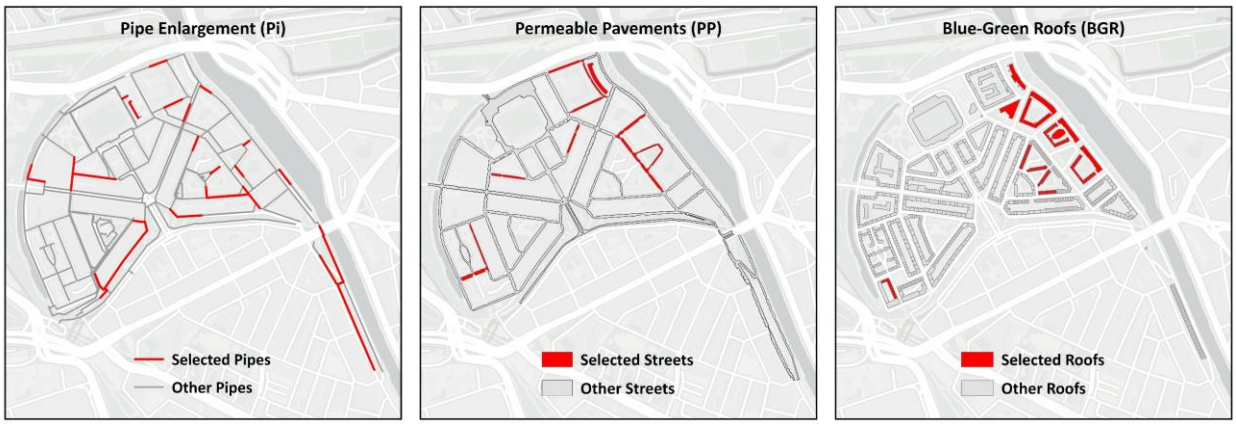

Figure 41 – Location of the risk-reduction measures proposed for Spangen: pipe enlargement, permeable pavements and blue-green roofs.

4.4.1 Flood Risk Assessment of Mitigation Interventions

The assessment is performed for different flood risk-reduction scenarios, considering each mitigation intervention individually as well as in combination (see Table 8 for a full list of intervention scenarios). Damage costs estimated across these scenarios for different return periods, under current and future climates, are presented in Annex H. Annual risk density curves derived from these estimates are presented in Figure 42.

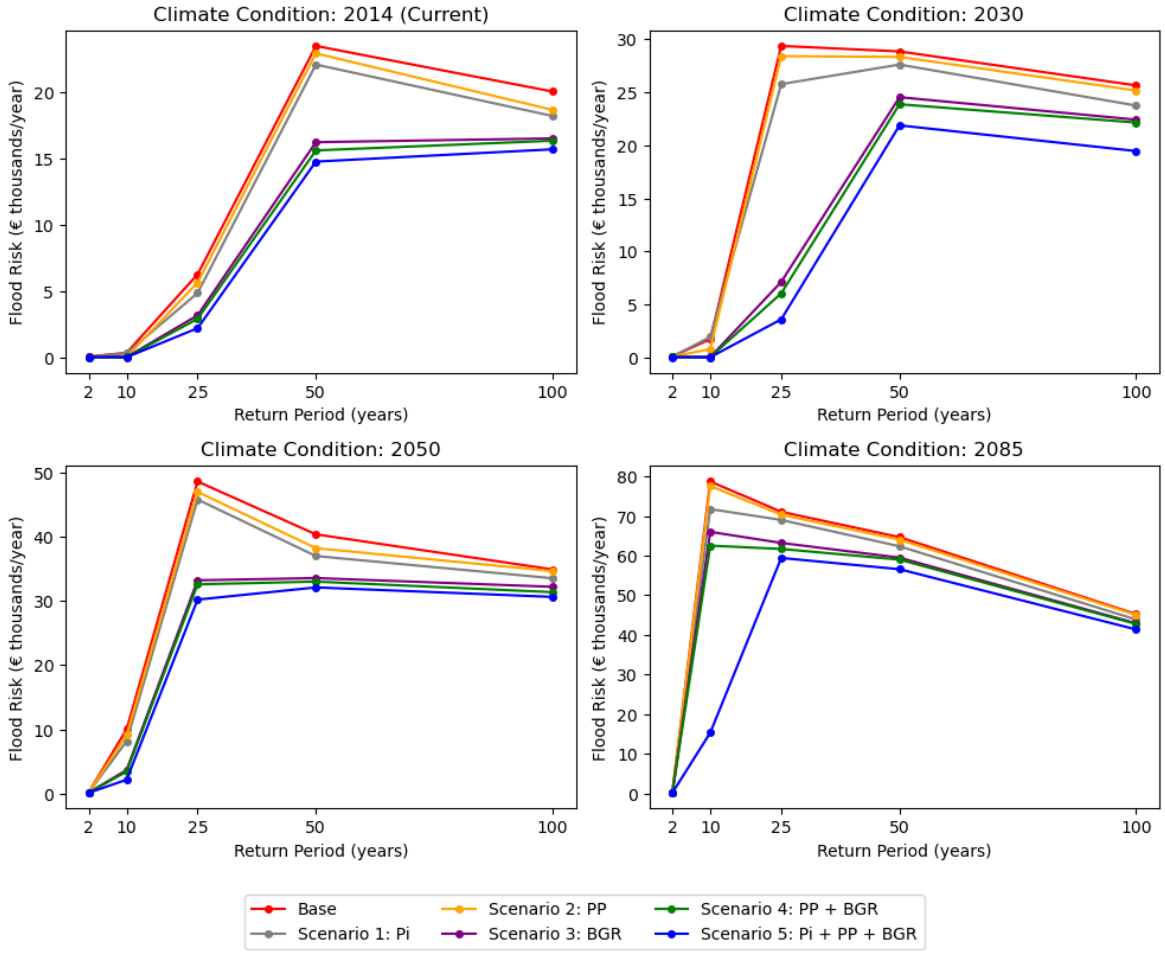

Figure 42 – Annual flood risk density curves for each risk-reduction scenario considering current and future climate conditions.

Despite permeable pavements providing more additional storage in Scenario 2 (250 m³) compared to enlarging pipes in Scenario 1 (218 m³), Scenario 1 consistently shows lower flood risks than Scenario 2 across all return periods. This difference arises because enlarging pipes increases storage but also reduces hydraulic losses by decreasing friction during pressurized flows, while permeable pavements only reduce runoff volumes without improving internal hydraulic conditions. Nevertheless, as it can be seen from Figure 44, neither solution significantly mitigates flood risks when applied independently. This is because runoff and/or node overflow abatement for these two scenarios are relevant only for events involving 'low' rainfall intensities (e.g., 2-year event), where flood damages are low without any risk-reduction measures (i.e., base scenario). In higher return period events, the additional storage from either solution proves insufficient, with the storage capacity often being completely utilized before the peak of the rainfall event.

On the other hand, the installation of blue-green roofs (Scenario 3), which provide an additional 1,190 m³ of storage (equivalent to 70 mm over 1.7 hectares of roofs), significantly reduces runoff volumes, even during high-intensity rainfall events. For example, under current climate conditions, when this solution is applied alone, the dominant return period increases to the 100-year event, compared to the 50-year event in the base scenario. Furthermore, results suggest that this additional storage capacity is still sufficient under future climate conditions, increasing the dominant return period to 50 years instead of 25 years for 2030 and 2050. However, flood damages from the 10-year event in 2085 remain high for such a moderate return period, leading to elevated flood risks. Further, when blue-green roofs are combined with permeable pavements (Scenario 4), only a minor reduction in estimated damages is observed compared to Scenario 3. This is again because the additional 25 mm of storage provided by the permeable pavements is insufficient to manage high-intensity rainfall, as its capacity is exceeded before the peak.

However, when all the proposed solutions are applied together (Scenario 5), a greater reduction in flood damages is achieved, particularly under the extreme future climate projected for 2085. For example, in a 10-year rainfall event, the estimated damage without any measures is €787 thousands, but this is reduced to €153 thousands. This significant reduction occurs because internal flooding is not predicted for buildings of the stadium, as the average water depth stays below the 5 cm threshold set in the exposure analysis. In contrast, other scenarios show these buildings experiencing flooding, with average water depths reaching 7 cm when no measures are implemented (see Figure 43). Therefore, the large EAD reduction by 2085 in Scenario 5 may stem from overestimating building damage by applying uniform flood depths to entire surface area, disproportionately affecting larger exposed buildings. Moreover, although the thresholds are derived from common doorstep heights in Rotterdam, they have not been validated for the specific catchment area and fail to consider different potential water entry points in buildings, and therefore that predicted flood depths may not accurately reflect actual flow intrusion risks.

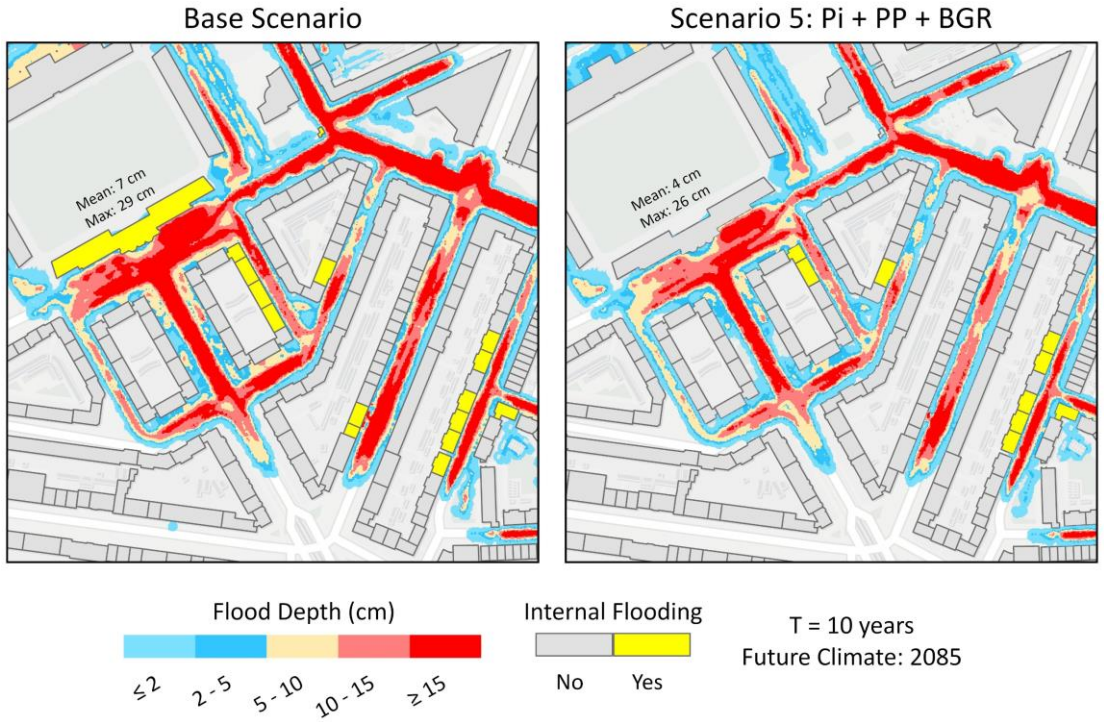

Figure 43 – Comparison of flood depths and building flooding status in baseline and scenario 5 for a 10-year rainfall event, projected for 2085.

Despite these uncertainties, the findings suggest that combining green infrastructure (to reduce runoff volumes) with pipe enlargement (to minimize hydraulic losses in sewer flows) can significantly mitigate flood hazards. However, the effectiveness of such measures diminishes during very extreme events as green solutions are more effective in flood reduction for lower intensity and smaller peak rainfall events (Zhu *et al.*, 2017). For example, flood reduction averages 27% for a 10-year storm in 2085 (see Figure 44, left panel), but only 18% for a 100-year event in 2085 (see Figure 44, right panel). Consequently, flood damage estimates for the 100-year event with all measures are €4.14 million, compared to €4.5 million without measures, resulting in a modest damage cost reduction of 8.1%.

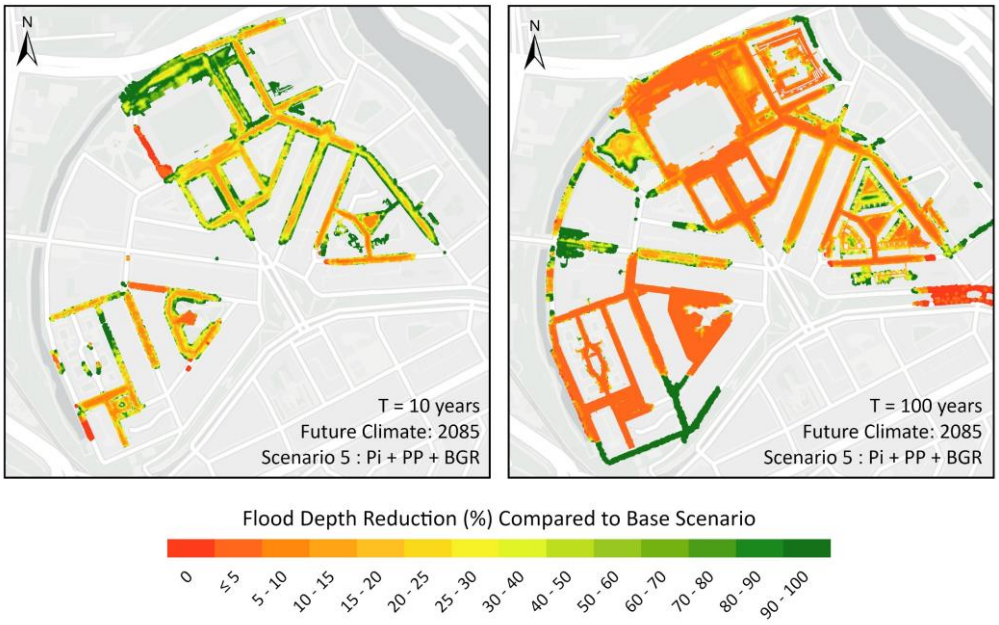

Figure 44 – Flood depth reduction for 10- and 100-year flood events in 2085 with all measures implemented (Scenario 5).

Despite the minimal impact during the extreme events projected for 2085, implementing all proposed solutions significantly lowers the EAD in that year, (Figure 45), largely due to decreased damage from more moderate, frequent events (e.g., 10-year flooding). Specifically, the EAD drops from approximately €325 thousands to €158 thousands, marking a 51% decrease compared to the baseline scenario of not implementing any measures.

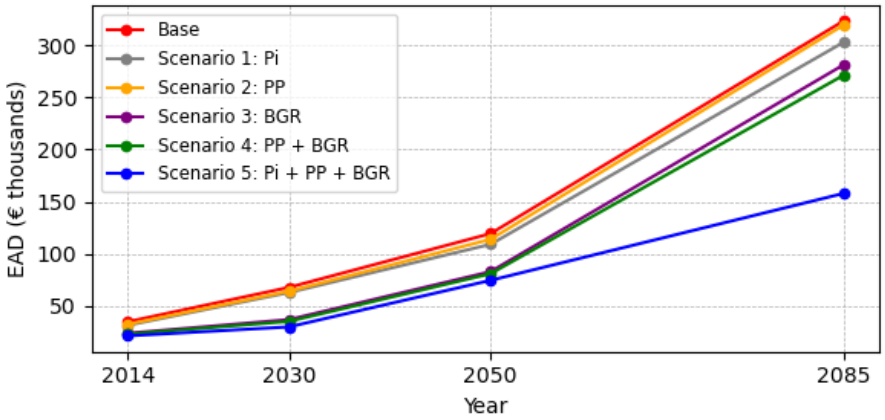

Figure 45 – Projected expected annual damage over time considering climate change impacts across the risk-reduction scenarios.

Further, Figure 46 shows the EAD reduction across the risk-reduction scenarios for present and future climates. It can be seen that implementing pipe enlargement or permeable pavement alone yields minimal primary benefits compared to other measures. In contrast, blue-green roofs alone achieve nearly the same flood risk mitigation effect as when combined with permeable pavements. The plot also indicates temporal variations in the effectiveness of each scenario. Specifically, scenarios incorporating blue-green roofs show peaking effectiveness by 2030, as the frequency of extreme weather events rises, highlighting their benefits mitigating damages from events like a 25-year flooding (refer to Figure 42). Over time, however, the effectiveness of these solutions diminishes as their storage capacities become insufficient for increasingly intense future rainfall events. Despite this decline, Scenario 5, which integrates all proposed measures, continues to provide substantial EAD reductions by 2085. This significant reduction, as previously discussed, is largely driven by the notably lower flood damage estimated for the 10-year storm occurring that year.

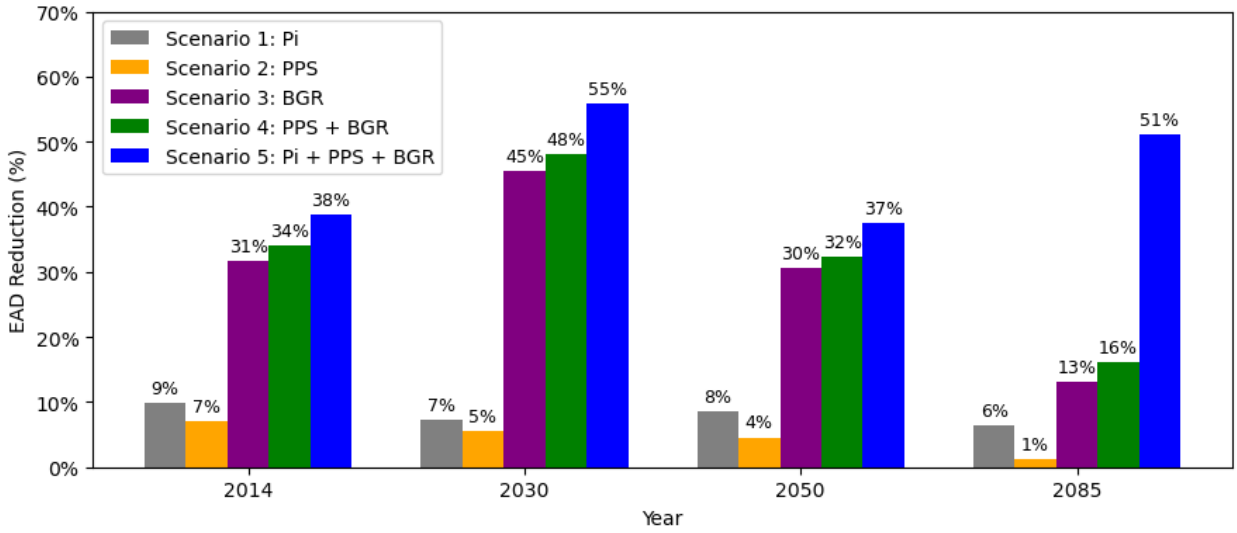

Figure 46 – Expected annual damage reduction compared to the baseline across the risk-reduction scenarios.

Although the evaluation suggests that combining gray and green infrastructure might significantly reduce EAD, using these results to guide flood-risk management decisions requires careful consideration. The model simplifies green infrastructure by assuming a fixed initial water loss to mimic infiltration and storage. Yet, in practice, the volume of 250 m³ presumed to be absorbed by permeable pavements is not entirely infiltrated to deep soil layers but rather slowly released into surface waters or the sewer system via drainage pipes due to high groundwater levels. Furthermore, the effectiveness of blue-green roofs hinges on whether the water retention layer is emptied prior to rainfall events. Nonetheless, “smart blue-green roofs” might improve hydrological efficiency by using prediction-based controls to empty storage before heavy rainfall (Cirkel *et al.*, 2018). Additionally, it is assumed that initial loss remains constant over time, even though permeable pavements are susceptible to physical and biological clogging that can lead to premature degradation and maintenance challenges (Veldkamp *et al.*, 2022). For blue-green roofs, the aging processes and their impacts on hydrological performance are still not well understood, representing a significant gap in research (Andenæs *et al.*, 2018).

Finally, it is crucial to note that the impact of climate change is considered to be large in these future climate projections. While all climate conditions projected by the KNMI (Klein *et al.*, 2014) show an increase in extreme precipitation intensities over time, changes in summer precipitation extremes, which are typically localized and characterized by very high precipitation peaks, are remain particularly uncertain. This uncertainty arises because accurately simulating weather fronts does not necessarily improve predictions for this specific type of rainfall, which largely depends on local processes. Given the significant uncertainty band of these extreme precipitation projections, it is also advisable to evaluate the effectiveness of the risk-reduction measures under scenarios assuming minor climate change impacts.

4.4.2 Cost-Benefit Analysis

Figure 47 presents the cost, primary benefit and net present values across the risk-reduction scenarios using the discounting rate of 2.25 as suggested by the Ministry of Infrastructure and Water Management (Rijkswaterstaat, 2021). It can be seen that all five mitigation options result in a negative net values, where costs outweigh primary benefits. This aligns with expectations, as previous analysis suggests that without considering the discount rate and focusing solely on primary benefits, a maximum investment of around €8 million would be justifiable only if it could maintain future flood risks at current climate levels. However, investments like Scenario 5, despite having the highest primary benefit-cost ratio of 0.26 and nearing €8 million in present value costs, still fail to reduce future flood risks to present levels, as the additional storage remains insufficient to significantly avoid damages from extreme rainfall events projected under future climates.

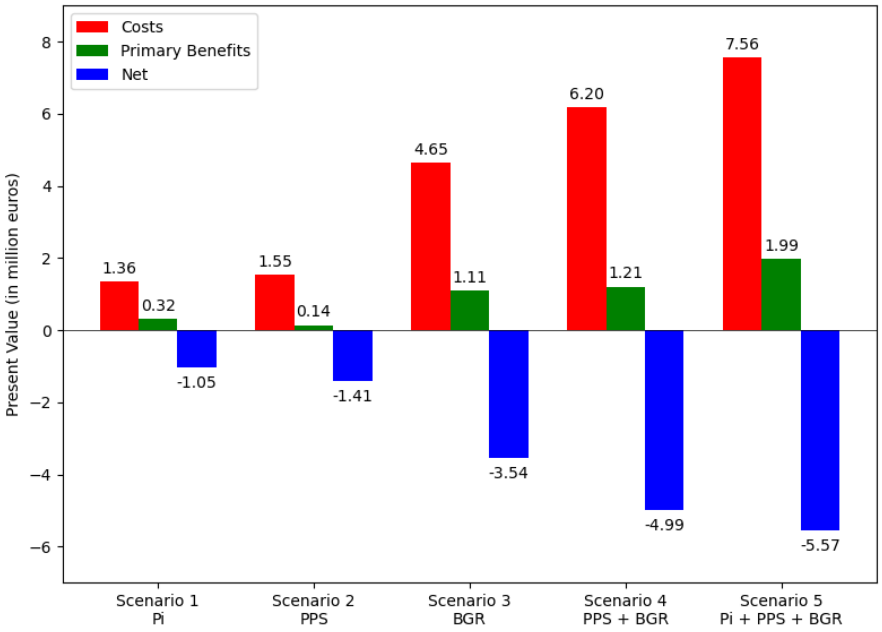

Figure 47 – Cost, primary benefit and net present values by risk-reduction scenario.

Furthermore, while Scenario 5 provides an additional 1,658 m³ of storage, previous investments have already contributed 2,583 m³ of extra capacity (refer to Table 2 and Annex A), likely having a significant impact on reducing flood risks. Consequently, Spangen may be experiencing diminishing returns on further investments (i.e., overspending for only marginal improvement) since the existing infrastructure is already capable of preventing substantial flood damage under

both current and future climate conditions. Therefore, justifying further adaptation measures solely based on primary benefits poses a challenge.

Although primary benefits may show diminishing returns, it is important to also consider the co-benefits of these investments in decision-making. Installing permeable pavements, for instance, enhances urban cooling by increasing evaporation and decreasing surface reflection (Foster *et al.*, 2011). Previously underestimated, the urban heat island effect is notably significant in the Netherlands, with Rotterdam experiencing temperatures above heat stress thresholds for about 15 days each year (Steeneveld *et al.*, 2011). Therefore, permeable pavements serve as an effective measure heat stress reduction, especially in densely populated areas such as Spangen. Beyond temperature regulation, the cooling effect can also reduce energy consumption, subsequently lowering air pollution and greenhouse gas emissions, depending on the sources of electricity. Additionally, cooler temperatures contribute to slowing the formation of ground-level ozone and reducing evaporative emissions from vehicles (USEPA, 2012).

Similarly, green roofs offer extensive benefits beyond runoff reduction, complementing the cooling and environmental advantages provided by permeable pavements. Serving as an insulating layer, green roofs enhance thermal regulation in buildings, thereby reducing cooling energy needs (Liu *et al.*, 2003). These roofs also address several environmental challenges: they mitigate urban heat islands, improve air quality by filtering dust, particulates, and nitrates (Peck *et al.*, 1999), and support biodiversity by offering habitats for butterflies, birds, and bees (Schrader *et al.*, 2006). Additionally, green roofs have a longer lifespan than traditional roofs, which reduces the frequency of replacement and associated landfill costs (Bianchini *et al.*, 2012). They also elevate property values and can offer recreational spaces, enhancing both the aesthetics and market appeal of urban areas (Wise *et al.*, 2010).

Lastly, the stormwater retention potential of the proposed green solutions offers additional benefits beyond flood risk mitigation. For example, these measures reduce the volume of stormwater entering combined sewer systems, thereby lowering CSO discharge. Cavadini *et al.* (2024) highlight that in future climate conditions, the cost-effectiveness of such solutions will improve due to an increase in total rainfall captured by blue-green infrastructure, leading to greater CSO volume reductions and substantially fewer environmental impacts. Furthermore, reducing runoff volume also reduces energy costs associated with pumping and treating combined sewer systems (Shakya *et al.*, 2021).

5 Conclusions

This research aims at: (i) identifying best approach to simulate pluvial flood hazards in an urban environment in a realistic, reliable and efficient manner, i.e. by using a simplified 1D-2D model without gully data; and (ii) developing an integrated flood risk assessment framework to guide the selection of cost-effective adaptation measures. The thesis evaluates flood mitigation strategies using an enhanced 1D-2D model that not only reduces data requirements but also accelerates simulation times, thus improving flood risk evaluations. To the best of the author's knowledge, this modeling approach is novel and has significant potential to benefit asset managers and aid informed decision-making. The conclusions are based on the model simulation results and data analysis, which addressed the main research question as follows:

"*How can the cost-effectiveness of climate adaptation measures be evaluated using flood hazard estimates derived from an efficient and reliable 1D-2D modeling approach without gully data?"*,

The main conclusion is that simplified 1D-2D urban drainage model (i.e., without gully data) can be used to estimate pluvial flood hazards in a realistic manner. Consequently, this enhances confidence in flood risk assessments and supports subsequent evaluations of the cost-effectiveness of climate adaptation measures. This main conclusion is based on the following answers to the research sub-questions:

1) *How can gully flow be modelled in a simplified manner (resulting in reduced data requirements and computational time) without significantly compromising the quality of obtained results?*

Computational time and data requirements for a coupled 1D-2D urban drainage model can be minimized by replacing individual gully inlet data with a constant infiltration rate applied across the entire 2D surface, routing the infiltrated volumes to selected nodes of the 1D network. Comparative analysis revealed that the simplified model closely matched the detailed model with gully data in predicting maximum flood depths for rainfall events from 2 to 100 years, despite minor discrepancies in locations with inlets but lacking manholes. In the urban catchment studied, these discrepancies occurred primarily in less critical areas, such as public parks, where flooding consequences are minor. The simplified model also performed simulations up to 6.6 times faster than the detailed model by effectively drying the 2D surface post-peak rainfall, thereby reducing the need for extensive 2D calculations. With its ability to deliver comparable flood hazard predictions, shorter execution times, and reduced data demands, the simplified model emerged as the preferred modeling approach.

2) *How best to incorporate climate change impacts into the evaluation of pluvial flood risks in the urban environment?*

Addressing climate change impacts in pluvial flood risk assessments can be done by using rainfall events to simulate system behavior for various return periods that reflect current and anticipated future climate conditions. This research used composite storms representing return periods of 2, 10, 25, 50, and 100 years, based on both existing climate data and projections for 2030, 2050, and 2085 derived from KNMI forecasts that considers large climate change impacts.

3) *How can estimates of pluvial flood risks be generated from simulated flood hazards using the simplified model?*

Pluvial flood risks can be quantified in monetary terms by calculating the expected annual damage. This involves estimating flood damage across various rainfall return periods and summing these losses, each weighted by the probability of its corresponding rainfall event. In this research, flood damages for different return periods were estimated using simulated flood hazards from the simplified model. Inundation data was intersected with detailed building

geometries through buffer analysis to determine buildings susceptible to internal flooding. These exposures can be converted into monetary terms using the web-based WSS tool developed by STOWA, which uses predefined asset values and damage functions.

4) *How can the effectiveness of climate adaptation measures be assessed using pluvial flood risk estimates?*

The effectiveness of climate adaptation measures can be assessed through cost-benefit analysis, where primary benefits are determined as the reduction in expected annual damage resulting from risk-reduction measures, estimated across the horizon under study. Five risk-reduction strategies were proposed: (i) enlarging pipes, (ii) installing permeable pavements, (iii) installing blue-green roofs, (iv) combining permeable pavements and blue-green roofs, and (v) combining all three measures. Simulated flood hazards and damage estimates for each strategy were compared with the base scenario (i.e., no adaptation measures) to compute the primary benefits. For the specific catchment under study, the greatest damage reduction occurred when all measures were combined, especially for future climate conditions (e.g., reducing damage from €787 thousands to €153 thousands in a 10-year event by 2085). However, despite having the highest primary benefit-cost ratio, this scenario resulted in a negative net present value. This may be attributed to substantial initial investments in existing infrastructure upgrades, which already significantly mitigate pluvial flood risks, leading to diminishing returns on additional adaptations. While this analysis focuses only on primary benefits related to flood management, it is important to also consider co-benefits such as urban cooling, air quality enhancement, and biodiversity improvements in the decision-making process.

6 Recommendations

Based on the obtained results and conclusions, the following recommendations are made:

1) The coupled 1D-2D models proposed for this research require further calibration and validation. It is recommended that the municipality engage in continuous monitoring of the network, using the collected data to regularly assess the model's predictions. More critically, the models should be tested with events that represent extreme weather conditions. Ideally, comparing the model results with actual flood extent and depth records would enhance validation efforts. Additionally, flood complaints or surveys from residents in areas prone to flooding might also serve as valuable data for validating the model's accuracy.

2) In the simplified model, the optimal constant infiltration rate for the 2D surface was defined using flood hazard predictions from the detailed model that includes individual inlets. As this rate is site-specific and depends on factors like inlet density and hydraulic capacities, it requires inlet data for each application. Further research is therefore recommended to explore how this methodology might be generalized for other areas without needing detailed gully data.

3) The 1D-2D simulations do not explicitly account for flow intrusion into buildings; rather, flood exposure at the building level was determined using GIS analysis based on nearby simulated water depths. The depth thresholds used in this analysis have not been validated yet, so it is recommended to test them via e.g., resident surveys n areas known or suspected to have experienced flooding. Additionally, mapping water entry points like doors and windows with LiDAR data and integrating these detections into the model could allow the simulation of flow intrusion and better estimates of internal flood depths, though this method would also need validation to confirm its accuracy.

4) The economic flood risk assessment conducted in this research, which also considers future climate conditions, is based solely on projections from KNMI that assume significant climate

change impacts. It is recommended that future research also evaluate conditions that account for minor climate change impacts.

5) The assumption that all building within the same functional class have the same damage characteristics and average values is questionable. For instance, stadium facilities are classified as commercial; however, they usually feature assets like seating and concession stands, which are less financially valuable than those typical of retail buildings. Consequently, it is recommended to pursue additional research to refine our understanding of asset values and the relationship between flood depth and damage across more specific land use categories.

6) The economic flood risk assessment presented in this research does not account for indirect damages to roads, direct damage to vehicles, or intangible damages such as impacts on public health, environmental effects, psychological trauma, and casualties. Therefore, it is imperative that future research includes these types of damages to provide a more comprehensive assessment.

7) This research focused on three specific solutions (pipe upsizing, permeable pavements, and green roofs) for mitigate flood risks in the area; however, additional measures such as enhancing pump capacities, downspout disconnection, and underground storage can also be implemented. Future research should explore these other solutions. Moreover, the optimal locations for these proposed solutions were not thoroughly examined. Identifying locations where flood risk reductions are maximized could enhance the effectiveness of these measures.

8) The cost-benefit analysis in this research primarily focused on the primary benefits related to flood damage reduction. However, green solutions also offer additional environmental and social benefits that extend beyond flood management. Future assessments should include these co-benefits. Additionally, benefits to economically disadvantaged individuals should be valued higher, based on the concept of diminishing marginal utility of income, where an additional dollar provides more well-being to a person with lower income compared to someone wealthier. Thus, incorporating equity weights in future analyses can ensure a fairer distribution of benefits.

References

Abdulla, B., Kiaghadi, A., Rifai, H. S., & Birgisson, B. (2020). Characterization of vulnerability of road networks to fluvial flooding using SIS network diffusion model. Journal of Infrastructure Preservation and Resilience, 1, 1-13.

Actueel Hoogtebestand Nederland. (2023). Retrieved September 8, 2024, from https://www.ahn.nl/ahn-4.

Alcrudo & Mulet-Martí, J. (2015). Urban inundation models based upon the shallow water equations. Numerical and practical issues. In: Proceedings of Finite Volumes for Complex Applications IV. Problems and Perspectives, Hermes Science Publishing, London, pp. 1–12.

Ally, M. (2011). Modelling road gullies. Richard Allitt Associates Ltd: West Sussex, UK.

Alves, A., Gersonius, B., Kapelan, Z., Vojinovic, Z., & Sanchez, A. (2019). Assessing the Co-Benefits of green-blue-grey infrastructure for sustainable urban flood risk management. Journal of environmental management, 239, 244-254.

Andenæs, E.; Kvande, T.; Muthanna, T.M.; Lohne, J. (2018). Performance of Blue-Green Roofs in Cold Climates: A Scoping Review. Buildings 2018, 8, 55.

Aronica, G., Freni, G., & Oliveri, E. (2005). Uncertainty analysis of the influence of rainfall time resolution in the modelling of urban drainage systems. Hydrological Processes: An International Journal, 19(5), 1055-1071.

Bagheri, S., Kabiri-Samani, A. R., & Heidarpour, M. (2014). Discharge coefficient of rectangular sharp-crested side weirs, Part I: Traditional weir equation. Flow Measurement and Instrumentation, 35, 109-115.

Barreiro, J.; Santos, F.; Ferreira, F.; Neves, R.; Matos, J.S. (2023). Development of a 1D/2D Urban Flood Model Using the Open-Source Models SWMM and MOHID Land. Sustainability 2023, 15, 707. https://doi.org/10.3390/su15010707.

Beersma, J., Hakvoort, H., Jilderda, R., Overeem, A., & Versteeg, R. (2019). Neerslagstatistiek en -reeksen voor het waterbeheer 2019. STOWA-rapport 2019-19

Benedetti, L., Langeveld, J., van Nieuwenhuijzen, A. F., de Jonge, J., de Klein, J., Flameling, T., Nopens, I., van Zanten, O., and Weijers, S. (2013). Cost-effective solutions for water quality improvement in the dommel river supported by sewer–wwtp–river integrated modelling. Water Science and Technology, 68(5):965–973.

Bertsch, R., Glenis, V., & Kilsby, C. (2022). Building level flood exposure analysis using a hydrodynamic model. Environmental Modelling & Software, 156, 105490.

Boogaard F.C. (2019) Bodemvervuiling in wadi's onderzocht met nieuwe methode. H2O Waternetwerk. Retrieved September 12, 2024, from <https://www.h2owaternetwerk.nl/images/2019/mei/Bodemvervuiling_in_wadis_onderzocht_met_nieuwe_methode.pdf.>.

Bianchini, F., & Hewage, K. (2012). Probabilistic social cost-benefit analysis for green roofs: A lifecycle approach. Building and environment, 58, 152-162.

Bulti, D.T., Abebe, B.G. (2020). A review of flood modelling methods for urban pluvial flood application. Model. Earth Syst. Environ. 6, 1293–1302. https://doi.org/10.1007/s40808-020-00803-z.

Busker, T., de Moel, H., Haer, T., Schmeits, M., van den Hurk, B., Myers, K., ... & Aerts, J. (2022). Blue-green roofs with forecast-based operation to reduce the impact of weather extremes. Journal of Environmental Management, 301, 113750.

Butler, D., Digman, C. J., Makropoulos, C., & Davies, J. W. (2018). Urban drainage. Crc Press.

Cavadini, G. B., Rodriguez, M., Nguyen, T., & Cook, L. M. (2024). Can blue–green infrastructure counteract the effects of climate change on combined sewer overflows? Study of a swiss catchment. Environmental Research Letters, 19(9), 094025.

Chang, T. J., C. H. Wang, and A. S. Chen. (2015). A Novel Approach to Model Dynamic Flow Interactions between Storm Sewer System and Overland Surface for Different Land Covers in Urban Areas. Journal of Hydrology 524: 662–679. doi:10.1016/j.jhydrol.2015.03.014.

Chang, T. J., Wang, C. H., Chen, A. S., & Djordjević, S. (2018). The effect of inclusion of inlets in dual drainage modelling. Journal of Hydrology, 559, 541-555.

Chen, A. S., Djordjevic, S., Leandro, J., & Savic, D. (2007). The urban inundation model with bidirectional flow interaction between 2D overland surface and 1D sewer networks. In Novatech 2007-6ème Conférence sur les techniques et stratégies durables pour la gestion des eaux urbaines par temps de pluie/Sixth International Conference on Sustainable Techniques and Strategies in Urban Water Management. GRAIE, Lyon, France.

Cheng, X., Wang, H., Chen, B., Li, Z., & Zhou, J. (2024). Comparative analysis of flood prevention and control at LID facilities with runoff and flooding as control objectives based on InfoWorks ICM. Water, 16(3), 374.

Cirkel, D.G.; Voortman, B.R.; van Veen, T.; Bartholomeus, R.P. (2018). Evaporation from (Blue-) Green Roofs: Assessing the Benefits of a Storage and Capillary Irrigation System Based on M-easurements and Modeling. Water 2018, 10, 1253

Costa, S., Peters, R., Martins, R., Postmes, L., Keizer, J. J., & Roebeling, P. (2021). Effectiveness of nature-based solutions on pluvial flood hazard mitigation: The case study of the city of eindhoven (The Netherlands). Resources, 10(3), 24.

Dai, L., Wörner, R., & van Rijswick, H. F. (2018). Rainproof cities in the Netherlands: Approaches in Dutch water governance to climate-adaptive urban planning. International Journal of Water Resources Development, 34(4), 652-674.

Delta Programme (2020) Delta Programme 2021: Staying on track in climate-proofing. The Netherlands. Ministry of Infrastructure and Water Management, The Hague. Retrieved October, 2, 2024 from: <https://english.deltaprogramma.nl/documents/publications/2020/09/15/dp2021-eng-printversie>.

de Bruin, K., Goosen, H., van Ierland, E. C., & Groeneveld, R. A. (2014). Costs and benefits of adapting spatial planning to climate change: lessons learned from a large-scale urban development project in the Netherlands. *Regional Environmental Change*, *14*, 1009-1020.

de Graaf-van Dinther, R., Leskens, A., Veldkamp, T., Kluck, J., & Boogaard, F. (2021). From pilot projects to transformative infrastructures, exploring market receptivity for permeable pavement in the Netherlands. Sustainability, 13(9), 4925.

Deletic, A., Dotto, C. B. S., McCarthy, D. T., Kleidorfer, M., Freni, G., Mannina, G., & Tait, S. (2012). Assessing uncertainties in urban drainage models. Physics and Chemistry of the Earth, Parts A/B/C, 42, 3-10.

Depietri, Y., & McPhearson, T. (2017). Integrating the grey, green, and blue in cities: Nature-based solutions for climate change adaptation and risk reduction. Nature-based solutions to climate change adaptation in urban areas: Linkages between science, policy and practice, 91-109.

DiGiano, F. A., Adrian, D. D., & Mangarella, P. A. (Eds.). (1977). Short Course Proceedings: Applications of Stormwater Management Models, 1976 (Vol. 1). Environmental Protection Agency, Office of Research and Development, Municipal Environmental Research Laboratory.

Dirckx, G., Fenu, A., Wambecq, T., Kroll, S., & Weemaes, M. (2019). Dilution of sewage: Is it, after all, really worth the bother?. Journal of Hydrology, 571, 437-447.

Dirksen, J., Baars, E. J., Langeveld, J. G., & Clemens, F. H. L. R. (2013). Quality and use of sewer invert measurements. Structure and Infrastructure Engineering, 10(3), 295–304. doi:10.1080/15732479.2012.751430.

Djordjević, S., Prodanović, D., & Maksimović, Č. (1999). An approach to simulation of dual drainage. Water Science and Technology, 39(9), 95–103. doi:10.2166/wst.1999.0451.

Djordjević, S., Saul, A. J., Tabor, G. R., Blanksby, J., Galambos, I., Sabtu, N., & Sailor, G. (2013). Experimental and numerical investigation of interactions between above and below ground drainage systems. Water Science and Technology, 67(3), 535–542. doi:10.2166/wst.2012.570.

Engman, E.T., “Roughness Coefficients for Routing Surface Runoff”, Journal of Irrigation and Drainage Engineering, ASCE, Vol. 112, No. 1, February 1986, pp. 39-53.

ESRI. (2024a). How Derive Continuous Flow works. Retrieved September 12, 2024, from <https://pro.arcgis.com/en/pro-app/latest/tool-reference/spatial-analyst/how-derive-continuous-flow-works.htm#:~:text=The%20Derive%20Continuous%20Flow%20tool,across%20the%20input%20surface%20raster.>.

ESRI. (2024b). How Watershed works. Retrieved September 12, 2024, from <https://pro.arcgis.com/en/pro-app/latest/tool-reference/spatial-analyst/how-watershed-works.htm>.

European Commission. (2021). Forging a climate-resilient Europe - the new EU Strategy on Adaptation to Climate Change (COM/2021/82 final). Communication from the Commission to the European Parliament, the Council, the European Economic and Social Committee and the Committee of the Regions.

Feng, Y., Xiao, Q., Brenner, C., Peche, A., Yang, J., Feuerhake, U., & Sester, M. (2022). Determination of building flood risk maps from LiDAR mobile mapping data. Computers, Environment and Urban Systems, 93, 101759.

Fenn, T., Clarke, C., Burgess-Gamble, L., Harding, E., Ogunyoye, F., Hick, E., & Chatterton, J. (2016). The costs and impacts of the winter 2013/14 floods in England and Wales. In E3S web of conferences (Vol. 7, p. 05004). EDP Sciences.

Ferreira, C.S.S., Potočki, K., Kapović-Solomun, M., Kalantari, Z. (2021). Nature-Based Solutions for Flood Mitigation and Resilience in Urban Areas. In: Ferreira, C.S.S., Kalantari, Z., Hartmann, T., Pereira, P. (eds) Nature-Based Solutions for Flood Mitigation. The Handbook of Environmental Chemistry, vol 107. Springer, Cham. https://doi.org/10.1007/698_2021_758

FLOODsite. (2009). Flood Risk Assessment and Flood risk Management. An Introduction and Guidance Based on Experiences and Findings of FLOODsite (an EU-funded Integrated Project). Deltares, Delft, the Netherlands (ISBN 978 90 8 |4067|0)

Foster, J., Lowe, A., & Winkelman, S. (2011). The value of green infrastructure for urban climate adaptation. Center for Clean Air Policy, 750(1), 1-52.

Freni, G., La Loggia, G., & Notaro, V. (2010). Uncertainty in urban flood damage assessment due to urban drainage modelling and depth-damage curve estimation. Water Science and Technology, 61(12), 2979–2993. doi:10.2166/wst.2010.177

Gehrels, H., Goosen, H., van de Ven, F., Brolsma, R., Hofland, S., Snep, R., & Koekoek, A. (2018). NKWK Klimaatbestendige Stad: Rapportage Onderzoeksprogramma 2018. Nationaal Kennis-en innovatieprogramma Water en Klimaat (NKWK).

Godunov, S. K. (1959). A difference scheme for numerical solution of discontinuous solution of hydrodynamic equations. Math. Sbornik, 47, 271-306.

Gupta, H. V., Clark, M. P., Vrugt, J. A., Abramowitz, G. & Ye, M. (2012). Towards a comprehensive assessment of model structural adequacy. Water Resources Research 48, 1–16. https://doi.org/10.1029/2011WR011044

Hoogmoet, G. (2019). Analysing the effects of extreme precipitation for municipalities and waterboards: Do they need to connect their sewer and surface water models?. MSc Thesis. Delft University of Technology, Delft, the Netherlands.

Innovyze (2012). Representation of inlets in InfoWorks. Thechnical paper. Retrieved August 20, 2024 form <https://help2.innovyze.com/infoworksicm/Content/HTML/TechNotes/Representation_of_Inlets.htm>.

Innovyze. (2023a). InfoWorks ICM key concepts. InfoWorks® ICM version 2023.2. Retrieved January 29, 2024, from <https://help2.innovyze.com/infoworksicm/Content/HTML/ICM_IN_ILCM/InfoWorks_Key_Concepts.htm>.

Innovyze. (2023b). Hydraulic Theory. InfoWorks® ICM version 2023.2. Retrieved September 12, 2024, from <https://help2.innovyze.com/infoworksicm/Content/HTML/ICM_ILCM/Hydraulic_Theory.htm>.

Innovyze. (2023c). Basic 2D Hydraulic Theory. InfoWorks® ICM version 2023.2. Retrieved September 12, 2024, from <https://help2.innovyze.com/infoworksicm/Content/HTML/ICM_ILCM/Basic_2D_Hydraulic_Theory.htm>.

Innovyze. (2023d). 2D Mesh Generation Methodology. InfoWorks® ICM version 2023.2. Retrieved September 12, 2024, from < https://help2.innovyze.com/infoworksicm/Content/HTML/ICM_ILCM/2D_Mesh_Generation_Methodology.htm>.

Innovyze (2023e). Defining 2D nodes. InfoWorks® ICM version 2023.2. Retrieved August 20, 2024, from <https://help2.innovyze.com/infoworksicm/Content/HTML/ICM_ILCM/Defining_2D_Nodes.htm>.

Innovyze (2023f). Permeable Zone (2D). InfoWorks® ICM version 2023.2. Retrieved August 20, 2024, from <https://help2.innovyze.com/infoworksicm/Content/HTML/ICM_ILCM/2D_Permeable_Zones.htm>.

Innovyze (2023g). Infiltration Zone (2D). InfoWorks® ICM version 2023.2. Retrieved August 20, 2024, from <https://help2.innovyze.com/infoworksicm/Content/HTML/ICM_ILCM/2D_Infiltration_Zones.htm>.

Innovyze (2023h). SWMM Model. Retrieved September, 8, 2024, from <https://help2.innovyze.com/infoworksicm/Content/HTML/ICM_ILCM/SWMM_Model.htm>.

IPCC. (2021). Climate Change 2021: The Physical Science Basis. Contribution of Working Group I to the Sixth Assessment Report of the Intergovernmental Panel on Climate Change. Technical report, IPCC. Masson-Delmotte V, Zhai P, Pirani A, Connors SL, Pean C, Berger S, Caud N, Chen Y, Goldfarb L, Gomis MI, Huang M, Leitzell K, Lonnoy E, Matthews JBR, Maycock TK, Waterfield T, Yelekci O, Yu R, Zhou B (eds.) In press.

Jang, J. H., Chang, T. H., & Chen, W. B. (2018). Effect of inlet modelling on surface drainage in coupled urban flood simulation. Journal of Hydrology, 562, 168-180.

Jansen, D. H. B. R. (2023). Land subsidence related damage to residential real estate and cost-effective adaptation strategies. From sinking to solutions: a methodological approach to assess the cost-effectiveness of adaptation strategies to counteract land subsidence related damage to residential real estate. Master Thesis. Delft, University of Technology.

Kadaster J. (2022). Dataset: Basisregistratie Grootschalige Topografie (BGT). Retrieved October 8, 2024, from <https://www.pdok.nl/introductie/-/article/basisregistratie-grootschalige-topografie-bgt-> .

Kabat, P., van Vierssen, W., Veraart, J., Vellinga, P., & Aerts, J. (2005). Climate proofing the Netherlands. Nature, 438(7066), 283–284. doi:10.1038/438283a.

Kaplan, S., & Garrick, B. J. (1981). On The Quantitative Definition of Risk. Risk Analysis, 1(1), 11–27. doi:10.1111/j.1539-6924.1981.tb01350.x

Keifer, C. J., & Chu, H. H. (1957). Synthetic storm pattern for drainage design. ASCE Journal of the Hydraulics Division, 83(HY4), 1-25.

Kellens, W.; Vanneuville, W.; Verfaillie, E.; Meire, E.; Deckers, P.; De Maeyer, P. (2013). Flood risk management in Flanders: Past developments and future challenges. Water Resour. Manag. 2013, 27, 3585–3606.

Kindsvater, C. E., & Carter, R. W. (1957). Discharge characteristics of rectangular thin-plate weirs. Journal of the Hydraulics Division, 83(6), 1453-1.

Klein Tank, A., Beersma, J., Bessembinder, J., Van den Hurk, B., & Lenderink, G. (2014). KNMI'14: Climate scenarios for the Netherlands: A guide for professionals inclimate adaption. KNMI, De Bilt.

Koning, J., & Boogaard, F. C. (2023). Mapping, Assessing, and Evaluating the Effectiveness of Urban Nature-Based Solutions to Climate Change Effects in the Netherlands. In Handbook of Nature-Based Solutions to Mitigation and Adaptation to Climate Change (pp. 1-32). Cham: Springer International Publishing.

Korving, H., & Clemens, F. (2005). Impact of dimension uncertainty and model calibration on sewer system assessment. Water Science and Technology, 52(5), 35–42. doi:10.2166/wst.2005.0103

Kreibich, H.; Seifert, I.; Merz, B.; Thieken, A.H. (2010). Development of FLEMOcs—A new model for the estimation of flood losses in the commercial sector. Hydrol. Sci. J. 2010, 55, 1302–1314

Langewen, J., Holstein, A. N., Spaan, K., van den Buuse, D., van Winden, W., Switzer, A., & Morel, M. (2022). RESILIO Final report: A roof journey.

Leandro, J., Chen, A. S., Djordjević, S., & Savić, D. A. (2009). Comparison of 1D/1D and 1D/2D coupled (sewer/surface) hydraulic models for urban flood simulation. Journal of hydraulic engineering, 135(6), 495-504.

Leitão, J. P., Simões, N. E., Pina, R. D., Ochoa-Rodriguez, S., Onof, C., & Sá Marques, A. (2017). Stochastic evaluation of the impact of sewer inlets' hydraulic capacity on urban pluvial flooding. Stochastic environmental research and risk assessment, 31, 1907-1922.

Lerer, S. M., Arnbjerg-Nielsen, K., & Mikkelsen, P. S. (2015). A mapping of tools for informing water sensitive urban design planning decisions—questions, aspects and context sensitivity. Water, 7(3), 993-1012.

Liu, K., & Baskaran, B. (2003). Thermal performance of green roofs through field evaluation.

Mark, O., Weesakul, S., Apirumanekul, C., Aroonnet, S. B., and Djordjević, S. (2004). "Potential and limitations of 1D modelling of urban flooding." J. Hydrol., 299(3–4), 284–299.

Marvi, M. T. (2020). A review of flood damage analysis for a building structure and contents. Natural Hazards, 102(3), 967-995.

Meng, X., Currit, N., Zhao, K. (2010). Ground filtering algorithms for airborne LiDAR data. A Review of Critical Issues' 2, 833–860. https://doi.org/10.3390/rs2030833.

Meng, M. (2022). How to model an underground storage unit. Medium. Retrieved September 29, 2024, from https://mel-meng-pe.medium.com/how-to-model-an-underground-storage-unit-a3ff006b9479

Merz, B., Elmer, F., Thieken, A.H. (2009). Significance of 'high probability/low damage' versus 'low probability/high damage' flood events. Nat. Hazards Earth Syst. Sci. 9 (3), 1033–1046

Merz, B.; Kreibich, H.; Schwarze, R.; Thieken, A. (2010). Review article "Assessment of economic flood damage". Nat. Hazards Earth Syst. Sci. 2010, 10, 1697–1724.

Ministry of Transport & Water Mangement (1998) Vierde nota waterhuishouding: Regeringsbeslissing. Ministry of Transport & Water Mangement, The Hague.

Moore, S.L., Stovin, V.R., Wall, M., Ashley, R.M. (2012). A GIS-based methodology for selecting stormwater disconnection opportunities. Water Sci. Technol. 66, 275–283. https://doi.org/10.2166/wst.2012.172.

Montoya-Coronado VA, Tedoldi D, Lenormand E, Castebrunet H, Molle P, Lipeme Kouyi G. (2024) Combined sewer overflow mitigation through SUDS - A review on modelling practices, scenario elaboration, and related performances. J Environ Manage. Jun;362:121073. doi: 10.1016/j.jenvman.2024.121073. Epub 2024 Jun 4. PMID: 38833926.

Moreno Rodenas, A. (2019). Uncertainty analysis in integrated catchment modelling. [Dissertation (TU Delft), Delft University of Technology]. https://doi.org/10.4233/uuid: a8577854-a254-44a4-bdb2- b63218454828

Moriasi, D. N., Arnold, J. G., Van Liew, M. W., Bingner, R. L., Harmel, R. D., & Veith, T. L. (2007). Model evaluation guidelines for systematic quantification of accuracy in watershed simulations. Transactions of the ASABE, 50(3), 885-900.

Municipality of Rotterdam (2021). Gemeentelijk rioleringsplan, Planperiode 2021–2025: Van Buis Naar buitenruimte. Rotterdam: Municipality of Rotterdam. Retrieved from https://www.rotterdam.nl/grp.

Nicklin, H., Leicher, A. M., Dieperink, C., & Van Leeuwen, K. (2019). Understanding the costs of inaction–an assessment of pluvial flood damages in two European cities. Water, 11(4), 801.

Nikuradse, J. (1933). Strömungsgesetze in rauhen Rohren. In: Ver. Deut. Ing. Forschungsheft 361.

Ortiz, A., Velasco, M. J., Esbri, O., Medina, V., & Russo, B. (2021). The economic impact of climate change on urban drainage master planning in Barcelona. Sustainability, 13(1), 71. https://doi.org/10.3390/su13010071

Peck S, Callaghan C, Kuhn M, Bass B. (1999). Greenbacks from Green Roofs: Forging a new industry in Canada. Status report on benefits, barriers and opportunities for green roof and vertical garden technology diffusion. Prepared for Canada Mortgage and Housing Corporation.

Pedersen, A. N., Borup, M., Brink-Kjær, A., Christiansen, L. E., & Mikkelsen, P. S. (2021). Living and prototyping digital twins for urban water systems: towards multi-purpose value creation using models and sensors. Water, 13(5), 592.

Pedersen, A. N., Pedersen, J. W., Borup, M., Brink-Kjær, A., Christiansen, L. E., & Mikkelsen, P. S. (2022a). Using multi-event hydrologic and hydraulic signatures from water level sensors to diagnose locations of uncertainty in integrated urban drainage models used in living digital twins. Water Science and Technology, 85(6), 1981-1998.

Pedersen, A. N., Brink-Kjær, A., & Mikkelsen, P. S. (2022b). All models are wrong, but are they useful? Assessing reliability across multiple sites to build trust in urban drainage modelling. Hydrology and Earth System Sciences, 26(22), 5879-5898.

Pelorosso, R., Petroselli, A., Apollonio, C., Grimaldi, S. (2021). Blue-green roofs: hydrological evaluation of a case study in Viterbo, Central Italy. In: Lecture Notes in Civil Engineering. Springer, Cham, pp. 3–13. https://doi.org/10.1007/978-3-030-68824-0_1.

Penning-Rowsell, E.C.; Priest, S.; Parker, D.; Morris, J.; Tunstall, S.; Viavattene, C.; Chatterton, J.; Owen, D. (2013) Flood and Coastal Erosion Risk Management: A Manual for Economic Appraisal; Routledge: London, UK, 2013; ISBN 978-0415815154.

Pina, R., Ochoa-Rodriguez, S., Simões, N., Mijic, A., Marques, A., & Maksimović, Č. (2016). Semi- vs. Fully-Distributed Urban Stormwater Models: Model Set Up and Comparison with Two Real Case Studies. Water, 8(2), 58. doi:10.3390/w8020058'

Prokofieva, I., & Thorsen, B. J. (2011). Protocol for performing Cost-Benefit Analysis (CBA) and Cost-Efficiency Analysis (CEA) in EFORWOOD. European Forest Institute, Finland, 19.

Pushpalatha, R.; Perrin, C.; Le Moine, N.; Andréassian, V. (2012). A review of efficiency criteria suitable for evaluating low-flow simulations. J. Hydrol. 2012, 420, 171–182.

Rehder, T. S. (2024). Enhancing Municipal Flood Risk Communication and Community Adaptability Through Serious Gaming. A Case Study of the 'WhereWeMove' Game. Master Thesis. Delft, University of Technology. https://resolver.tudelft.nl/uuid:f891ab5c-f8ba-42f0-a57e-82b3e7537566.

Rijkswaterstaat. (2021). Discontovoet. Retrieved September 18, 2024, from https://www.rwseconomie.nl/discontovoet

RIONED. (2004). Urban drainage guideline. Module C2100 'Hydraulic performance sewerage calculations'. Leidraad Riolering. Module C2100. Rioleringsberekeningen, hydraulisch functioneren (in Dutch). August 2004. Kluwer, Alphen aan den Rijn, the Netherlands.

RIONED (2019). Modelleren hydraulisch functioneren. Retrieved September 28, 2024, from <https://www.riool.net/kennisbank/onderzoek/modelleren-hydraulisch-functioneren>.

RIONED (2022). Ontwerp en beheermaatregelen. Retrieved July 11, 2024, from <https://www.riool.net/kennisbank/ontwerp-en-beheermaatregelen>.

Rosenzweig, B. R., McPhillips, L., Chang, H., Cheng, C., Welty, C., Matsler, M., & Davidson, C. I. (2018). Pluvial flood risk and opportunities for resilience. Wiley Interdisciplinary Reviews: Water, 5(6), e1302. doi:10.1002/wat2.1302.

Rossman, L. A.; Huber, W. C. (2016) Storm Water Management Model Reference Manual Volume I – Hydrology. Cincinnati (EUA): USEPA (United States Environment Protection Agency).

Russo, B., Sunyer, D., Velasco, M., & Djordjević, S. (2015). Analysis of extreme flooding events through a calibrated 1D/2D coupled model: the case of Barcelona (Spain). Journal of Hydroinformatics, 17(3), 473-491.

Schrader, S., & Böning, M. (2006). Soil formation on green roofs and its contribution to urban biodiversity with emphasis on Collembolans. Pedobiologia, 50(4), 347-356.

Schröter, K.; Kreibich, H.; Vogel, K.; Riggelsen, C.; Scherbaum, F.; Merz, B. (2014). How useful are complex flood damage models? Water Resour. Res. 2014, 50, 3378–3395

Shakya, R., & Ahiablame, L. (2021). A synthesis of social and economic benefits linked to green infrastructure. Water, 13(24), 3651.

Shewchuk J. R. (1996). Engineering a 2D quality mesh generator and Delaunay triangulator. Applied Computational Geometry towards Geometric Engineering. Vol. 1148 of Lecture Notes in Computer Science. Berlin, Heidelberg, Springer, 203–222.

Smith, D. I. (1994). Flood damage estimation-A review of urban stage-damage curves and loss functions. Water Sa, 20(3), 231-238.

Smith, J.B., Schellnhuber, H.-J., Mirza, M.M.Q. (2001). Vulnerability to climate change and reasons for concern: a synthesis. In: McCarthy, J.J. *et al.* (Eds.), Climate Change 2001: Impacts, Adaptation and Vulnerability. Contribution of Working Group II to the Third Assessment Report of the Intergovernmental Panel on Climate Change. Cambridge University Press.

Snep, R. P., Klostermann, J., Lehner, M., & Weppelman, I. (2023). Social housing as focus area for Nature-based Solutions to strengthen urban resilience and justice: Lessons from practice in the Netherlands. Environmental Science & Policy, 145, 164-174.

Spekkers MH, ten Velduis JAE, Kok M, Clemens FHLR. (2012). Analysis of pluvial flood damage based on data from insurance companies in the Netherlands.

Stanić, N., Clemens, F. H., & Langeveld, J. G. (2017). Estimation of hydraulic roughness of concrete sewer pipes by laser scanning. Journal of Hydraulic Engineering, 143(2), 04016079.

Steeneveld, G. J., Koopmans, S., Heusinkveld, B. G., Van Hove, L. W. A., & Holtslag, A. A. M. (2011). Quantifying urban heat island effects and human comfort for cities of variable size and urban morphology in the Netherlands. Journal of Geophysical Research: Atmospheres, 116(D20).

Stovin, V. R., Moore, S. L., Wall, M., & Ashley, R. M. (2013). The potential to retrofit sustainable drainage systems to address combined sewer overflow discharges in the Thames Tideway catchment. Water and Environment Journal, 27(2), 216-228.

Suryanto, A. (2021). Optimal Rehabilitation of Urban Drainage Systems: Application of single-objective optimisation for the implementation of Green-Blue-Grey Infrastructures in changing climate. https://resolver.tudelft.nl/uuid:2c9aef02-d0b7-4973-bf1f-ccda469b9616

Sušnik, J.; Strehl, C.; Postmes, L.A.; Vamvakeridou-Lyroudia, L.S.; Savi´c, D.A.; Kapelan, Z.; Mälzer, H.J. (2015). Assessment of the effectiveness of a risk-reduction measure on pluvial flooding and economic loss in Eindhoven, the Netherlands. Procedia Eng. 2014, 70, 1619–1628.

Ten Veldhuis, J. A. E., Clemens, F. H. L. R., Sterk, G., & Berends, B. R. (2010). Microbial risks associated with exposure to pathogens in contaminated urban flood water. Water research, 44(9), 2910-2918.

TRUEGRID. (2024). Permeable Paver Maintenance: the Only Guide You'll Need in 2024. Retrieved September 18, 2024, from https://www.truegridpaver.com/permeable-paver-maintenance/.

Tscheikner-Gratl, F.; Zeisl, P.; Kinzel, C.; Leimgruber, J.; Ertl, T.; Rauch, W.; Kleidorfer, M. (2017). Lost in calibration: Why people still do not calibrate their models, and why they still should—A case study from urban drainage modelling. Water Sci. Technol. 2016, 74, 2337–2348.

USEPA .(2012). "Cool Pavements." In: Reducing Urban Heat Islands: Compendium of Strategies. https://www.epa.gov/heat-islands/heat-island-compendium.

Vaes, G., Berlamont, J. (1996). Composietbuien als neerslaginvoer voor rioleringsberekeningen. Water nr. 88.

Van Bijnen, M., Korving, H., & Clemens, F. (2012). Impact of sewer condition on urban flooding: an uncertainty analysis based on field observations and Monte Carlo simulations on full hydrodynamic models. Water Science and Technology, 65(12), 2219–2227. doi:10.2166/wst.2012.134

van Ginkel, K. C. H., Dottori, F., Alfieri, L., Feyen, L., and Koks, E. E. (2021). Flood risk assessment of the European road network, Nat. Hazards Earth Syst. Sci., 21, 1011–1027, https://doi.org/10.5194/nhess-21-1011-2021, 2021.

van Leth, T. C., Leijnse, H., Overeem, A., & Uijlenhoet, R. (2021). Rainfall Spatiotemporal Correlation and Intermittency Structure from Micro-γ to Meso-β Scale in the Netherlands. Journal of Hydrometeorology, 22(8), 2227-2240.

Veldkamp, T. I. E., Boogaard, F. C., & Kluck, J. (2022). Unlocking the potential of permeable pavements in practice: A large-scale field study of performance factors of permeable pavements in the Netherlands. Water, 14(13), 2080.

Wagenaar, D. J., De Bruijn, K. M., Bouwer, L. M., & de Moel, H. (2016). Uncertainty in flood damage estimates and its potential effect on investment decisions. Natural Hazards and Earth System Sciences, 16(1), 1-14.

Walker, W., Harremoës, P., Rotmans, J., van der Sluijs, J. P., van Asselt, M., Janssen, P. & Krayer von Krauss, M. (2003). Defining uncertainty: a conceptual basis for uncertainty management. Integrated Assessment 4, 5–17. https://doi.org/10.1076/iaij.4.1.5.16466.

Wei, H., Zhang, L., & Liu, J. (2022). Hydrodynamic modelling and flood risk analysis of urban catchments under multiple scenarios: a case study of Dongfeng Canal District, Zhengzhou. International journal of environmental research and public health, 19(22), 14630.

Woodward, M., Gouldby, B., Kapelan, Z., Khu, S. T., & Townend, I. (2011). Real Options in flood risk management decision making. Journal of Flood Risk Management, 4(4), 339-349.

Willems, P., & Olsson, J. (2012). Impacts of climate change on rainfall extremes and urban drainage systems. IWA publishing.

Wise, S., Braden, J., Ghalayini, D., Grant, J., Kloss, C., MacMullan, E., & Yu, C. (2010). Integrating valuation methods to recognize green infrastructure's multiple benefits. In Low impact development 2010: Redefining water in the city (pp. 1123-1143).

Yang, Y., Sun, L., Li, R., Yin, J., & Yu, D. (2020). Linking a storm water management model to a novel two-dimensional model for urban pluvial flood modeling. International Journal of Disaster Risk Science, 11, 508-518.

Yen B.C. (1973). Open channel flow equations revisited.J. Eng. Mech. Div. ASCE, Vol 99, No EM5

Zhang, Shouhong, Lin, Z., Zhang, Sunxun, Ge, D. (2021). Stormwater retention and detention performance of green roofs with different substrates: observational data and hydrological simulations. J. Environ. Manag. 291, 112682 https://doi.org/10.1016/j.jenvman.2021.112682.

Zhou, Q.; Mikkelsen, P.S.; Halsnæs, K.; Arnbjerg-Nielsen, K. (2012). Framework for economic pluvial flood risk assessment considering climate change effects and adaptation benefits. J. Hydrol. 2012, 414, 539–549

Zhou, Q., Panduro, T. E., Thorsen, B. J., & Arnbjerg-Nielsen, K. (2013). Verification of flood damage modelling using insurance data. Water science and technology, 68(2), 425-432.

Zhu, Z., & Chen, X. (2017). Evaluating the effects of low impact development practices on urban flooding under different rainfall intensities. Water, 9(7), 548.

Annex A – Combined and Stormwater Systems in Spangen

1. Combined System

In Spangen, wastewater from buildings is collected through a highly looped network of pipes, with dimensions ranging from 200 to 1500 mm. This dry sanitary flow is transported towards a pumping station (as shown in Figure 48) which has a maximum discharge capacity of 600 m³/h. The pumping station directs the flow to an adjacent city district, from where it is subsequently transported to a treatment plant. During periods of heavy rainfall, the capacity of the combined sewer system in Spangen may be exceeded, leading to discharges from the combined sewer overflow into the *Spaansebocht* canal.

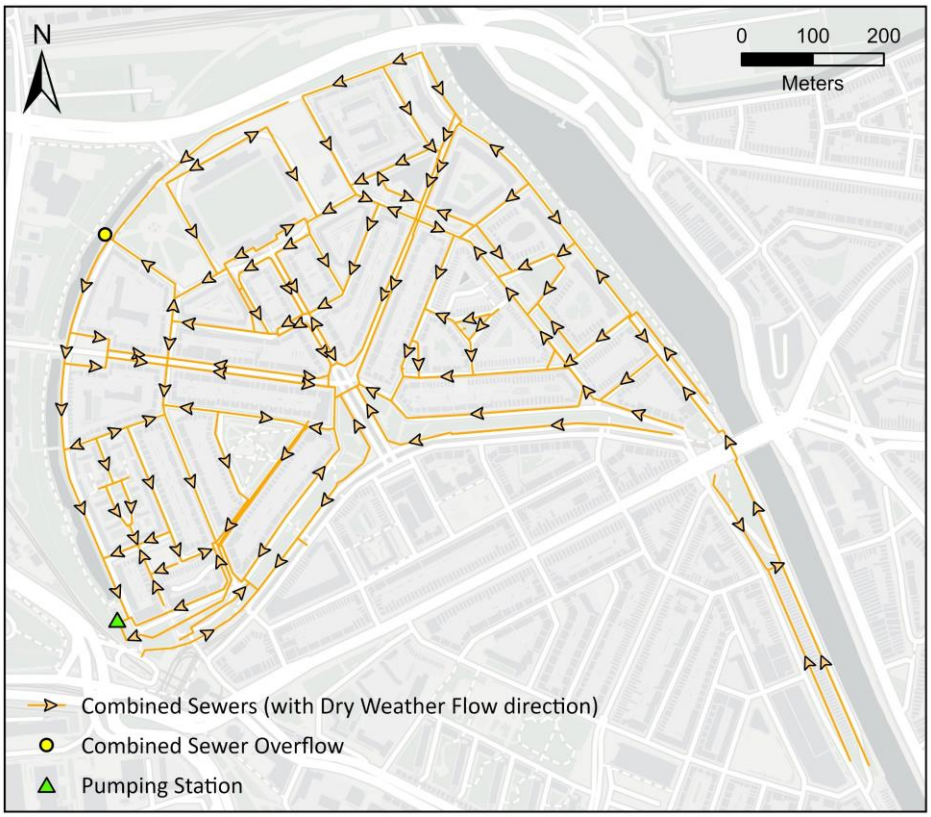

Figure 48 – Combined sewer system with dry weather flow direction.

2. Stormwater Systems

2.1. Urban Water Buffer

In 2018, an Urban Water Buffer (UWB) was implemented near Sparta Rotterdam's stadium, *Het Kasteel*, in the northern region of Spangen. This innovative system captures runoff from the stadium and parts of the nearby area, storing it in a buffer of underground crates with a total capacity of 1400 m³. Following storage, the water is purified using a vertical helophyte filter, then pumped into the first aquifer through a groundwater well. This rainwater is later recovered via the same well for purposes such as irrigating the stadium's field and providing cooling for the square. When the water buffer reaches its capacity, excess water is directed to an overflow weir that discharges into the *Spaansebocht* canal. Positioned just a few centimeters above the canal's normal level, the weir often operates submerged, which frequently leads to flooding around the stadium during periods of extreme precipitation.

Figure 49 illustrates the UWB's operational mechanism and its associated drainage network. In this research, the performance of the pre-treatment was not investigated.

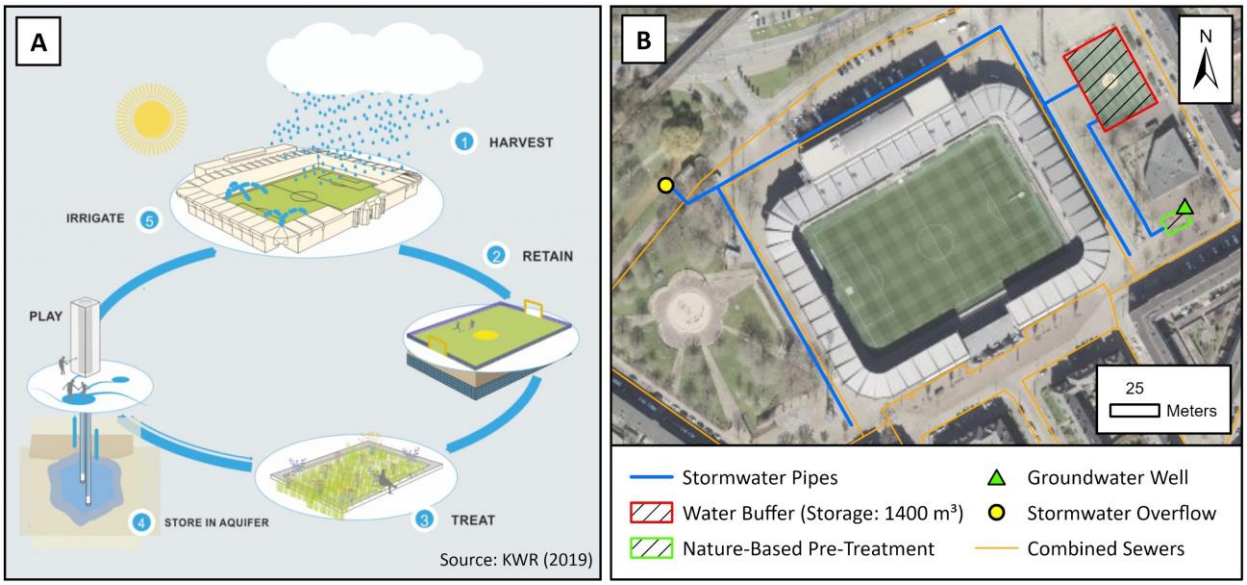

Figure 49 – Schematic of the UWB: (a) operational mechanism and (b) drainage network layout.

2.2. Bellamyplein Water Square

Bellamyplein, situated in the eastern part of Spangen and one of the district's lowest regions, has historically faced significant drainage challenges. In response to frequent water nuisances, a pioneering water square was constructed in 2012, the first of its kind in the Netherlands. This innovative square captures stormwater from adjacent paved areas through a combination of surface channels and underground pipes, directing the flow towards a large concrete retention tank with a capacity of 191 m³ (Figure 50). Additionally, the roofs of surrounding buildings have been modified to have disconnected downspouts, which channel runoff directly to the paved areas linked to this concrete tank.

Figure 50 – Photo of the concrete retention tank at Bellamyplein water square.

After a certain time, the water stored in the tank is pre-purified via two underground crates and it is slowly infiltrated into the phreatic soil. Runoff from specific areas of the square can be routed directly to these crates via gully inlets connected to a system of infiltration pipes, bypassing the retention tank. Due to the inadequate infiltration capacity of these crates during wet periods, a groundwater well is utilized to infiltrate the water into the first aquifer.

When the capacity of the underground crates is exceeded, two overflow weirs allow excess water to flow from the infiltration pipes back into the stormwater pipes. Additionally, water from this system can be discharged into the combined sewer system via an overflow weir located in the southern part and/or through a pumping system in the northern part. The layout of this stormwater system's drainage network is presented in Figure 51.

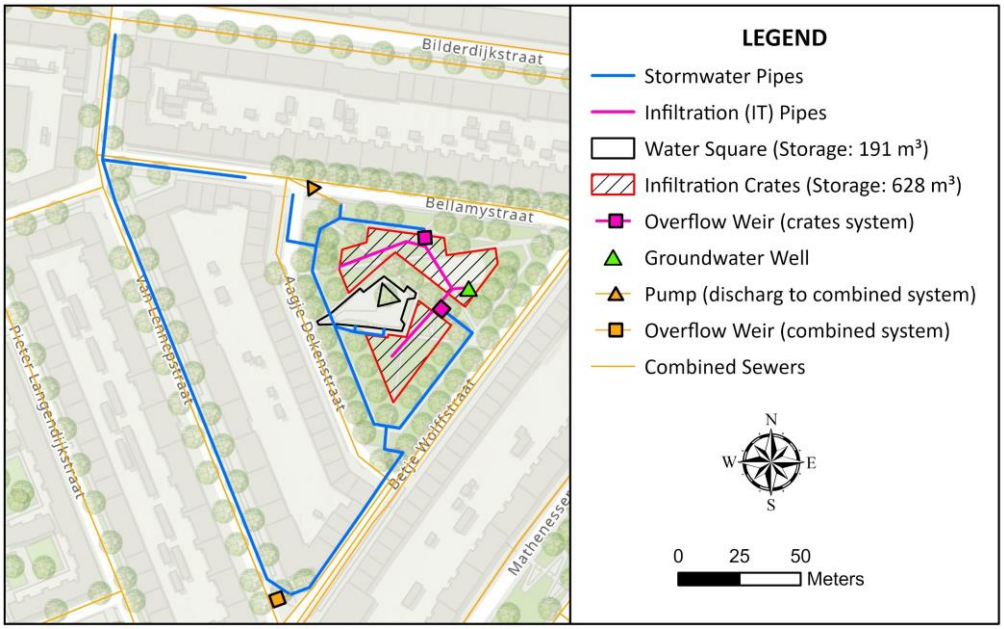

Figure 51 – Drainage network layout in Bellamy water square.

2.3. Staringplein Stormwater System

Located in the eastern part of Spangen, the homes and outdoor spaces at Staringplein were in need of renovation and improvement. The Municipality of Rotterdam therefore decided to redesign the neighborhood. Since many of the homes were owned by the housing corporation Woonstad, the municipality partnered with them to initiate a redevelopment project in 2018.

In addition to energy-efficient measures such as extra insulation, heat pumps, and solar panels, flood mitigation strategies were also implemented. Staringplein now features a green appearance, including a large lawn between the houses, under which lies an underground infiltration crate system with an effective storage capacity of about 105 m³. Figure 52 shows photos of the square during the renovation works and after completion.

Figure 52 – Staringplein during renovation works (left) and after completion (right).

In this system, rainwater is collected separately as much as possible. Runoff from adjacent streets and sidewalks is collected through gullies and routed into a network of stormwater pipes. Similarly, roofs of the new homes drains now separately, with runoff also being directed through stormwater pipes. All collected rainwater is then routed towards the bottom of the infiltration crate. Additionally, a small infiltration crate with a storage capacity of approximately 20 m³ has been installed near Multatulistraat to handle runoff from the southern part of the system. Both crates are equipped with an overflow weir, which allows excess water to be discharged into the combined sewer system when their capacity is exceeded. Figure 53 provides a visualization of the drainage network in Staringplein and its components.

Figure 53 – Drainage network layout of Staringplein stormwater system.

Annex B – Comparison of Design and Actual Ground Elevation (2016)

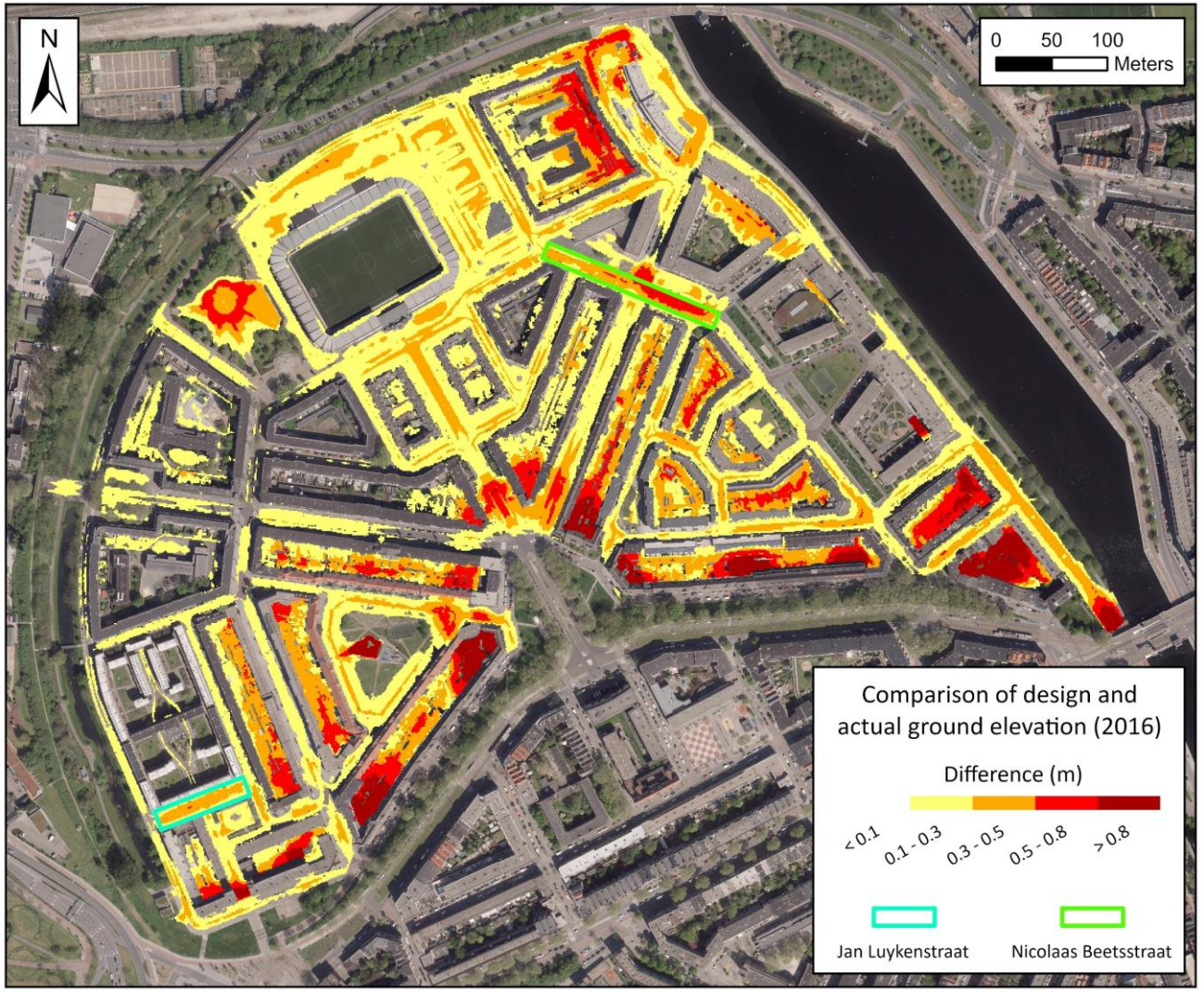

Figure 54 – Comparison of design and actual ground elevation (2016). Source: archives from The Municipality of Rotterdam.

Annex C – Observed Data

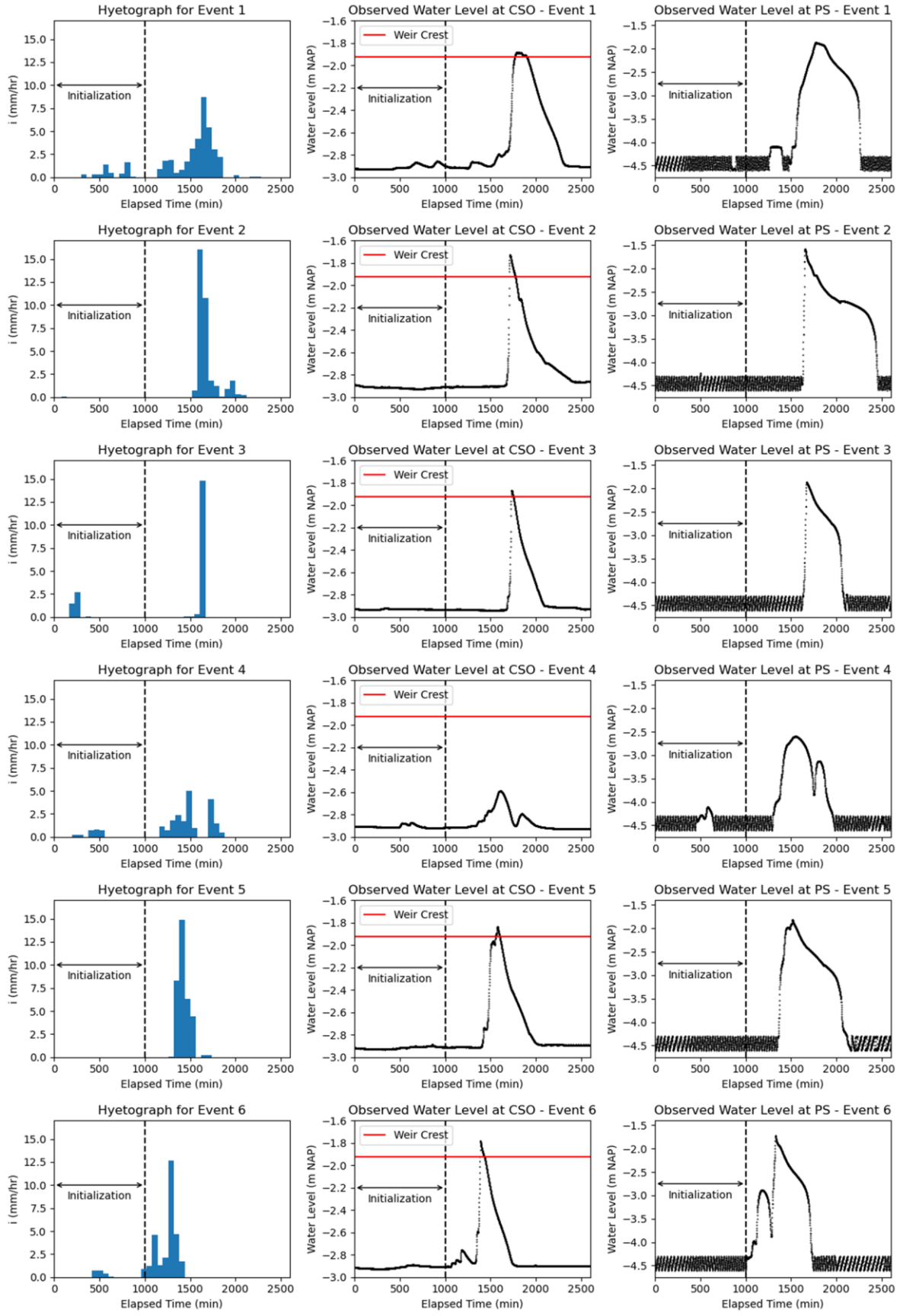

Figure 55 – Time series of the observed data used for calibration and validation.

Annex D – Rotterdam Doorstep Measurements

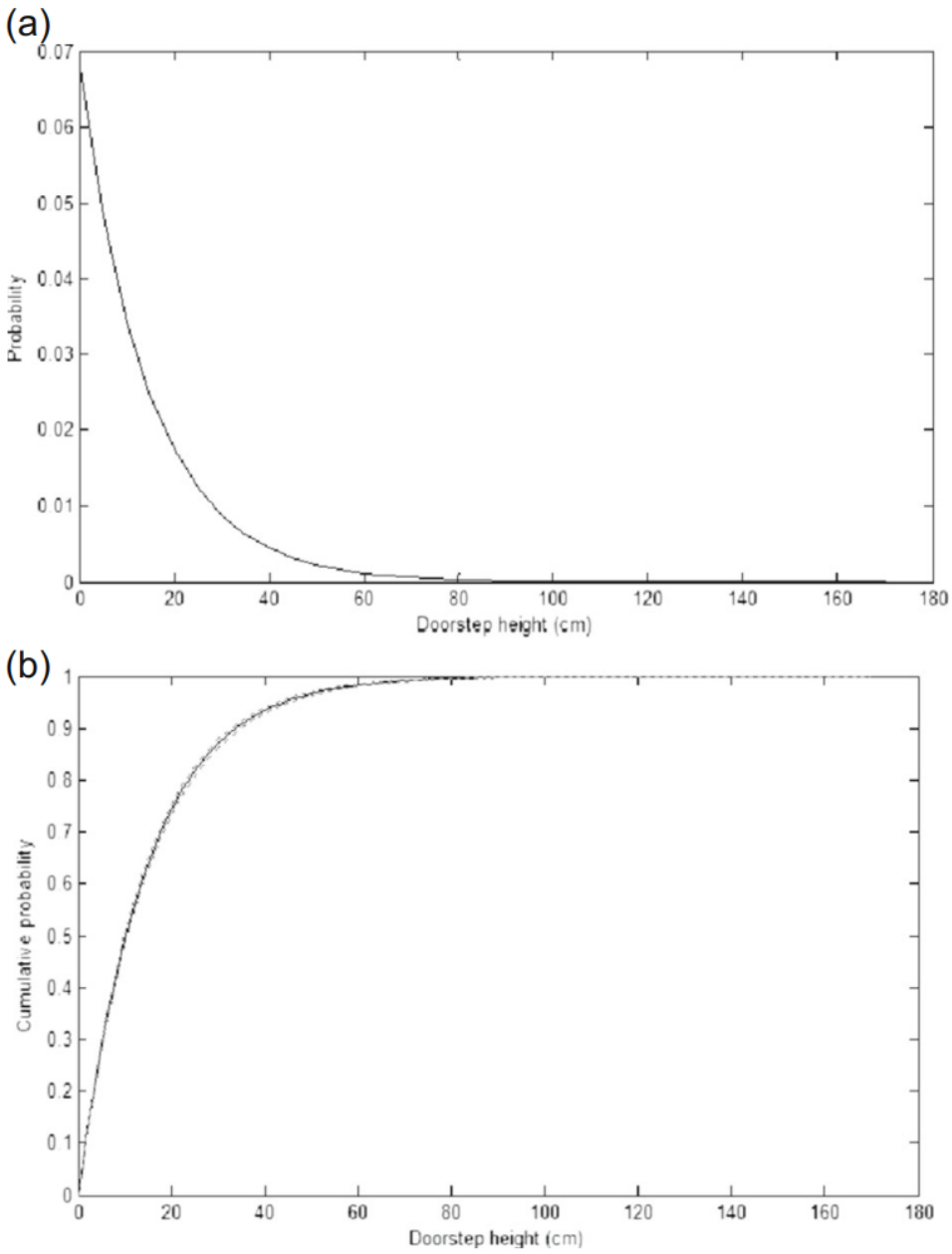

Figure 56 – (a) Probability- and (b) Cumulative-density functions of Rotterdam doorstep measurements (Sušnik *et al.*, 2015).

Annex E – Functional Land Use Map

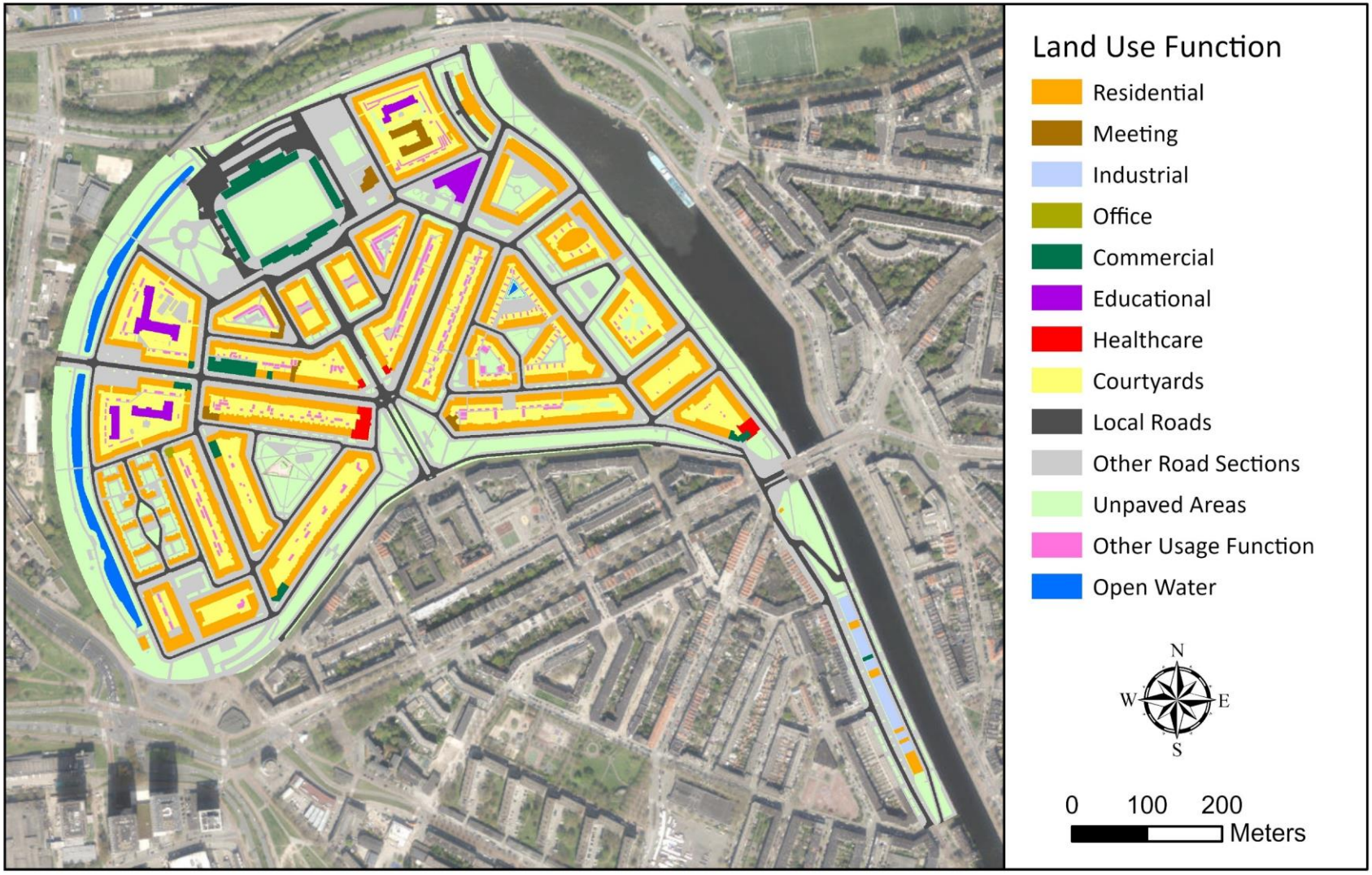

Figure 57 – Functional land use map for Spangen.

Annex F – Costs Data

Pipe enlargement

Cost data for enlarging pipes through excavation are sourced from the Dutch sewerage guidelines (RIONED, 2022) using 2021 prices. Maintenance costs after implementing this solution are assumed to be equivalent to current system maintenance, disregarding potential increases due to larger diameters, and thus omitted from this analysis. The base costs, including allowances, are €470 per meter for a 300 mm diameter sewer and €940 per meter for a 700 mm diameter sewer, with other sizes calculated as follows:

$$C_1 = 470 * 1.25^{\left(\frac{D-300}{135}\right)} \quad (13)$$

$$C_2 = 940 * 1.77^{\left(\frac{D-700}{135}\right)} \quad (14)$$

where C_1 and C_2 are the costs in euros per meter for diameters below and above 700 mm, respectively; and D is the new sewer pipe diameter in millimeters.

Permeable Pavements

Investment and maintenance costs for permeable pavements are obtained from the national guidelines (RIONED, 2022) using 2021 prices (Table 11).

Table 11 – Investment and maintenance costs for permeable pavements (RIONED, 2022)

Cost Category	Cost in 2021 (€)
Capital Cost (per m2)	115
Measuring Permeability Cost (per m² every 3 years)	1.1
Visual Inspection Cost (per m² per year)	0.25
Swepping Cost (per m² per year)	0.55
Deep Cleaning Cost (per m² every six years)	2.25
Fill Joints Cost (per m² after deep cleaning)	0.55

Blue-Green Roof

Costs for blue-green roofs were estimated based on the RESILIO project in Amsterdam (Langewen *et al.*, 2022). This project installed 7,449 m² of blue-green roofs at €245/m², totaling €1,825,000. Regular maintenance costs—covering green maintenance, gutter maintenance, maintenance of the smart roof weir/drop system and re-inspection—are significant, currently estimated at €4/m² per year. However, economies of scale could potentially reduce this to €2/m². For this study, a reduced rate of €2/m² was assumed, anticipating cost reductions over time due to technological advancements and wider adoption.

Annex G – Inundation and Exposure Maps for Current System

Figure 58 – Flood depth and building exposure for current system under varying return periods for current and future climate conditions.

Annex H – Damage Cost Estimates

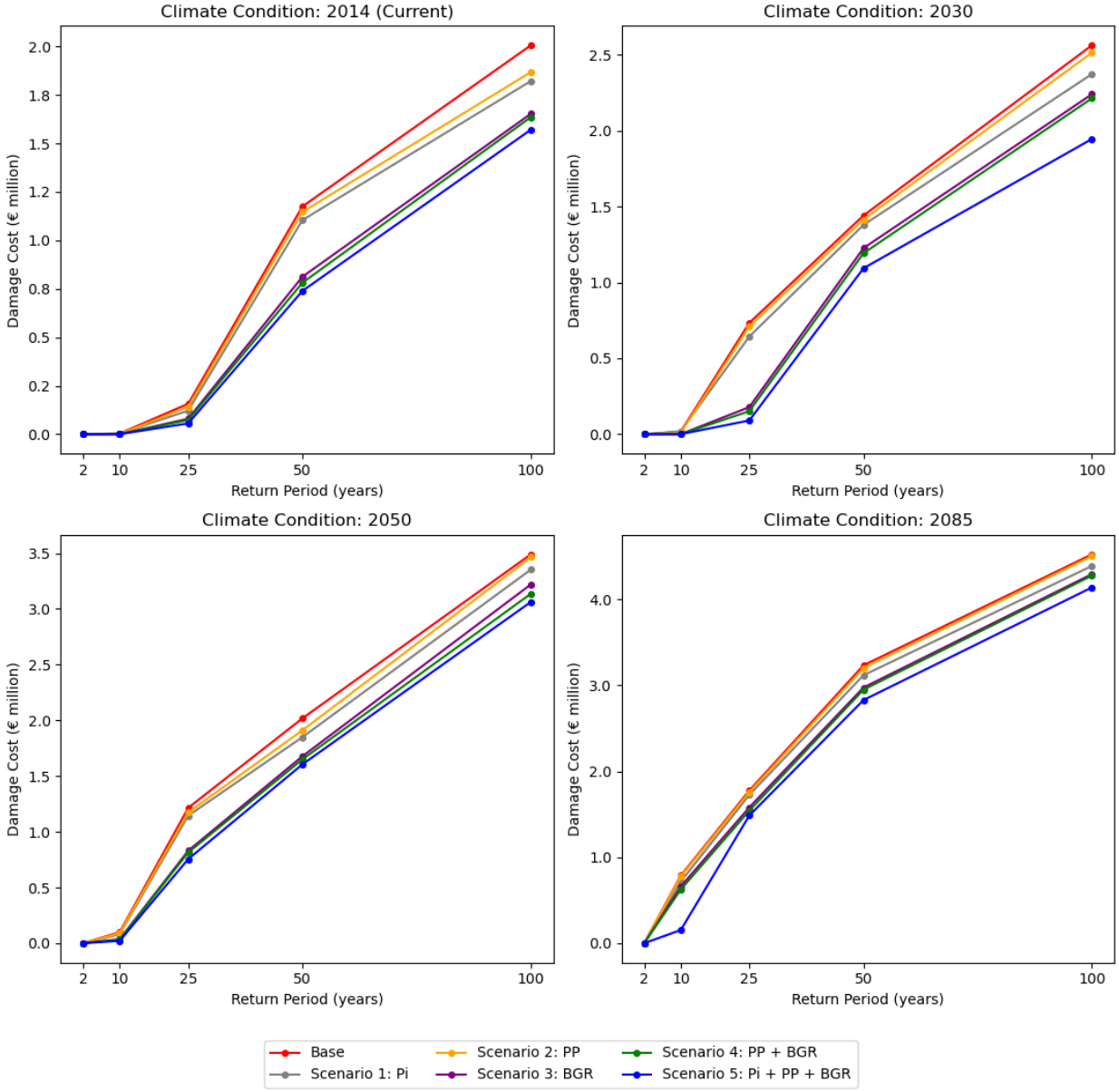

Figure 59 – Damage cost as function of the return period for different risk-reduction scenarios under present and future climate conditions.

TU Delft

Gemeenteraad
Gemeente Rotterdam